In presenting this thesis in partial fulfillment of the requirements for an advanced degree at Idaho State University, I agree that the Library shall make it freely available for inspection. I further state that permission for extensive copying of my thesis for scholarly purposes may be granted by the Dean of the Graduate School, Dean of my academic division, or by the University Librarian. It is understood that any copying or publication of this thesis for financial gain shall not be allowed without my written permission.

Signature ____________________________________

Date ____

Categorization and Evaluation of Spray Patterns from Pipe Leaks

By

Cody Michael Muchmore

A thesis

submitted in partial fulfillment of

the requirements for the degree of

Master of Science in the Department of Nuclear Science and Engineering

Idaho State University

Spring 2018

To the Graduate Faculty

The members of the committee appointed to examine the thesis of Cody Muchmore find it satisfactory and recommend that it be accepted.

Dr. Chad Pope,
Major Advisor

Dr. Bruce Savage,
Committee Member

Dr. Hossein Mousavinezhad
Graduate Faculty Representative

For Paige, forever and always, and for my parents for their endless love and support

Acknowledgements

I would like to thank Dr. Chad Pope for hiring me onto this project in my undergrad and allowing me to pursue a graduate degree on it. His constant mentoring and level-headed support of me and other students make this work and all other project work possible. I would also like to thank Dr. Bruce Savage for taking the time out of his day to constantly address all my complicated piping calculation questions that he broke down and made simple to understand. He is a credit to this project, and we would not have near the success we have had without him. I would like to thank the Idaho State Nuclear Engineering department for allowing me to succeed in a high-quality education as an undergraduate and a graduate. I would like to thank the Nuclear Regulatory Commission for funding my graduate school and stipend. I would like to thank Allison Wells for helping me with the piping assembly, and coming in on all the random days to help me switch parts out at the drop of a hat. I would like to thank the rest of the CFEL team for all the work they do.

Table of Contents

Table of Figures

Table of Tables

Table of Equations

Categorization and Evaluation of Spray Patterns

from Pipe Leaks

Thesis Abstract – Idaho State University (2018)

The goal of this project is to present a method for describing leaks from piping in nuclear power plants. The predominant failure types being from erosion/corrosion and fatigue vibration. One such piping type present in all power plants is fire sprinkler systems. This setup allowed for testing of three pipe diameters, 1-inch, 2-inch, and 3-inch. Three different pipe failures were tested - longitudinal cracks, circumferential cracks, and cracks on the outside of elbows. The leaks were tested by varying valves upstream and downstream of the test section. From these tests, three different leak types were identified. Type 1 acted as the baseline, Type 2 leaks display the lowest leak rates and velocities and Type 3 display the highest leak rates, pressures, and velocities. This thesis is early work in the assessment of leaks and leak patterns as a flooding type in nuclear power plants, and there is much future possible.

Key Words: pipe, leak, spray, pattern, pump, flooding, component, failure

Introduction

Since the Fukushima Daiichi power plant was destroyed by a tsunami in 2011, flooding has been of great interest in the nuclear power industry. The Light Water Reactor Sustainability Program (LWRS) contains a portion of the United States' efforts in nuclear power plant (NPP) flooding safety. The goal of the LWRS program is to determine if the current U.S. nuclear fleet can safely be licensed beyond their 60-year operating period, possibly up to another 20 years. Part of extending licensure for plants is ensuring reasonable plant safety from flooding events, or, as there will always be the hazard of flooding in plants, the probable risks associated with flooding. There have been several flooding events in U.S. plants, few of which had less than substantial news coverage, because of their low-damage nature. Few received much news coverage, because they did not result in serious damage. The reality is, these types of events are likely to happen, even if it is on a small scale. Little research has been currently dedicated on how power plant components will fail under flooding events. Efforts to assess the risks associated with flooding are lacking real failure data and rely on assumptions due to the lack of data.

Flooding events can be broken down into three major categories: rising water, wave impact, and water spray. The work presented in this thesis will be focusing on water spray events. Water spray is the most common type of flooding event, generally from smaller pipes, about 1 inch in diameter. The goal of this thesis is to examine water spray from different leak sizes and orientation in piping. The resulting sprays will be described as best as possible, qualitatively and quantitatively. The results of the experiments can then be loaded into a database, accessible by those individuals creating probabilistic risk assessments for power plants. The risk analyst will have a system of piping they want to have fail in a certain way, and knowing the type of piping (the flows, the pressure, the size, etc), they will be able to query a database. Based on the model parameters and the type of failure induced, the analyst will be able to know an approximation of the resultant spray, and eventually, how the modeled spray can damage different equipment.

The research for this project will be a part of one of the three types of water impact tested with the Component Flooding Evaluation Laboratory (CFEL). The Portal Evaluation Tank (PET) is currently used for water rise tests focusing on doors, the Wave Impact Simulation Device (WISD) will be for wave impact tests in the future, and this research will begin the water spray portion. The scope of this project will be in the experiment design for leak pattern testing, while trying to determine some patterns in quantitative data.

Literature Review

Pipe leakages in power plants has been considered greatly, but most research addresses how leaks can occur in pipes, and discusses the probabilities of them happening. Such papers include “The Probability of Leakage in Piping Systems of Pressurized Water Reactors on the Basis of Fracture Mechanics and Operating Experience” [1] and “Fracture Mechanics Analysis on the Initiation and Propagation of Circumferential and Longitudinal Cracks in Straight Pipes and Pipe Bends” [2]. The papers in [1] and [2] are generally concerned with pipes between 1 and 10 inches in diameter. Papers such as “Study on Crack Opening Area and Coolant Leak Rates on Pipe Cracks” [3] and “Estimation of Leak Rate Through Circumferential Cracks in Pipes in Nuclear Power Plants” [4] address methods of determining the leak rate through circumferential cracks using the Henry-Fauske flow model, but do not address what happens to the water once it leaves the pipes. These papers are most concerned with Loss-Of-Coolant Accidents (LOCA), and core damage. LOCAs and core damage may be the most important considerations for nuclear power plants, but the possibilities of damage occurring to equipment suffering water damage from a leak have not been studied. To put it another way, the lack of water being in a pipe has been studied, but what the water does outside of the pipe has not. The goal of this section is to address what has been studied in pipe failures relevant to nuclear power plant components, and to demonstrate where the knowledge is lacking. The basis for the experiments will be justified using data compiled from pipe failures in nuclear power plants.

Leak Before Break (LBB) is a key of this research, and of nuclear plant life in general. The concept states there should be more than the minimum detectable leak rate leaking from a pipe before catastrophic failure occurs, or pipes should leak before they rupture. These leaks range in size, the orientation of their stream, the exit velocity of the stream, crack characteristics, and more.

Flow rate is a parameter in these leak studies examined in depth in relation to crack parameters. The focus on internal pipe parameters is due more to the concern of LOCAs occurring rather than component damage accidents.

Swedish Nuclear Power Inspectorate Report

The Swedish Nuclear Power Inspectorate (SKI) performed a study of pipe failure events at United States NPPs from 1961-1995 [5]. The SKI database examines several report databases. The three most important report databases are Licensing Event Reports (LERs), Abnormal Occurrence Reports (AORs), and Reportable Occurrences (ROs). These three are all used, or have been used, by the NRC, and the LERs have the most extensive set of event data. In all, this study aggregated 1511 reports of piping failures in the US in the studied period, and created a Microsoft Access database for the events.

The SKI study uses six different terminologies to define pipe failures. The first term is leak, defined as a limited but finite amount of water being released, varying from leaks of cubic centimeters per hour to a liter or more a minute. The next term is crack/leak, defined as having finite depths and penetration of the pipe wall to create a leak, and is a subset of leaks. Thirdly, failure, which releases more water than a leak, but less than a full pipe break. In the context of these reports, failed is a vague term and is not used in any quantifying ways. The last three categories, rupture, severed, and breakage, are used synonymously and center on holes the size of the cross section of the pipe to full double-ended guillotine breaks. Each failure in the database is defined by one of these terms to indicate the severity of the damaged piping.

The following tables show some categorical breakdowns of data from the SKI database. Table 1 shows the numbers of failures sorted by pipe size. The first set of data contains 1055 reports where the pipe size was reported in ranges: less than 1 inch, 1 to 4 inches, 4 to 12 inches and greater than 12 inches. Most of the failures were in pipes of size less than 1 inch. The next set of data contains 382 reports where the exact size is unknown, but it could be classified as either less than 1 inch, greater than 1 inch, or a reducer. Lastly, 74 of the reports studied gave no indication of the pipe size. The reports categorized by size show most pipe failures in the reporting period were in pipes of less than 1 in.

Table 1. Number of Piping Failures for Various Pipe Sizes and Pipe Size Categories

Pipe Size/Category	Number of Failures
Actual Pipe Size	
≤ 1 inch	574
> 1 inch & ≤ 4 inches	252
> 4 inches & ≤ 12 inches	155
> 12 inches	74
Subtotal	1055
Pipe Size Category	
“<1”	227
“>1”	142
Reducer	13
Subtotal	382
Unknown/Undetermined Size/Category	74
Total	1511

The next data table from the SKI report, Table 2, shows the number of failures from the report based on the failure type. Failures from leaks were the largest category of failures, as is expected, as the LBB piping design principle from before described, minor leaks should be the most common failure. It is these types of failures being examined in this research. It must then be assessed how these pipes failed and the leaks occurred, and the last table from the SKI report reveal how.

Table 2. Number of Piping Failures by Type of Failure

Failure Type	Number of Failures
Leak	
Leak	1274
Crack/Leak	54
Failed	64
Rupture	
Breakage	13
Rupture	76
Severed	30
Total	1511

Finally, Table 3 discusses the failure mechanisms described in each report for each type of piping failure. The two biggest known causes of failure from Table 3 are Fatigue-Vibration (FV) with 364 failures, and Erosion/Corrosion (E/C) with 295 failures. The SKI report notes FV failure is mostly a contributor to pipes 1-inch and smaller, but is not visible in any of the presented tables. The SKI report describes a downward trend in failures after 1983, contributed to by changes in reporting requirements and increased safety standards, in all areas except ruptures. The lack of reduction in ruptures is due to E/C being the main cause of ruptures. The experiments in this project will seek to recreate these two failure types in tested pipes with machining.

Table 3. Number by Piping Failures for Each Failure Mechanism Category

Failure Mechanism (Code)	Number of Failures
Corrosion/Fatigue (C/F)	14
Construction Defects/Errors (CD)	184
Design-Dynamic Load (DDL)	8
Water Hammer (WH)	35
Fatigue-Vibration (FV)	364
Erosion/Corrosion (E/C)	295
Stress Corrosion / IGSCC SC	166
Corrosion (COR)	72
Thermal Fatigue (TF)	38
Other (OTH)	43
Unknown Causes (UNK)	292
Total	1511

The experiments for pipe leakage started with these failures in mind. The piping examined had a nominal diameter of less than 4-inches and focused on FV and E/C failure. Cracks were machined like in [4], as recreating FV and E/C proved too difficult to recreate. The paper in [4] focused on circumferential cracks, so they were one of the crack types analyzed for the experiments presented here. A safety advisory from the Canadian National Energy Board [6] indicated FV failure tended to happen where small diameter pipes tie into larger pipe. The failure occurs because these small pipes are not supported well enough, so vibration cause bending stresses at the pipe junction. The situation required to recreate FV, as well as E/C failure, would have taken too much time to recreate in the scope of this experiment. No ruptures were examined for this experiment- leaks through cracks were the focus. Lastly, the specific pipe material was needed, and since it was difficult to find information on power plant piping, general fire sprinkler piping was used as an example instead.

Fire Sprinkler Systems

Most of these small-bore pipes are likely either fire suppression systems, or for water lines for human use (sinks, toilets). The design of the experiment will be based on the pressure ratings of these lines, specifically fire sprinklers. From the National Fire Protection Association's NFPA 13 Standard for the Installation of Sprinkler Systems [7], the minimum pressure rating for fire sprinklers is 7 psi, and most fire sprinkler heads are rated to a maximum about 150-175 psi. Fire sprinklers will be chosen for the model as they are ubiquitous not only to every plant, but most plant rooms as well. One aspect of fire sprinkler lines not to be examined is the impurities present in fire lines over time. Impurities in water and degradation of the piping is one-way fire sprinkler lines can leak, as water sits in the piping for long periods of time and rusts away the pipe. The water becomes filled with particulate, which may affect the way water leaks. It would be difficult to recreate this in the available lab space, although it is worth acknowledging, the water in the lab contains a noticeable amount of sawdust, dust, dirt, and other contaminates, due to the open tank. Some of this may be pumped into the test piping, but it would be difficult to quantify how much and what affect it would have.

NFPA specifies the types of piping which may be used in fire sprinkler lines as well. Usable piping types include ferrous piping (welded and seamless), copper tube, CPVC, brass pipe, and stainless-steel pipe [7]. Fittings can be cast iron, malleable iron and steel in addition to the types previously mentioned. The type of pipe chosen for these experiments is schedule 40 galvanized steel. Galvanized steel falls in the category of ferrous piping, and is like the black steel piping often used for fire sprinkler. Steel was chosen over other materials, as it seems to be the most common material used for sprinkler piping.

INL Spray Simulation Work

The Idaho National Laboratory (INL) published a paper in September 2016 [8] concerning the modeling of seismic events in NPPs with advanced probabilistic risk assessment tools. It uses many codes and programs such as EMRALD, SAPHIRE, Mastodon, and Neutrino. The paper first discusses the development of the tools, and then goes on to describe a demonstration of how this can be applied.

Part of the demonstration is a seismic-flooding-thermalhydraulic dynamic probabilistic risk assessment demonstration. In which, a three-dimensional spacial model of a fire suppression system is created. The building in the fire suppression system seems to be an external switching room at a NPP. The fire suppression system consists of 6-inch stand pipes, 4-inch main lines, and branch lines with pipe diameters of 1.5-inches and 1.25-inches. The piping was then simulated with earthquakes, with peak ground accelerations (PGAs) from 0.3g to 1.5g at intervals of 0.1g.

Figure 1 shows the results of the simulations, given an x-directional PGA input of 1.5g from the earthquake. Figure 1 represents the plan view of a switch room at an NPP. The black lines represent the piping in the room. It is not certain what the scale of the room is from the report, but it is intended to represent a generic switch building, so it is likely large.

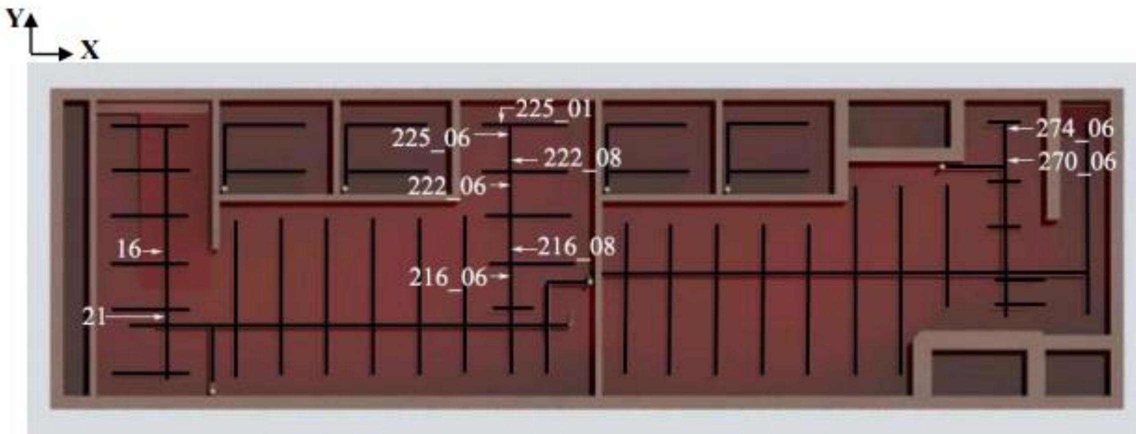

Figure 1. Leakage locations on piping system - X direction input. [8]

Seismic fragility curves were then developed from these simulations. Figure 2 shows an example for one of these charts for the first leak probability. These curves correlate to the positions in the piping of Figure 1.

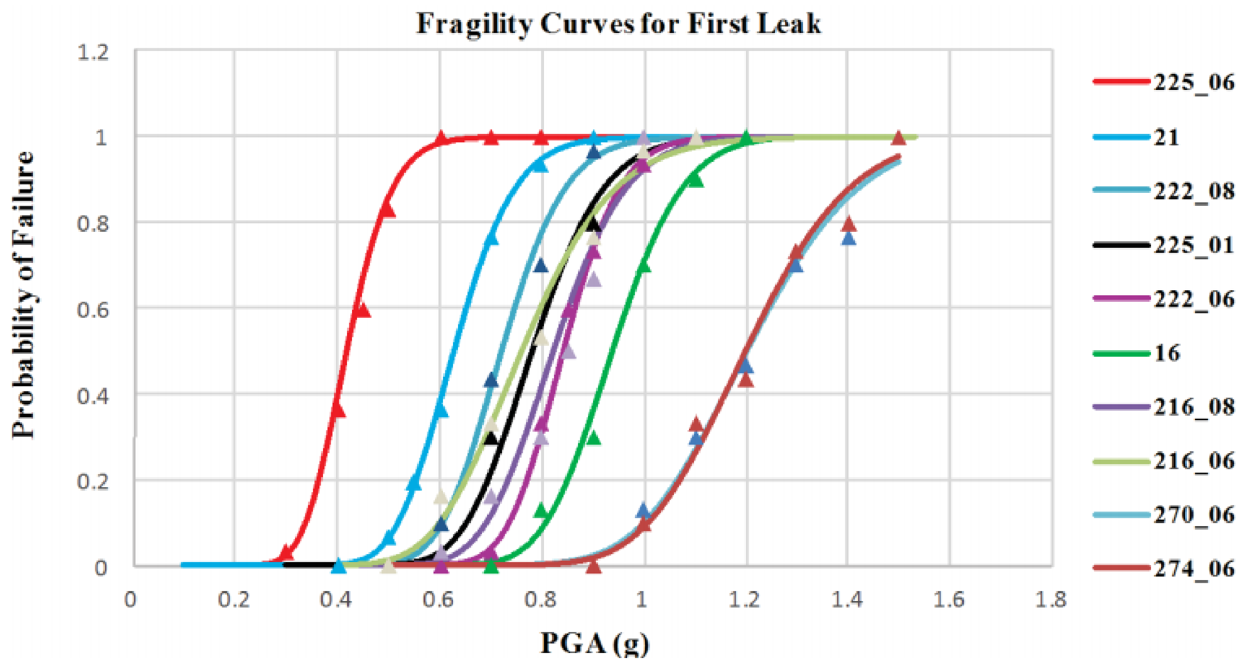

Figure 2. Fragility curves for first leak. [8]

The demonstration then uses EMRALD, a dynamic Probabilistic Risk Assessment (PRA) code, to simulate damage cases to the piping based on a random seismic input. Using the results from the EMRALD model, the demonstration then goes on to set parameters in Neutrino, a Smoothed Particle Hydrodynamics (SPH) program, such as the flowrate and the break size. Three break sizes are used, a small break (0.001 cm), a medium break (0.003 cm) and a large break (0.005 cm). Along with these parameters, desired event data is also loaded. These can be sent back to EMRALD as the simulation runs. Inside a simulation, Neutrino monitors the interaction with the components' measurement fields. The components have failure criteria under spray and rising water. If any failure criteria are met, a failure message is sent back to EMRALD to be processed. Figure 3 shows the example from the report of the switch room being modeled inside of Neutrino.

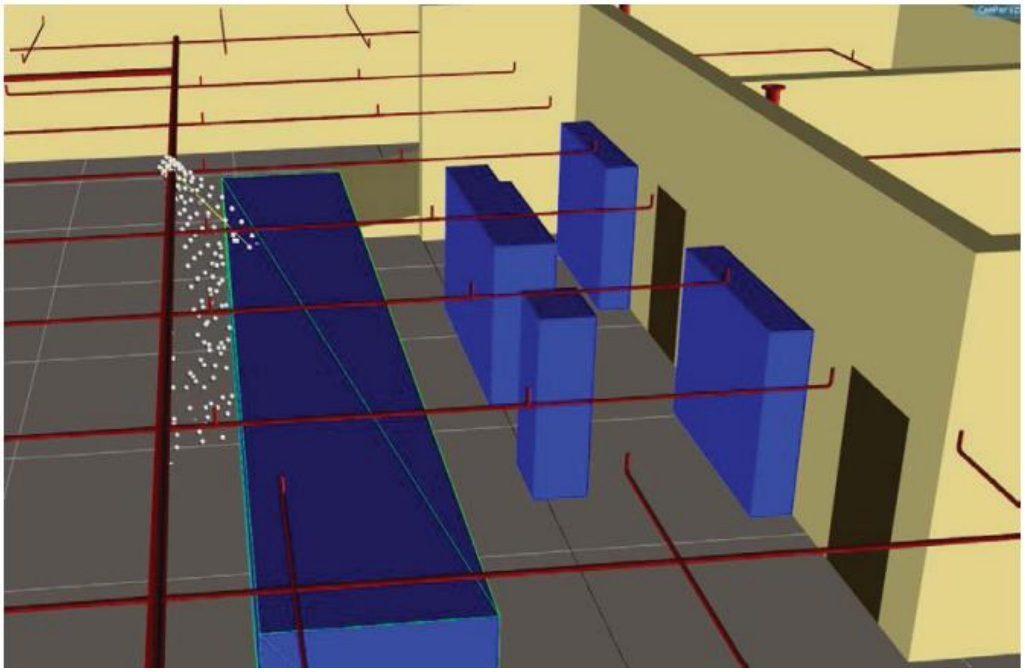

Figure 3. Example of a pipe fracture using Neutrino. [8]

The part of highest interest to this research is what they include as the needed enhancements for this demonstration. Most significant for the real pipe leak experiments is the mention of a lack of spray patterns for areas affected. The need for spray patterns data may be an issue of how the simulation is modeling spray, as the simulation only emits particles in the given direction. Figure 4 shows the figure they included in the report with their drawn in example of the types of spray patterns they desire. Implementing these desired spray patterns is possibly difficult, and impossible to do accurately as the data does not exist. These real pipe spray experiments will endeavor to inform these kinds of simulations in how sprays behave, from the flowrates to the pattern and area affected.

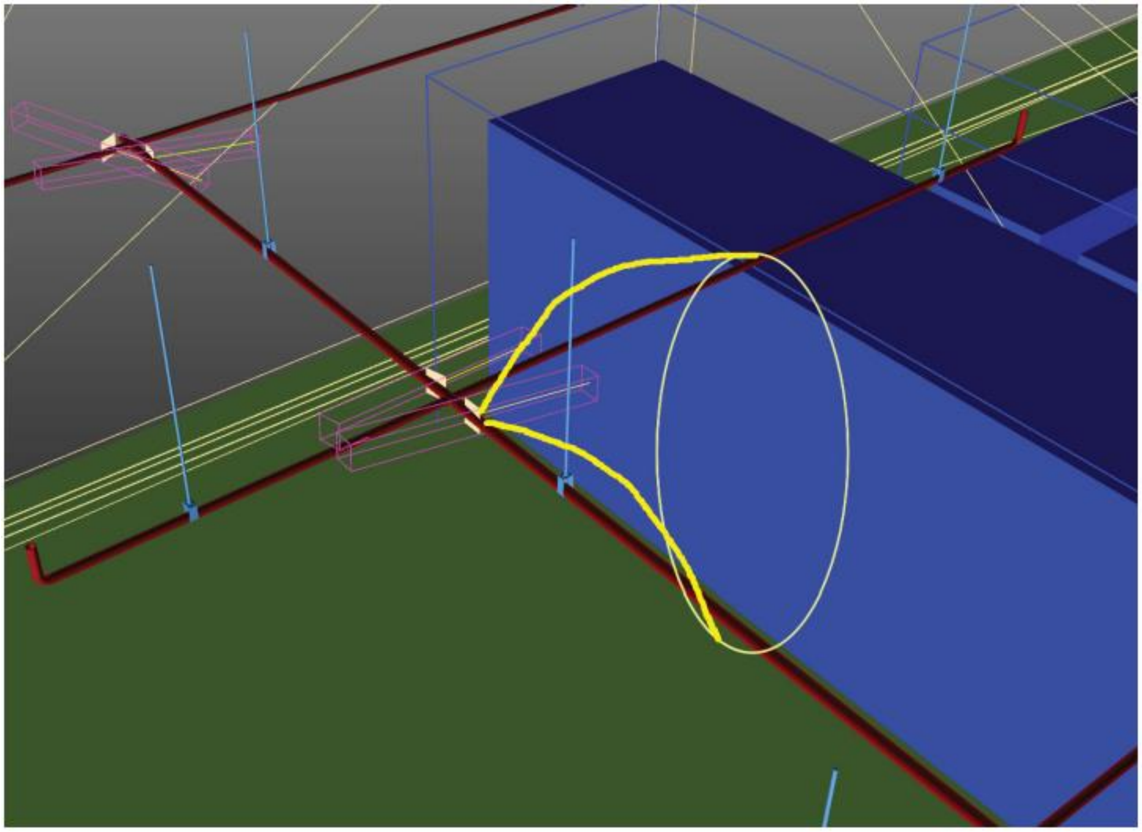

Figure 4. Needed emitter with spray pattern capability. [8]

Literature Review Summary

The literature review has been useful in identifying what work has been done previously in pipe leaks, and guiding the development of pipe leak experiments. Most of the research into pipe leaks has been done to examine the risks of causing a damaging LOCA. The focus on LOCAs makes sense as it is the event with the most risk for nuclear power plants. However, since LOCAs are well understood, there is now interest in what happens when there are water impacting components. The research from this experiment will likely be of interest to the INL in their efforts in modeling power plant floods with codes like Neutrino and EMRALD.

The research presented in this literature review drove the piping design of this experiment. The piping was modeled to simulate fire sprinkler piping as standardized by NFPA. The design parameters include the pressures used, and the types of piping material used in fire sprinkler lines.

These pipes were the small bore, denoted as the most likely to fail from the SKI report. Rather than looking at big ruptures, small leaks were the subject of interest instead. The failures were not able to represent the most likely types of failure (FV and E/C) due to the difficulty of recreating them in the lab.

Experiment Design

The goal of the experiment design was to create a piping setup allowing fast and easy adjustments in the diameter of the failed pipes examined, as well as the failed pipes themselves. The design also needed to be noninvasive to allow for other experiments to take place in the PET. A pump was present in the Water Resource Laboratory from a previous experiment for rising water door failure tests. The pump present in the lab was a 3-inch high volume dewatering sump pump from Global Pump. The pump curve and specifications for this can be found in Appendix B. The PET was originally designed to accommodate this pump and the 3-inch piping associated with it. The literature review found most pipe leaks were in pipes less than or equal to 1-inch, with the next most likely being in pipes between 1 and 4-inches in diameter. Based on this, three pipe diameters were chosen for these tests: 1-inch, 2-inch, and 3-inch sections.

Theoretical Operating Point

It is useful to know what kinds of flows would be expected from these experiments, so an examination of the piping system was performed for each test section individually to determine the operating point for each line. These calculations were made with a few assumptions. First it was assumed any tee joints the water flowed through with one direction ending in a closed valve were modeled as regular elbows. Next, for reducing tees, with flow only going one direction, the same assumption as before was made, but also including a sudden reduction in the line. The next assumption is for the starting point and the end. It is assumed the starting point is at the surface of the water in the tank, and the outlet back into the tank is the exit. The difference in height between the outlet and the surface of the water was measured to be 14.5 inches at the time of the experiments.

To calculate the head losses, the one-dimension energy equation was used, as seen in Equation 1.

$$\frac{P_1}{\rho g}+\frac{V_1^2}{2g}+z_1+h_p=\frac{P_2}{\rho g}+\frac{V_2^2}{2g}+z_2+\sum\left(\frac{fL}{D}\frac{v^2}{2g}\right)+\sum\left(k\frac{v^2}{2g}\right)$$

Equation 1. One-dimension energy equation for fluid flow

The P terms refer to the pressure at points in the system, the V terms the velocity, and the z terms to the elevation. The subscripts 1 and 2 refer to the two points of interest to the analysis. h_p is the head provided by the pump, ρ is the density of the water, and g is the acceleration due to gravity. The summation terms on the left represent the losses in the system due to the piping itself. These are the specific terms to be used to find the operation point of the pump. Each term is a summation as they change with different diameters and piping materials, as will be seen with this experiment. The first term is the major loss term and represents the friction losses in the piping system. f is the friction coefficient in the pipes, L is the total length for each piping section, D is the inside diameter of the section, and v the velocity for each unique section. The second loss term is the minor loss term, which represents the losses due to components in the system such as valves bends and tees, where k is the minor loss coefficient. The values of the minor loss coefficient have been measured and recorded previously, and can be referenced. One such reference, the Crane Flow of Fluids Through Valves, Fitting and Pipe [9], will be used here.

The friction factor in the major losses also needs to be known, and will be calculated with the Haaland equation, which is Equation 2.

$$\frac{1}{\sqrt{f}}\approx -1.8\,log_{10}\left(\frac{6.9}{Re}+\left(\frac{\varepsilon}{3.7D}\right)^{1.11}\right)$$

Equation 2. Haaland equation for the pipe friction factor

Where Re is the Reynolds number, ε is the absolute pipe roughness, and D is the pipe diameter. The Reynolds number can be calculated with Equation 3.

$$Re = \frac{\rho v D}{\mu}$$

Equation 3. Reynolds number equation

Again, D is the pipe diameter, v the velocity, ρ the density, and μ is the dynamic viscosity of the fluid.

Simplifying these equations gives Equation 4, which is used to find the system curves and the operating points for each line. It is assumed the first point used is at the surface of the water in the floor tank, and the second point is at the outlet of the piping back into the tank. These two points mean the P_1 and P_2 are equal, and V_1 is approximately zero. As there is a variety of different values occurring from the pump for h_p, the values on the right side of the equation must be calculated at several points to develop a curve. The system curves calculated can then be compared to the provided pump curve to find the operating point of the pump. The flow and head of each configuration can then be found.

$$h_p = \frac{V_2^2}{2g} + z_2 + \sum\left(\frac{fL}{D}\frac{v^2}{2g}\right) + \sum\left(k\frac{v^2}{2g}\right)$$

Equation 4: Simplified piping loss equation for pump operating point

The result of this can be seen in Figure 5. Three curves were developed, as there are three different operating conditions. The smaller the pipe diameter, the higher the head losses, and the lower the operating flow. The larger the pipe diameter, the lower the major head losses from friction, so a higher flow with a lower pressure is expected.

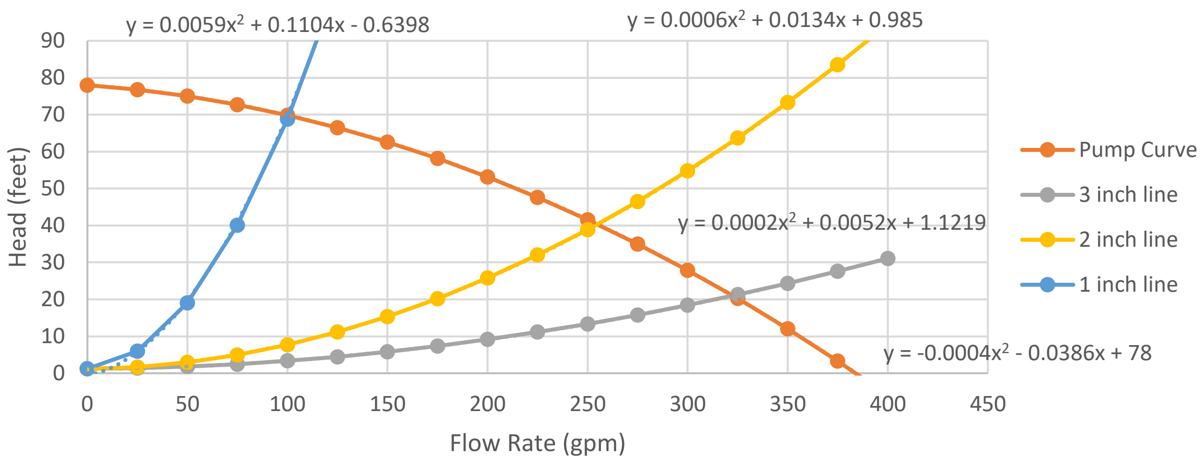

Figure 5. Pump curve operating point calculations.

Figure 5 gives the operating points of the system at the points where the loss curves cross the pump curve. These equations for the head loss curves and the pump curve can be seen in Equation 5. The system curves were then solved with the pump curve to determine the three operating points, as can be seen in Table 4. Once the piping setup was complete however, the operating flows were revealed to be less than what was calculated, also shown on Table 4. The difference between the theoretical and actual flows means the pump is operating less efficiently than expected, or the losses were miscalculated and are higher than what was determined, or some combination of the two.

$$\boldsymbol{Pump\ Curve}: \quad \boldsymbol{y = -0.0004x^2 - 0.0386x + 78}$$
$$\boldsymbol{3 - inch}: \quad \boldsymbol{y = 0.0002x^2 + 0.0052x + 1.1219}$$
$$\boldsymbol{2 - inch}: \quad \boldsymbol{y = 0.0006x^2 + 0.0134x + 0.985}$$
$$\boldsymbol{1 - inch}: \quad \boldsymbol{y = 0.0059x^2 + 0.1104x - 0.6398}$$

Equation 5. Pump curve and system curve equations

Table 4. Theoretical and Actual Operating Points

	Theoretical Operating Flow (gpm)	Actual Operating Flow (gpm)
3-inch	323.31	236.94
2-inch	252.73	176.64
1-inch	100.52	69.08

It is assumed the reason for the computed losses being lower than the actual system was some minor loss coefficient, or could be modeled as such if it was not. Values for k to be added to each branch were guessed, and the operating point checked and compared to the actual values. The final values can be seen in

Table 5 and the results plotted in Figure 6. The equations used to compute the operating point are seen in Equation 6. It is unclear whether the pump is working less efficiently compared to the pump curve, or whether some losses were not considered well enough, but this was overcome with additional minor losses. It makes sense that the 3-inch needed the largest adjustment, and the 1-inch the smallest, because the 3-inch line had further to shift than the 1-inch or 2-inch. Also, the 1-inch branch has much larger losses from friction than the 3-inch due to the higher velocities.

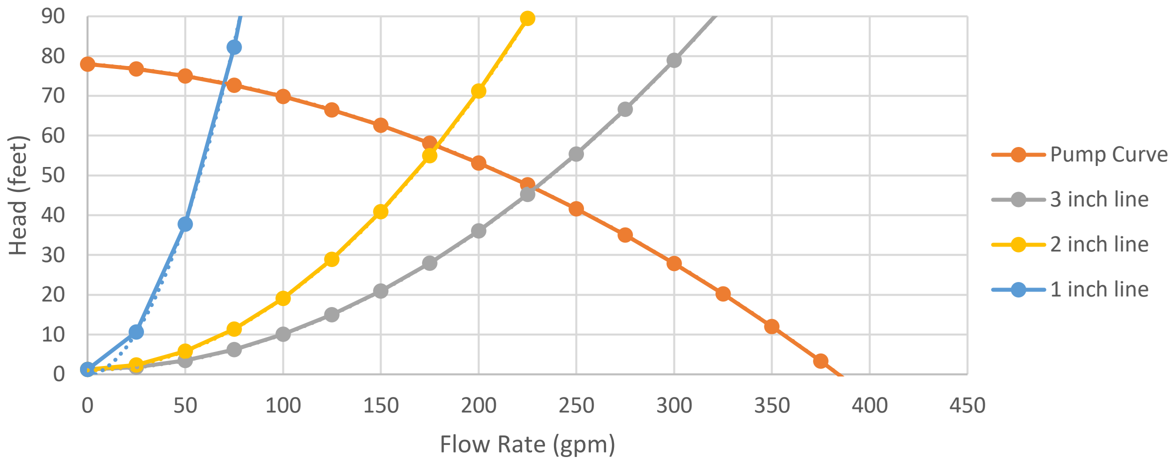

Figure 6. Pump curve operating point calculations, adjusted.

Table 5. Theoretical and Actual Operating Points, Adjusted

	Theoretical Operating Flow (gpm)	Actual Operating Flow (gpm)	Added Minor loss
3-inch	235.52	236.94	23
2-inch	179.52	176.64	8
1-inch	70.28	69.08	3.5

$$\boldsymbol{Pump\ Curve}: \quad \boldsymbol{y = -0.0004x^2 - 0.0386x + 78}$$
$$\boldsymbol{3 - inch}: \quad \boldsymbol{y = 0.0075x^2 + 0.4995x + 4.5893}$$
$$\boldsymbol{2 - inch}: \quad \boldsymbol{y = 0.0017x^2 + 0.0134x + 0.9850}$$
$$\boldsymbol{1 - inch}: \quad \boldsymbol{y = 0.0134x^2 + 0.1104x - 0.6398}$$

Equation 6. Pump curve and system curve equations, adjusted

Piping Setup

Figure 7 shows the completed test section inside the PET tank. Three test sections, of three different pipe diameters (1-inch, 2-inch, and 3-inch), are built in and are intended to run independently. Each test section has a u-bend of galvanized steel piping. These sections will be where failure will be induced. The galvanized pipe is where the failure will be produced, because of its similarity to fire sprinkler piping. Fire sprinkler piping is generally black steel piping as it is more fire resistant, and lines are allowed range in size from schedule 10 to schedule 40 [7]. Galvanized pipe was chosen over black steel as the parts in the size required were more readily available. Failure will be induced with milling equipment to ensure a slot of consistent and known size can be created. The u-bend setup allows for several positions of cracks in piping to be tested, as failure can be tested in horizontal and vertical sections of piping, as well in elbows. On each piece of piping, different orientations of cracks can be tested as well - for instance, on pipe runs, two simple slots can be created, circumferentially or longitudinally. For simplicity in the rest of this thesis, parts of the piping will be referred to as either upstream or downstream of the test sections. Lastly, the 12-inch stand pipe behind the test section is not a part of these experiments, and was installed at the time of the photo of Figure 7. A wall was later installed in the PET for the water rise door tests, and the stand pipe would be removed for the pipe leak experiments.

Figure 7. Inside PET test section setup.

In addition to the u-bend section of galvanized steel, each test section included two valves on each side to isolate each test section when they are not being tested. Inside of the valves are two tees reducing to ¼ inch to allow for the installation of pressure gauges. The idea being if the pressure on each side of the piping can be known, with and without any failures, then the pressure loss through the crack will be known as well. The location of one of these gauges can be seen in the middle test section in Figure 7 to the right of the steel pipe. The 1-inch (middle section) and the 2-inch (top section) piping also include compression couplers in their design. The couplers allow easy removal and replacement of test section components once experiments begin. The couplers for the 3-inch line, and one on the 2-inch section caused the piping to be too long for the tank, and had to be left out, though they were used in other piping. Figure 8 shows this, as this is the piping for the upstream side of the tank. In it, the pipe rupture piping can be seen working around the 12-inch PET piping. All the piping used in this project was designed and built to be easily removable to not interfere with the door testing experiments. Figure 9 shows the downstream piping after the tank as well. In both figures, flow meters can be seen on either side of the tank. The two flow meters allow for flow to be measured through the and cracks in the piping, as the difference between upstream and downstream flowmeters will be the flow through the crack. In the downstream side of the tank, at the outlet, there is another u-bend. The ending u-bend is to create a low point for the downstream flow meter. Flow meters are required to be at low points in the systems so they will be completely full to operate properly. The flow meters also require a certain amount of straight piping upstream and downstream of themselves to operate properly, 30 inches upstream and 6 inches downstream for these. The piping design met these requirements.

Figure 8. Piping upstream of tank.

Figure 9. Piping downstream of tank.

Lastly, Figure 10 shows a P&ID diagram for the setup. The different pipe sizes used are denoted by the different line thicknesses, and the steel test section has been denoted with red lines. Figure 10 makes it appears there are six pressure gauges, two for each leg, however this is just to demonstrate the places in the diagram where the flowmeters are used in each line. The valves are numbered as they will be referred to in following sections. Each line has four different valves associated with it. Valves 1 and 4 are the 3-inch brass valves on the outside of the PET, and are the same for all test setups. Valves 2 and 3 are line dependent, but refer to valves in the same position relative to each line's test section. Valves will be referred to with these numbers from here, or as upstream/downstream and PVC/brass.

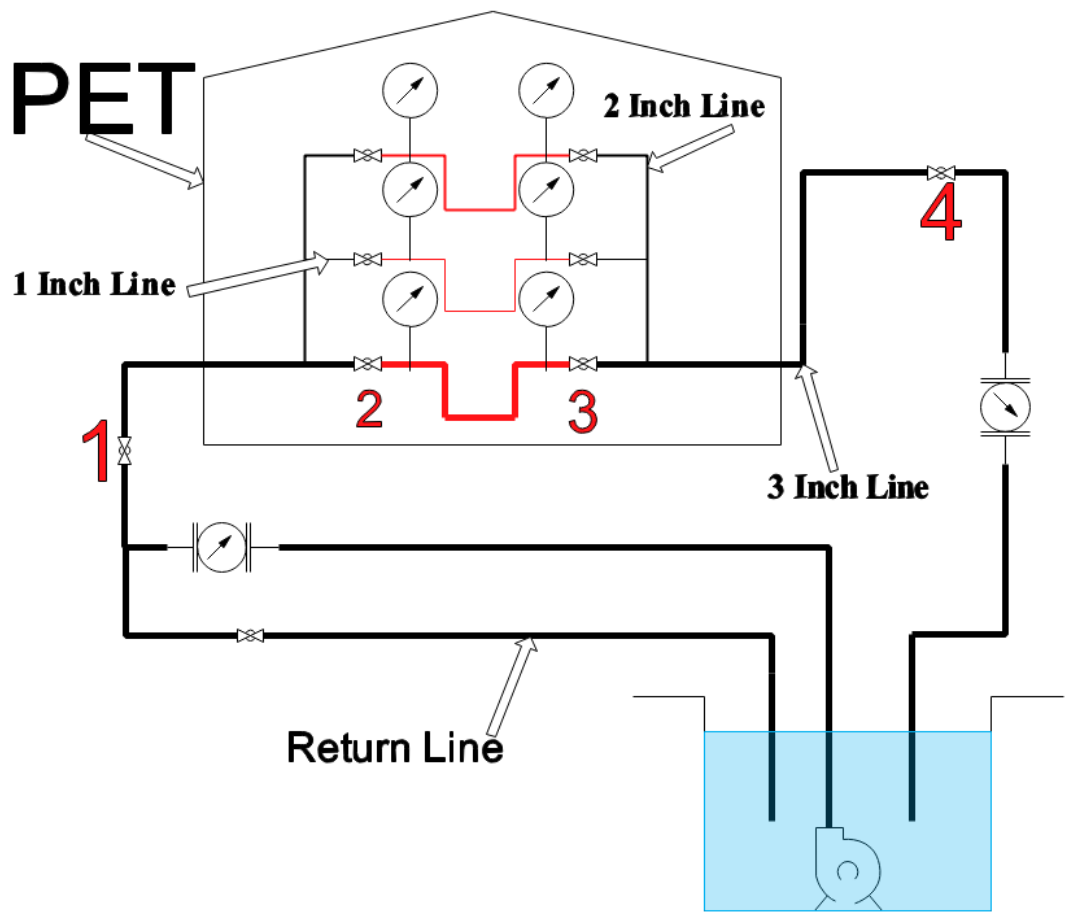

Figure 10. P&ID diagram of pipe leak setup.

The experimental procedure is simple. After installing the failed pipes for all three diameters, set all the valves to full open for one line. Close the two PVC valves on each of the other lines to isolate them. Set up a camera to record the leak. Turn the pump on and record the flow data, the pressure data, and the videos, as well as taking any necessary pictures. After recording for four minutes, partially close valve 1, then record for four more minutes. Continue downstream through the valves, partially closing them, then recording for four minutes. After all, four valves are partially closed and recorded, open valves 1, 2, and 3, then working from downstream to upstream repeat the recordings, closing valve 3 then 2. Valve 1 was not partially closed from downstream to upstream because it would be repeating data already collected upstream to downstream.

Several issues were noted in the experimental setup. The first is the size and capacity of the pump. The pump only produces 80 feet (34.65 psi) of head at maximum, and fire sprinkler systems can operate up to pressures of 175 psi. As mentioned earlier, the minimum pressure at a sprinkler head is 7 psi, so the experiments presented here are likely to represent the ends of branches near where the fire sprinkler heads are located. The location assumption is advantageous due to the maximum limits of the pressure gauges. A gauge, previously purchased for the same rising water experiment as the pump, was used with an identical one being purchased. These pressure gauges have a maximum pressure of 30 psi which is close to the maximum the pump can deliver. The 30-psi limit is likely the reason why the gauge was purchased originally, but this means gauges with a larger limit would need to be purchased to accommodate a larger capacity pump.

Failed Pipes

Three leak types were tested in this experiment. All the cracks were milled by Gem State Machining using a thin blade in a milling machine. The first failure type tested is a longitudinal crack. The tested section is the middle, galvanized nipple seen in Figure 7 for each diameter. The crack was made to be 2 inches externally. As the disk used to cut it was circular, the inner hole is not the same 2 inches and is slightly smaller. The size of the hole was measured with calipers, and can be seen in Table 6. Pictures of the three nipples can be seen in Figure 11.

Table 6. Longitudinal Slit Measurements

	3-inch	**2-inch**	**1-inch**
Length (inches)	1.970	1.978	1.990
Width (inches)	0.039	0.049	0.042
Area (in^2)	0.077	0.097	0.084

Figure 11. Longitudinally slotted galvanized nipples; top to bottom: 3-inch, 2-inch, 1-inch.

The next crack type is a circumferential crack on the same straight nipple section (referred as circumferential from here on), on new pipe. As the pipes have different diameters, the cracks were milled to be about a 90° arc. It was wished to have the cracks in the middle like the longitudinal cracks, for consistencies sake, but it ended up not being feasible for the machinist to mill it in the middle. The cracks ended up being about 3 inches from one of the ends. Table 7 shows the arc length for each crack, the width of the crack, and the depth. Figure 12 shows the three nipples side by side.

Table 7. Circumferential Slit Measurements

	3-inch	**2-inch**	**1-inch**
Length (inches)	2.707	1.835	1.057
Width (inches)	0.039	0.043	0.037
Length from End	3.014	2.939	3.021
Area (in^2)	0.083	0.062	0.031

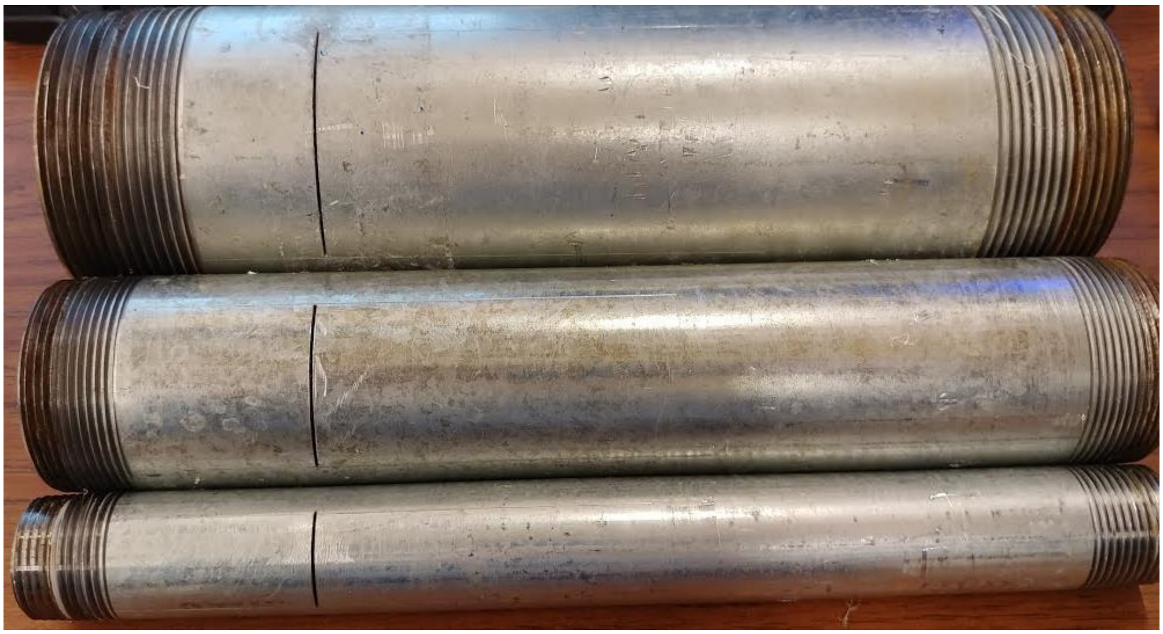

Figure 12. Circumferential slotted galvanized nipples; top to bottom: 3-inch, 2-inch, 1-inch.

The last type of crack tested was on the outside of a threaded elbow. The elbow position of the elbows can be seen in Figure 13. The elbow position was chosen as it allowed the water to have a straight run before the leak, as well as being positioned vertically without otherwise changing the piping. Other positions would have required repositioning of the test section to have the slit vertical. The same idea was taken for the elbows as was the circumferential cut pipes, the elbows were cut circumferentially to a 90° arc, centered on the back of the elbow. A picture of the three elbows can be seen in Figure 13 and Table 8 shows the size of the cracks and the arc length of the cracks.

Table 8. Elbow Slit Measurements

	3-inch	2-inch	1-inch
Length (inches)	3.131	2.162	1.356
Width (inches)	0.045	0.041	0.038
Area (in^2)	0.111	0.070	0.040

Figure 13. Galvanized slotted elbows; left to right: 1-inch, 2-inch, 3-inch.

Instrument Consistency and Flow Meter Corrections

Flow Calibration

One of the issues present in this experiment was the lack of calibration between the two flowmeters used. To solve this issue the data collected from the flow meters were adjusted. It is not clear as to which meter is not calibrated correctly, so the flow was assumed to be the average of the two meters. The flows from the leak tests were then adjusted based on the upstream flow by parameters determined from a system with no leaks

The setup seen in Figure 7 was used without employing any of the failed parts. Water was run through the system and the pressure and flow was recorded for four minutes. The four-minute time gave enough results even with the lowering of recording points from the HART system. One of the valves in the system was then adjusted to be about half open, then the test was repeated. The described procedure was repeated for each of the three lines, giving several points of flow data. These data were then plotted against each other, as seen in Figure 14, with the x-axis being the upstream flow rate, and the downstream the y-axis. Figure 14 also shows a graph of the line y=x. Ideally, the flow rate data would match to this line, but it does not. At the lower flowrates, the downstream data is higher than the upstream data, but the opposite is true at higher flows. However, the data at the higher flow appears to be very well behaved.

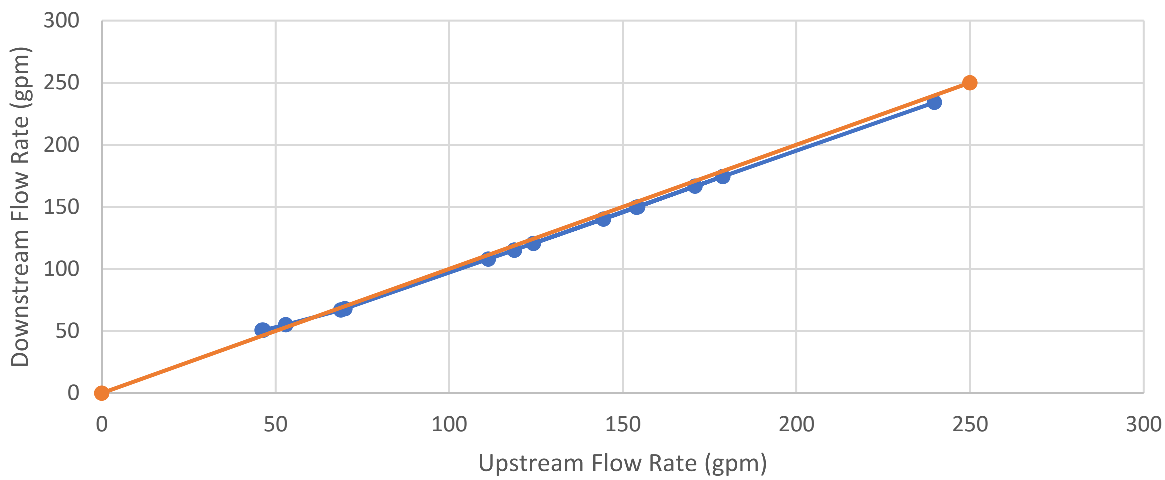

Figure 14. System calibration test data.

Some correction factors were needed to be able to determine the leak flowrate with the failed pipes. The data from Figure 14 was used to determine the percentage difference between the two flow meters. The percentage differences were then plotted and can be seen in Figure 15. Figure 15 shows at about 70 gpm the percent difference starts to behave more consistently, only being off by about 3%. At higher flows, this difference dropped again to 2.5%. The problem then comes with flows less than 70 gpm, when the downstream meter reads higher than the upstream. The flow meters are not very well behaved in those regions, however negative correction factors were still used. Table 1 shows the flow ranges from the upstream meter correlated with a correction factor for the downstream flow meter. Four regions were chosen, as can be seen in the table, two for the negative, not well-behaved sections, and two for the well-behaved sections.

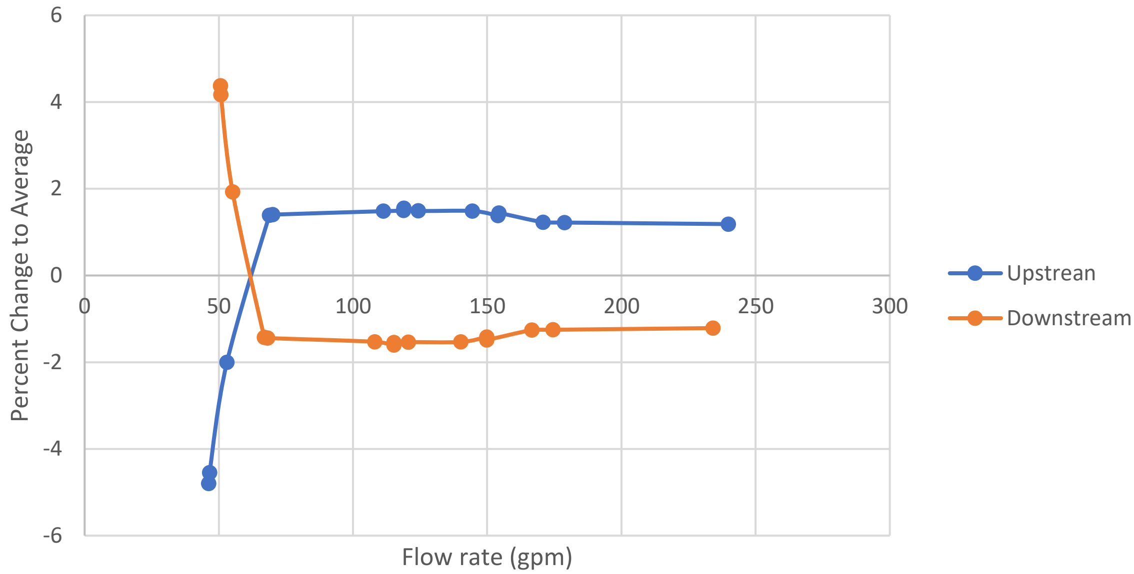

Figure 15. Upstream to downstream flow meter percent differences.

$$Q_{fixed} = Q_i * (1 - k/100)$$

Equation 7. Flow rate correction equation

Table 9. Upstream Flow Meter Correction Factors

Upstream Flow Range (gpm)	Upstream Correction Term k (%)	Downstream Correction Term k (%)
<50	-4.67	4.27
50 to 60	-2.01	1.93
60 to 165	1.46	-1.50
>165	1.21	-1.24

Instrumental Consistency

Four instruments were used for this experiment, two flow meters, and two pressure gauges. It is necessary to examine the consistency in these devices. The experiment ran the tests at steady state for four minutes per valve configuration, recording data on each device. For this analysis, a run from the circumferentially cut pipes was used. The run had three valves closed, valves 1,2, and 3. The consistency check is to examine whether any of the instruments had any trends over time that should not appear in a steady state experiment. Table 10 shows the overall averages for each instrument during the circumferential test. Table 10 also shows the amount of data collected from each instrument. The pressure gauges recorded consistently every second, and shows the test ran slightly longer than four minutes, as 240 data points would be expected. The flow meters recorded data about once every four seconds, however there was one minute during this test where only a few data points were recorded, 3 points with 20 seconds between for the upstream, and 2 points with 20 seconds between for the downstream. The inconsistencies in the flow meter data seems to be caused by the HART protocol they run on. The more meters on a multidrop connection, such as the setup here, the less consistent and the higher the time between recorded data. The problem with multidrop was suspected from observing the recorded data from the flow meters, and then confirmed by a document on the HART protocol from Siemens [10].

Table 10. Consistency Check Data

	Average (gpm)	Standard deviation (gpm)	Amount of Data Collected
Upstream Flow	137.67	0.65	52
Downstream Flow	129.57	0.46	51
Upstream Pressure	7.162	0.150	268
Downstream Pressure	6.707	0.045	267

The data from the flow meters does not have the correction factor described in the previous section, as this is just for examining the performance of the meter itself and whether there are any changes over time through a test. To accomplish this, four regions from each instrument during the test were analyzed. The flow meters were split into roughly four even sections of 13 data points, except for the last section of the downstream flowmeter, which had 12. The pressure gauges, which consistently recorded ever second, were analyzed by the first and last 30 seconds of the test, then the two 30 seconds periods about the middle of the test. The results of this can be seen in Figures Figure 16 toFigure 19. These figures show the average from the four analyzed sections compared to the average over the entire period of the test. The error bars represented here are the standard deviation for data each section.

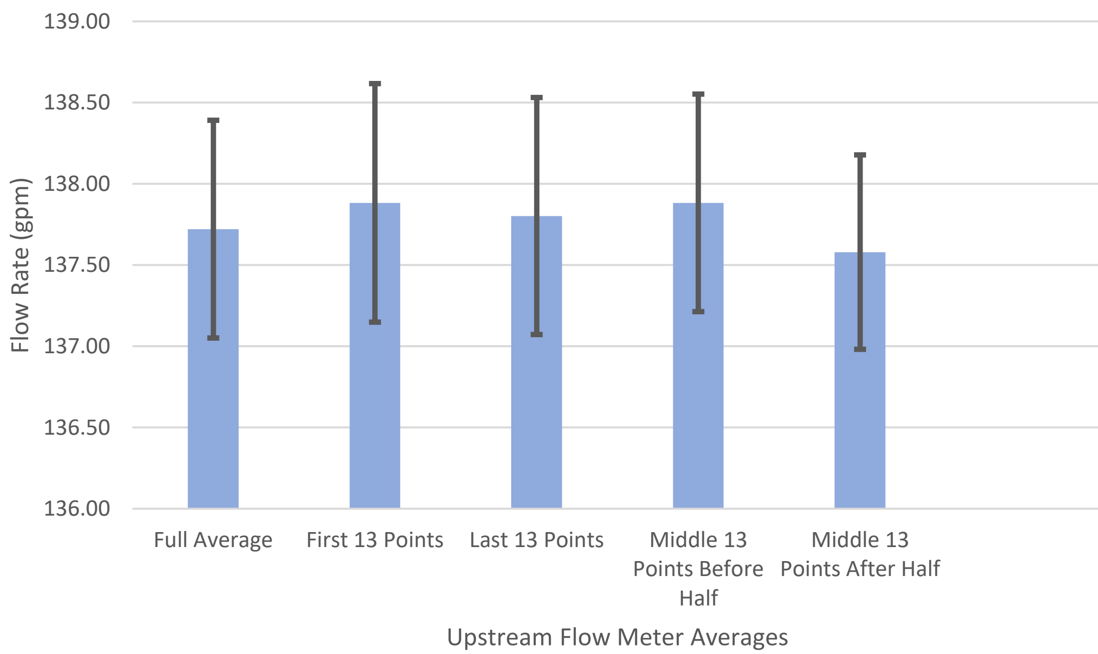

Figure 16. Upstream flow error analysis.

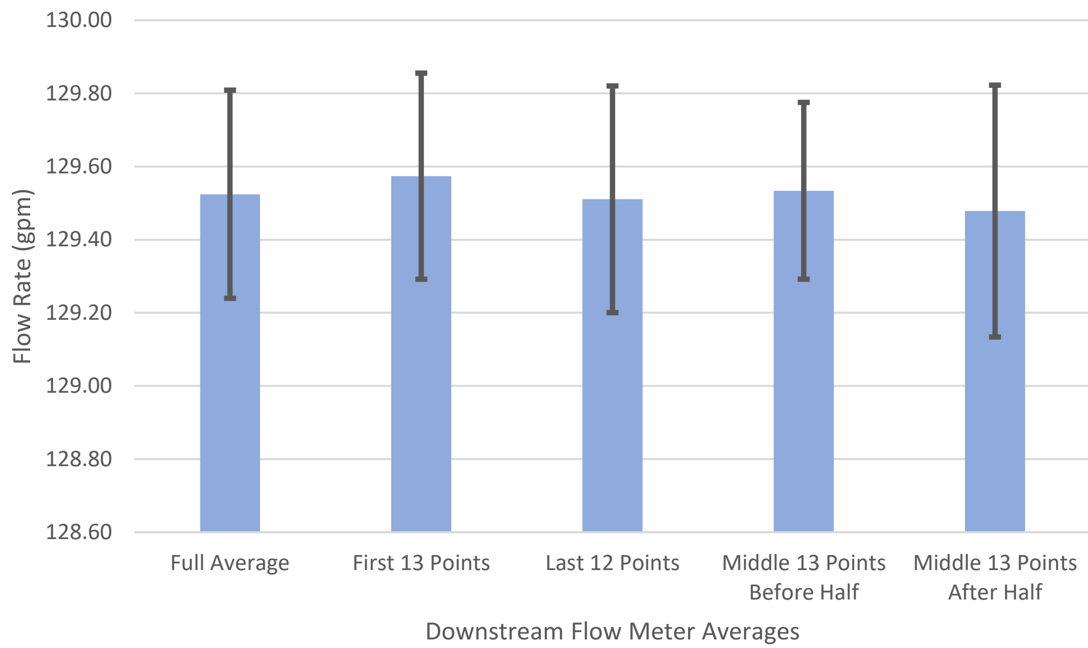

Figure 17. Downstream flow error analysis.

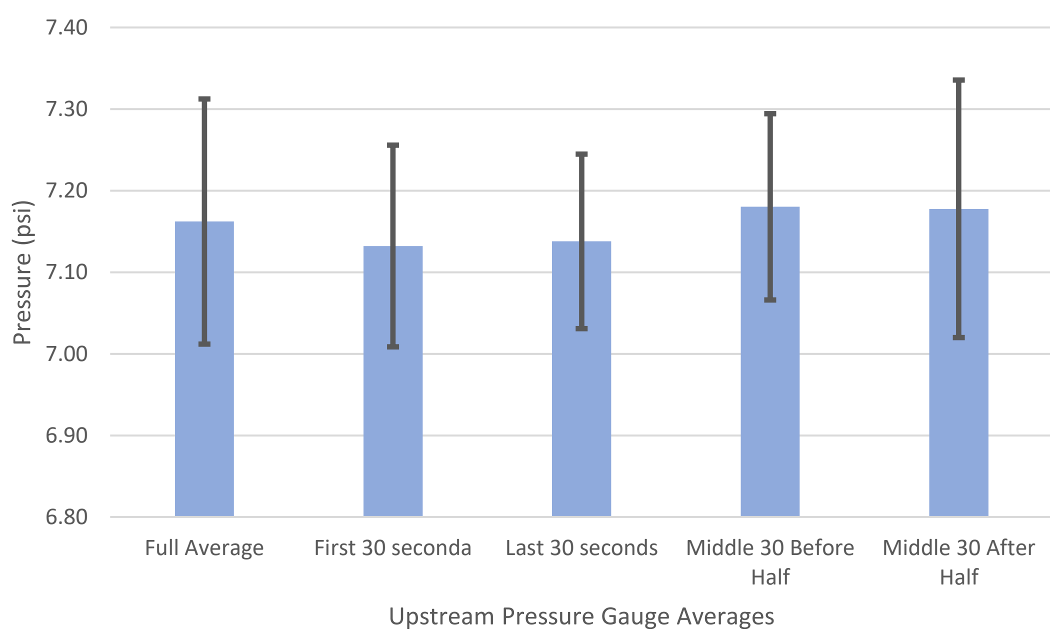

Figure 18. Upstream pressure error analysis.

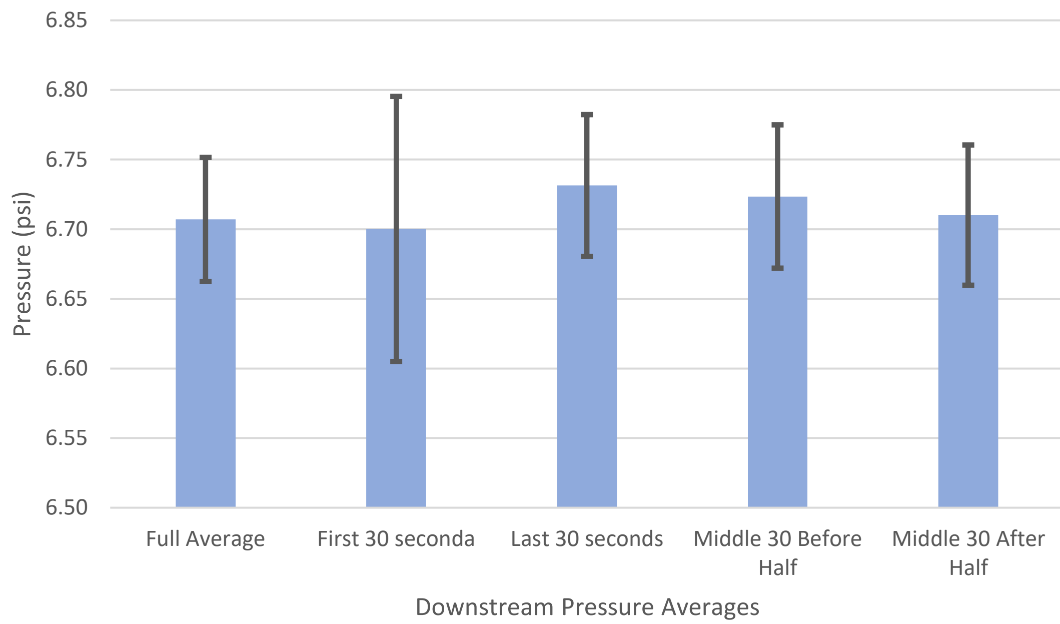

Figure 19. Downstream pressure analysis.

Figures Figure 16 to Figure 19 show there appears to be no trends in any of the instruments, up or down. Additionally, the average for each subsection analyzed falls within the error bars of the overall average and standard deviation calculation. It is reasonable to conclude then the error present in these instruments rises from random error only and not systematic error. There may be some systematic error, however, from the pump, and the variation in the instruments is likely in part due to the variation in the pump. As will be described in the next section, oscillations were observed in the leaks from the pipes. It is suspected the oscillations would not be seen if the city water source had been used instead of the pump, as any oscillatory effects from any city pumps would be attenuated out. Confirming whether the pump is causing these oscillatory effects would require further testing, which would be beyond the scope of this experiment. The error represented for the flow in the next section that will be the standard deviation as represented here.

Each of the data from these runs was then examined for the distribution of the data from the runs. The minimum and maximums were determined for each, then ten even bins were created, and the frequency of the results were plotted. Each of the frequency plots shows the data being distributed fairly consistently following a Gaussian distribution, however the flow meter data reflects the lack of data from these instruments, and are less consistent than the pressure gauges.

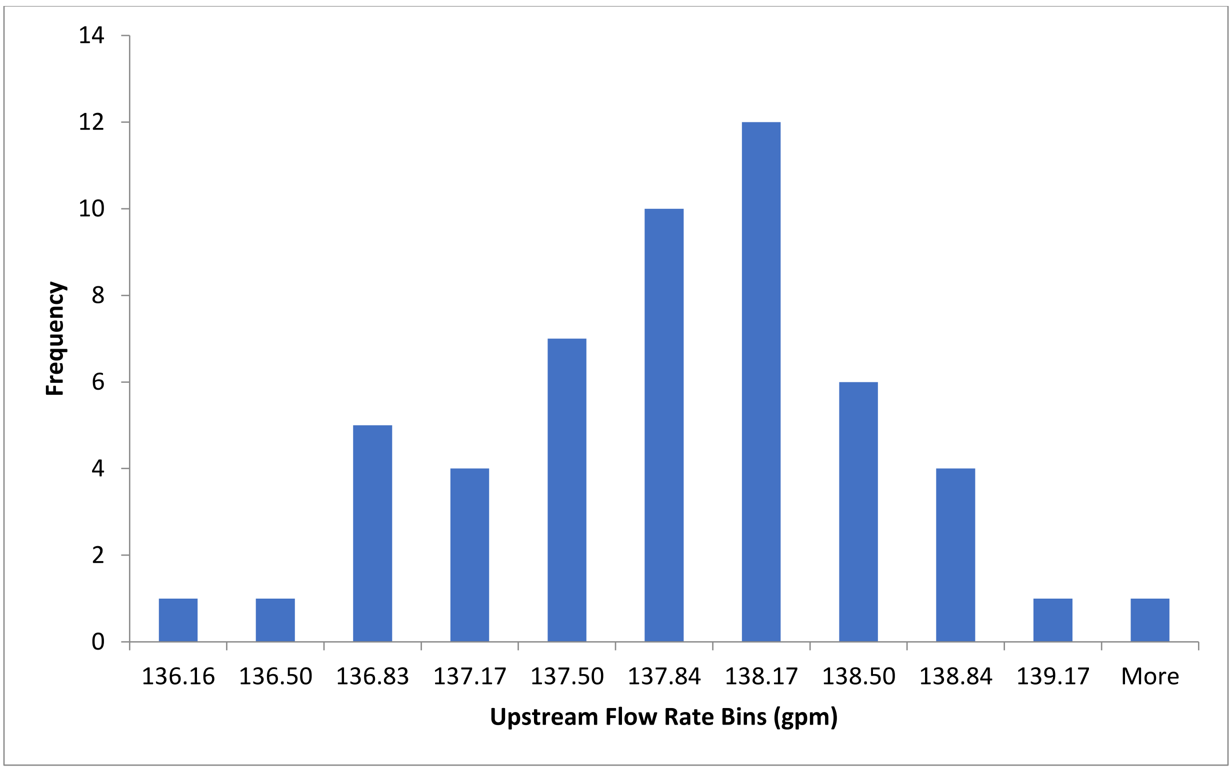

Figure 20. Upstream flow rate frequency analysis

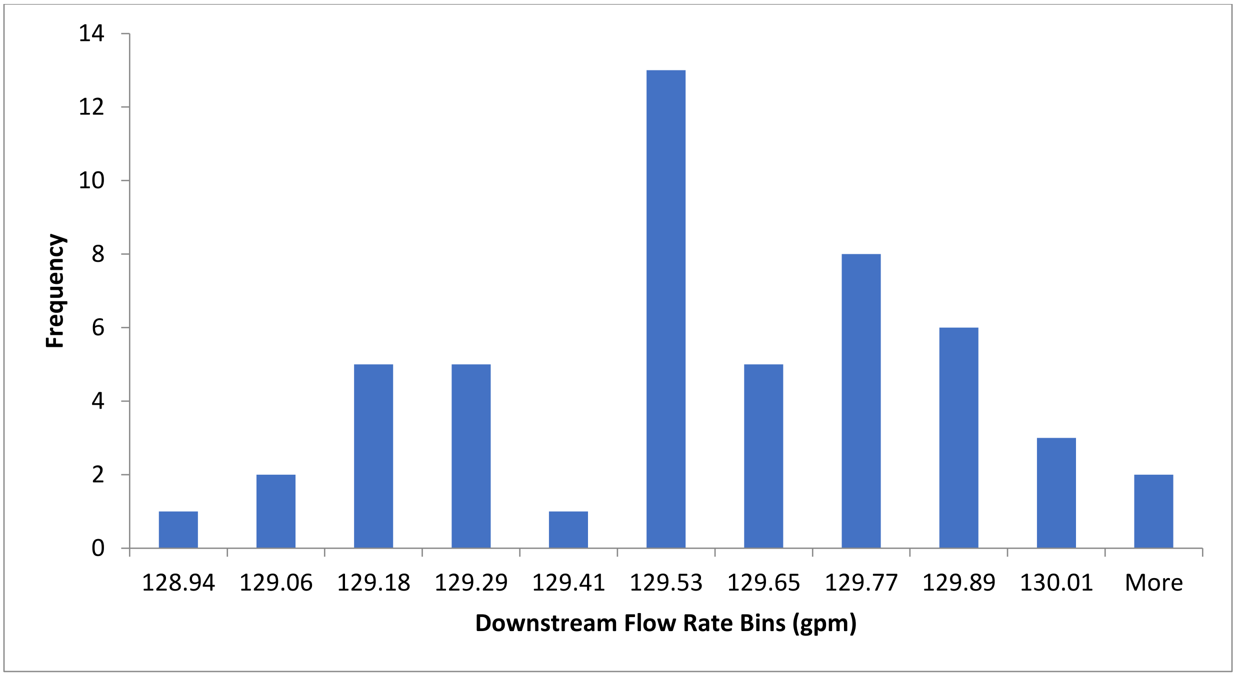

Figure 21. Downstream flowrate frequency analysis.

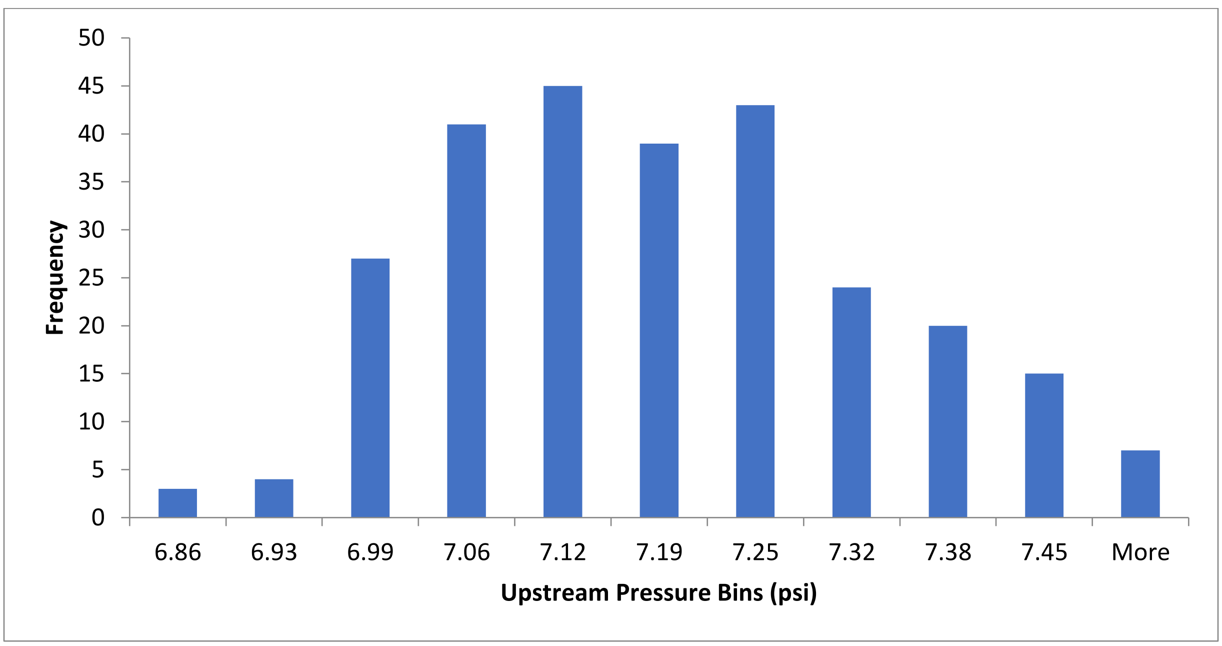

Figure 22. Upstream pressure frequency analysis.

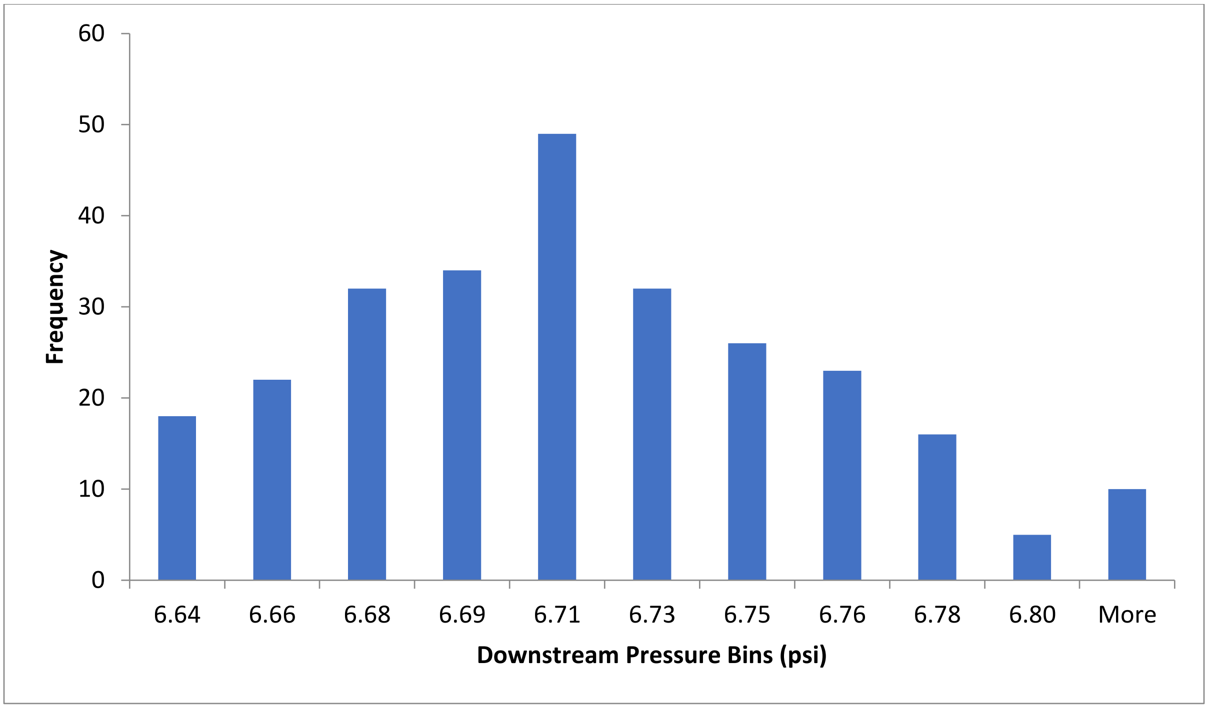

Figure 23. Downstream pressure frequency analysis.

Error Analysis

In addition to checking the consistency of the instruments to ensure none of them trended up or down over time, error analysis was performed for the data collected in these experiments. The error analysis performed was to propagate the inherent error in the data through to the calculations. All the error values reported in the experiment results section after the error analysis presented here will be the results of the error propagation.

The error propagation was done by addition in quadrature. The equation to calculate error on some value C, for example, where C is calculated with two independent variables A and B is given in Equation 8, where δA, δB, and δC are the errors associated with the values, where δA and δB are determined based on their associated measurements. $\frac{\partial C}{\partial A}$ and $\frac{\partial C}{\partial B}$ are the partial derivatives of the equation to calculate C with respect to A and B, respectively.

$$\boldsymbol{\delta C} = \sqrt{\left(\frac{\partial \boldsymbol{C}}{\partial \boldsymbol{A}}\boldsymbol{\delta A}\right)^2 + \left(\frac{\partial \boldsymbol{C}}{\partial \boldsymbol{B}}\boldsymbol{\delta B}\right)^2}$$

Equation 8. Method for error propagation in quadrature

Several equations were used for these experiments to determine desired values, the equations used will be presented here in full, but the error propagation equation for each will be excluded. An example will be presented instead, using the method to determine the velocity of the water through the cracks. The equation for the velocity through the split is simple, as seen in Equation 9, but both values are derived from other measured values. The flow through the split, $\boldsymbol{Q_{spit}}$, is determined by taking the difference between the corrected values of the flow meters as described previously. The area of the split $\boldsymbol{A_{slit}}$ was determined for each slit using a digital caliper. Equation 10 shows the simplified version of the error propagation method described with Equation 8, using Equation 9.

$$\boldsymbol{v_{split}} = \frac{\boldsymbol{Q_{slit}}}{\boldsymbol{A_{slit}}}$$

Equation 9. Velocity of water through a slit.

$$\boldsymbol{\delta v_{slit}} = \sqrt{\left(\frac{\boldsymbol{\delta Q_{slit}}}{\boldsymbol{A_{slit}}}\right)^2 + \left(-\frac{\boldsymbol{Q_{slit}}}{\boldsymbol{A_{slit}}^2}\boldsymbol{\delta A_{slit}}\right)^2}$$

Equation 10. Error for the velocity through a slit

The 3-inch longitudinal crack with no valves partially closed will be used as example. The slit flow rate, $\boldsymbol{Q_{slit}}$ was determined to be 4.81 ± 1.52 gpm. The area of the 3-inch longitudinal slit,

$\boldsymbol{A_{slit}}$, was determined to be 0.077 ±0.001 in^2. Plugging these values into Equation 10 (excluding necessary unit conversions) yields

$$\boldsymbol{\delta v_{slit}} = \sqrt{\left(\frac{\mathbf{1.52}\ \boldsymbol{gpm}}{\mathbf{0.077}\ \boldsymbol{in^2}}\right)^2 + \left(-\frac{\mathbf{4.81}\ \boldsymbol{gpm}}{(\mathbf{0.077}\boldsymbol{in^2})^2} * \mathbf{0.001}\ \boldsymbol{in^2}\right)^2}$$

Equation 11. Calculating the error of the velocity through the slit.

After converting gallons to cubic inches and minutes to seconds, the final calculated values for the velocity through the slit is 240.49 ± 21.27 in/s.

The rest of the equations used in the calculations in this project can be seen in Equation 12 through Equation 20, in no particular order. All calculated values have error associated with them. Values in the equation having associated error will be in bold. Non-bold errors are assumed to be well known and were not measured, such as the pipe diameters for schedule 40 piping.

$$\boldsymbol{Q_{ave}} = \frac{\boldsymbol{Q_{upstream}} + \boldsymbol{Q_{downstream}}}{\mathbf{2}}$$

Equation 12. Average flowrate between flow meters

$$\boldsymbol{Q_{fixed}} = \boldsymbol{Q_i} * \left(\mathbf{1} - \frac{\boldsymbol{k}}{\mathbf{100}}\right)$$

Equation 13. Flow rate correction equation

$$\boldsymbol{Q_{slit}} = \boldsymbol{Q_{upstream}} - \boldsymbol{Q_{downstream}}$$

Equation 14. Slit flow rate equation

$$\boldsymbol{v_{pipe}} = \frac{\boldsymbol{Q_i}}{\boldsymbol{A_i}}$$

Equation 15. Velocity of water in pipe i

$$Re = \frac{\rho * \boldsymbol{v} * d}{\mu}$$

Equation 16. Reynolds number equation

$$\frac{\mathbf{1}}{\sqrt{\boldsymbol{f}}} \approx -\mathbf{1.8}\ \boldsymbol{log_{10}}\left(\frac{\mathbf{6.9}}{\boldsymbol{Re}} + \left(\frac{\boldsymbol{\varepsilon}}{\mathbf{3.7}\boldsymbol{D}}\right)^{\mathbf{1.11}}\right)$$

Equation 17. Haaland equation for the pipe friction factor

$$\boldsymbol{P_{slit_{upstream/downstream}}} = \boldsymbol{P_{gauge}} + \boldsymbol{\rho}\left(\Delta\boldsymbol{z} \pm \left(\frac{\boldsymbol{f_1 L_1}}{\boldsymbol{D}} + \frac{\boldsymbol{f_2 L_1}}{\boldsymbol{D}}\right)\frac{\boldsymbol{v^2}}{\mathbf{2}\boldsymbol{g}} \pm \frac{\boldsymbol{kv^2}}{\mathbf{2}\boldsymbol{g}}\right)$$

Equation 18. Calculating the pressure at the slit on the upstream or downstream side

$$\boldsymbol{k_{no\ leak}} = \frac{\mathbf{2}\left(\boldsymbol{P_{upstream}} - \boldsymbol{P_{downstream}}\right)}{\boldsymbol{v^2\rho}} - \left(\frac{\boldsymbol{f_1 L}}{\boldsymbol{D}} + \frac{\boldsymbol{f_2 L}}{\boldsymbol{D}}\right)$$

Equation 19. Calculating total minor losses for the test section, simplification of Equation 1

$$\boldsymbol{k_{slit}} = \frac{\mathbf{2} * \Delta\boldsymbol{P}}{\boldsymbol{\rho v^2}}$$

Equation 20. Calculating minor loss through the slits

Experiment Results

There are several results of the leak tests this section will seek to present, some quantitative, some qualitative. The quantitative results are:

- Flowrate through the leak
- Velocity through the leak
- Pressure in the pipe at the leak
- Minor loss coefficient of the leak

The qualitative results are harder to define, but efforts are made to describe the spray and pattern in a categorical way. Each different crack style will be described and shown with typical traits of each crack. Different categories are presented with different examples from the three different crack styles. The demonstrations will mostly be done visually through videos and photos, and with some description. Each four-minute test had at least one picture and one video taken of the spray. These will be used as the evidence for these categories. As videos cannot be used here, stills will be presented as applicable.

Description of the Different Leaks

The contents of this section will explore the sprays from the three crack types: longitudinal, circumferential and elbows. General descriptions will be presented here from the three crack types, with the three different pipe sizes.

The first crack type examined was longitudinal. As discussed above, the cracks made in the pipes were approximately 2 inches long placed in the center of the pipes. Longitudinal cracks are the type of leak expected to be most like an E/C failure. Longitudinal cracks are the most directed type of the three sprays, coming out in a stream from the crack. There seems to be a velocity or pressure dependence on the angle of the stream as it exits the pipe, which will be explored further later. The angle of the spray always appears to be heading to the right in the figures presented here. The angle is most likely due to the momentum of the water, and in all of the picture in this thesis, the water is flowing from left to right. The spray often oscillates, which can be seen in Figure 24. Figure 24 (progressing left to right, top to bottom) shows the oscillation of a spray with no valves closed. The frames were taken over the course of 14 frames in the video recorded at 120 frames per second (fps). Calculating the period of oscillation for this configuration gives a period of about 0.12 seconds. The oscillations of the leaks may be caused by variances in the pump. There may be some natural frequency the pump operates on which gives rise to these oscillations. It is worth noting the oscillations, as simulated piping systems may be pump driven and may try to simulate them.

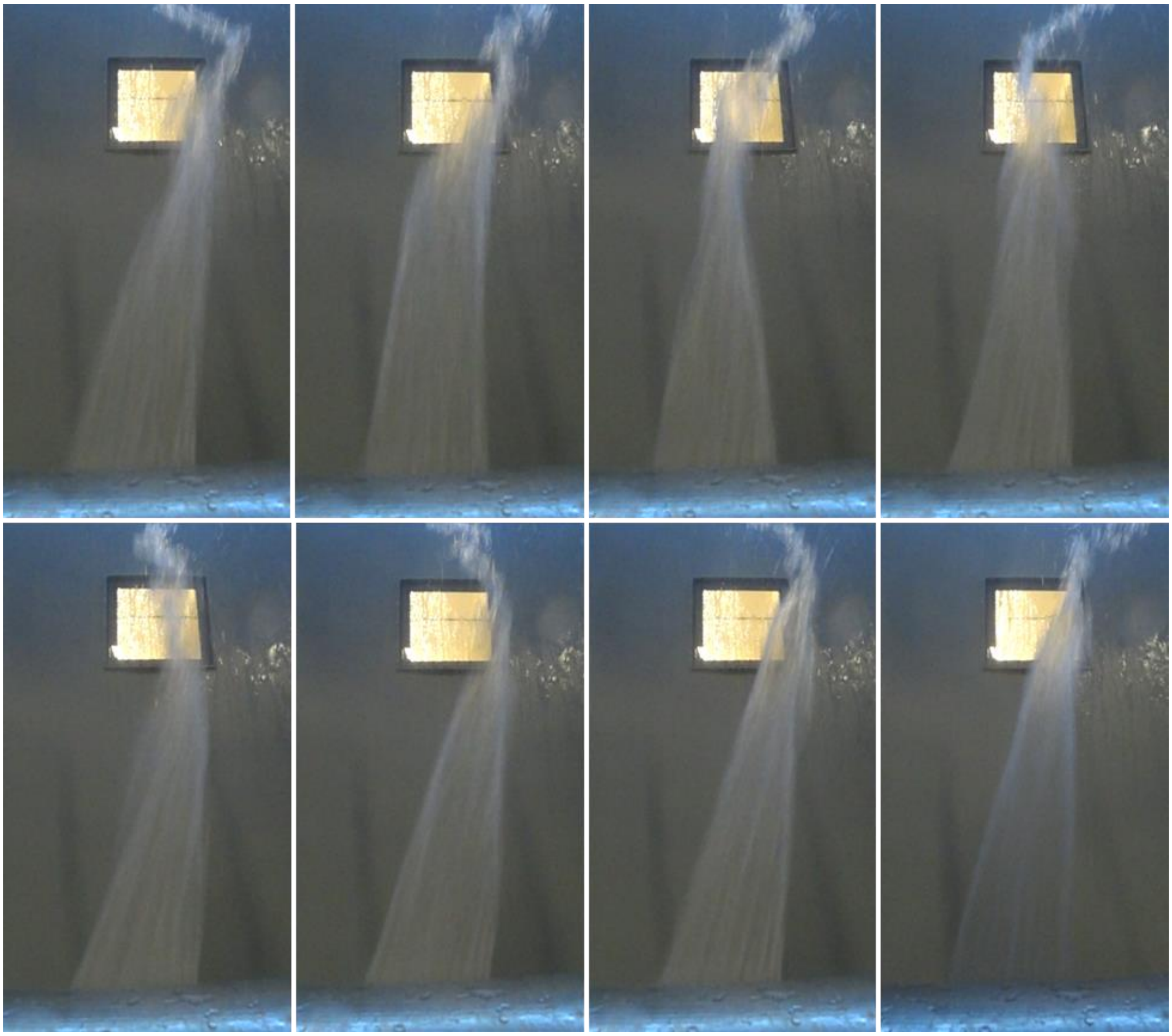

Figure 24. Oscillation in longitudinal slit, 3-inch diameter.

Figure 25 on the next page shows a wider view of the same 3-inch-no-valves-closed experiment. The water sprayed toward the back of the tank where it hits above the window (oval area) then splashed upward towards the ceiling, where some spray can be seen. The upwards direction seemed to be directly caused by the angle of the pipe in the threads, it appears the water came out normally through the pipe, and not at some upward angle. Longitudinally failed pipes are unique from the other two, as the cracks in all three pipes are of comparable size. As shown in Table 11, these leaks exhibit similar values for the leak rate, pressure, and velocity.

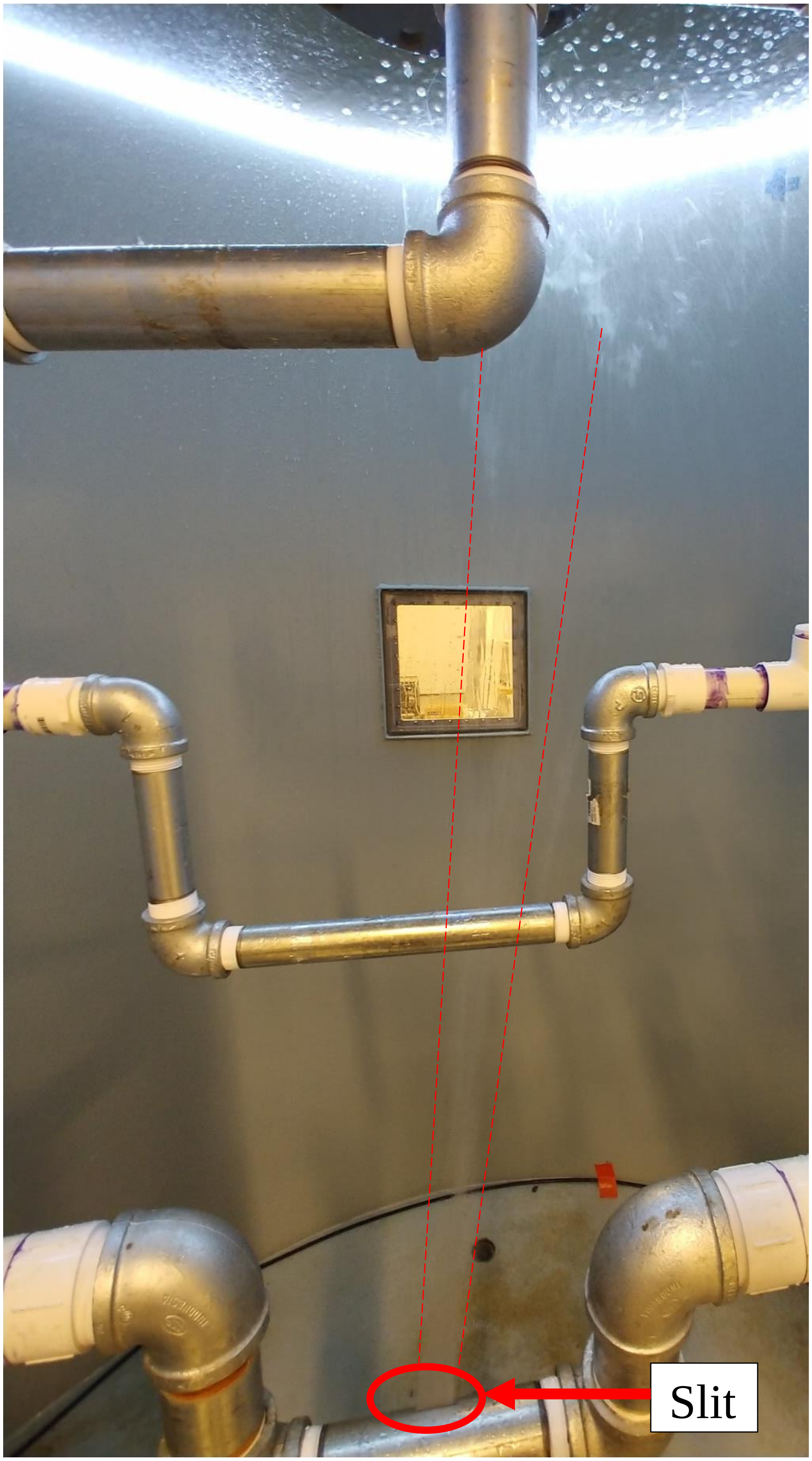

Figure 25. Larger view of longitudinal spray with no valves partially closed, 3-inch diameter.

The second crack type is circumferential, which type of crack is most likely related to FV failure, due to the bending stresses created from the vibration. Circumferential cracks result in a fan like spray, as seen in Figure 26. Figure 27 shows the side view of the same spray, so the fan shape is not visible from this picture. Figure 27 shows the height of the spray, and the resulting mist. The spray from circumferential cracks can reach to top of the PET, even though it is not as directed as the longitudinal spray. Circumferential leaks create more mist than the longitudinal slits as well. The mistiness observed means there are smaller water droplets in the air, making it feel far more humid, from observation, than the longitudinal. The mist may not be important for components directly in the spray failing, but may cause components to fail indirectly.

The biggest difference between the pipe diameters for this failure type is the difference in the failure area. As described before, the circumferential cracks were created to be as 90-degree arcs around the pipe, so the leakage area was lower for each pipe. Figure 28 and Figure 29 show the two-inch, and the one-inch circumferential cracks, respectively. A prominent feature here is the two-inch circumferential cut has burrs from the machining still inside of the crack. These burrs made the two-inch spray have several small streams, rather than appearing fan like, compared to the three-inch and the one-inch. Lastly, though the one-inch, and the three-inch appear similar, there is notably less flow through the one-inch crack, as expected. Note the clarity of the piping behind the spray is much sharper with the one-inch. Generally, for this crack type, as the pressure increased, and the crack area decreased due to smaller pipe diameter, the finer the resulting mist, and a lower the distance the mist could travel.

Figure 26. Fan spray from a circumferential crack, 3-inch pipe.

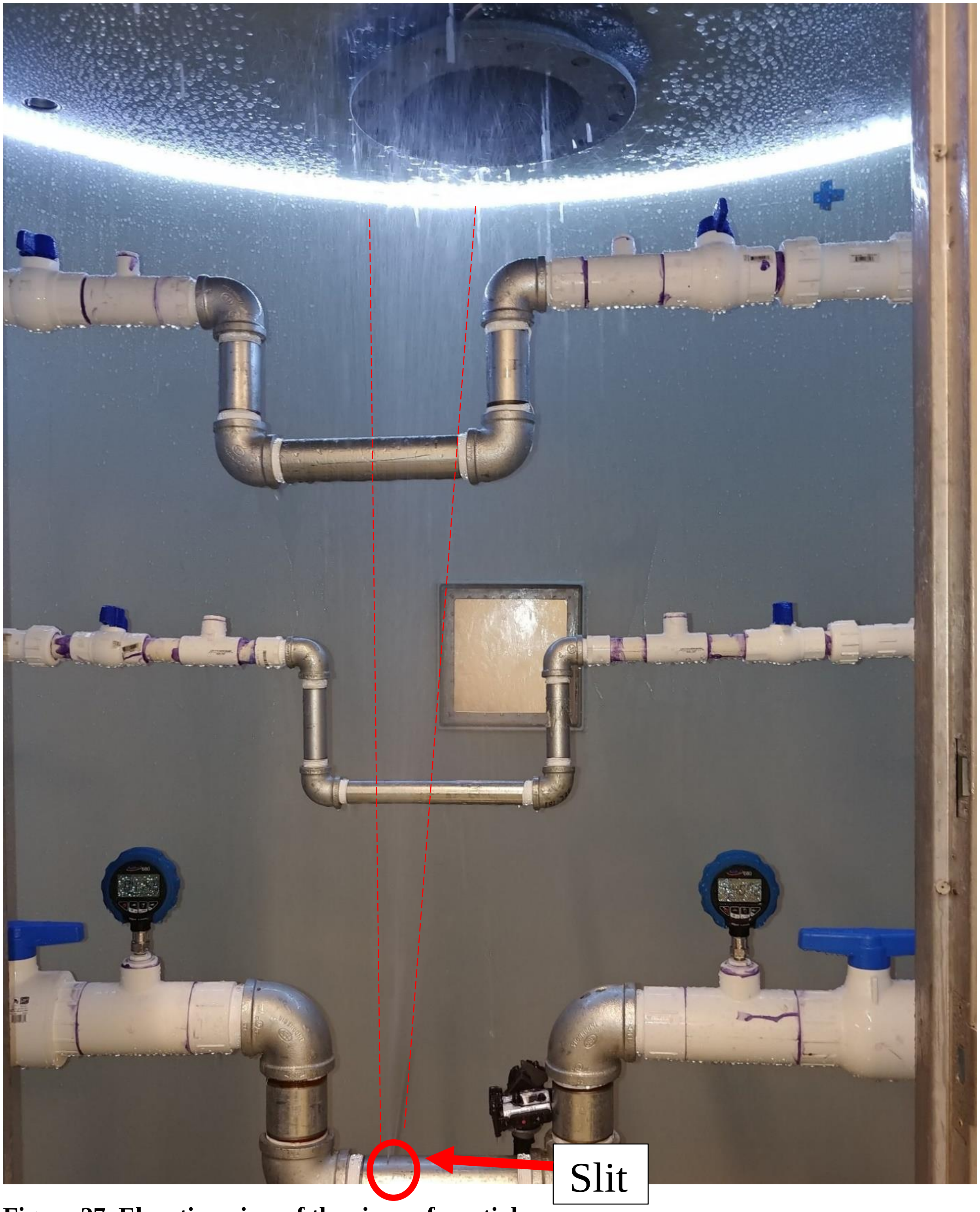

Figure 27. Elevation view of the circumferential spray.

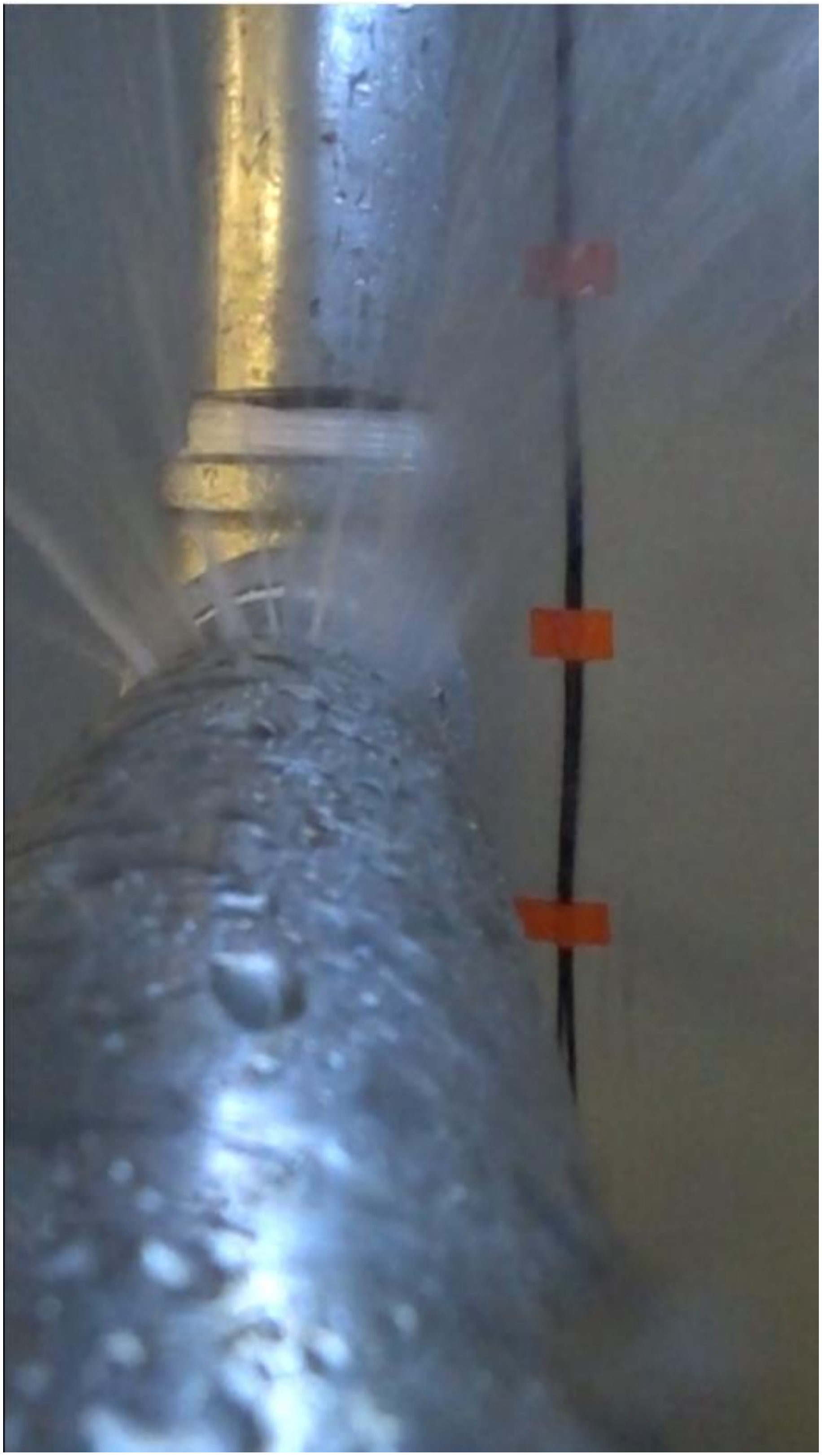

Figure 28. Fan spray from a circumferential crack, 2-inch pipe.

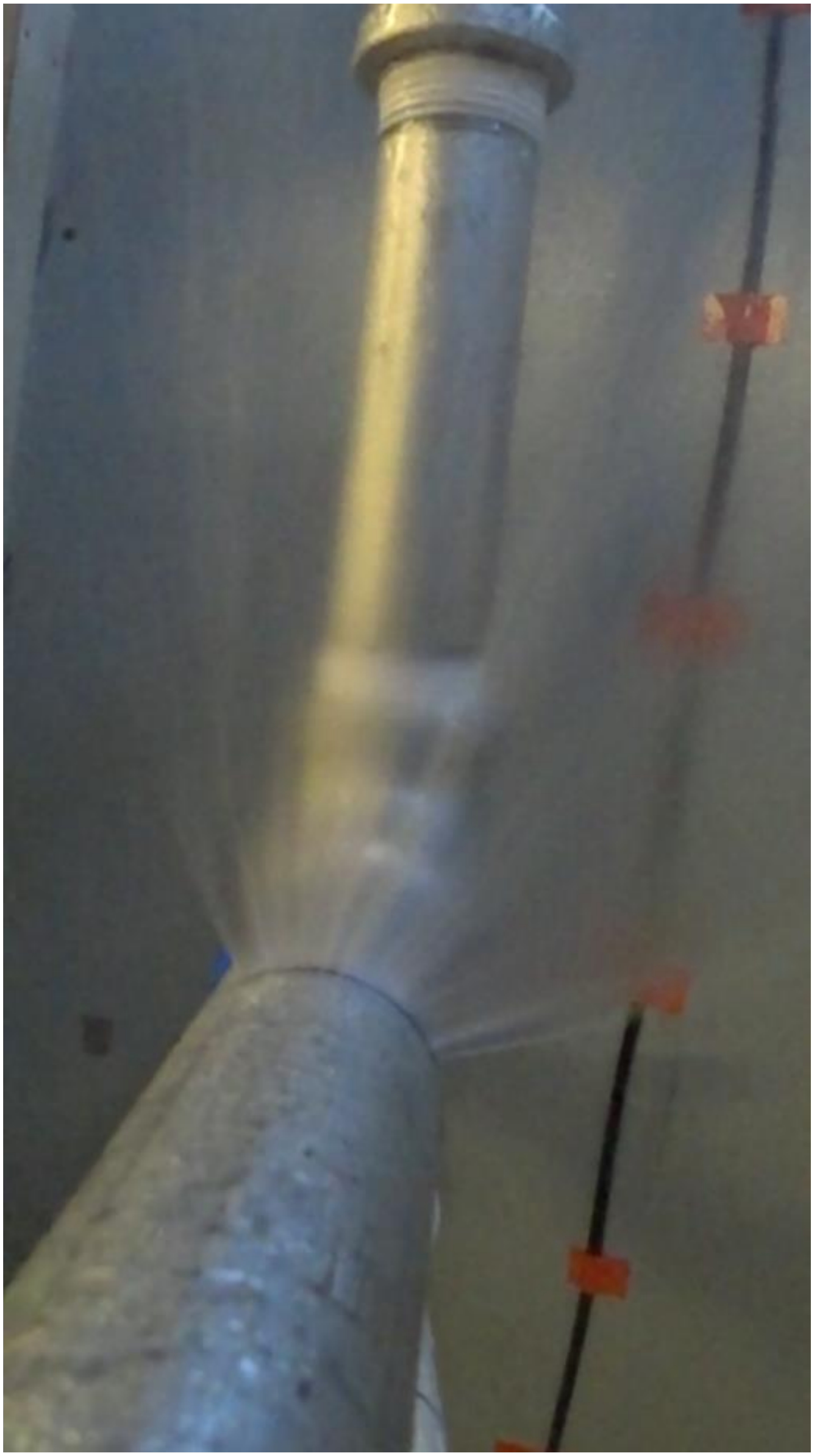

Figure 29 Fan spray from a circumferential crack, 1-inch pipe.

The last type of spray tested was leaks from elbows. Leaks from elbows, especially when they are somewhat circumferential, could also be described as FV failure if the piping had been secured poorly. Figure 30 shows a side view of an elbow leaking, and Figure 31 shows the view from the video camera, which was placed above the elbow looking down.

Elbow leaks of failure were a combination of the past two, the longitudinal and the circumferential. It is like the circumferential due to the fan like shape of the spray, as seen in Figure 31. The similarity is not very much of a surprise, as the slit is similarly somewhat circumferential. The elbow spray is like the longitudinal spray in the very directed manner of the spray, as can be seen in Figure 30. The elbow leaks tended to have higher leak flows compared to the other leak types with similar pipe flows. The higher leak rates are likely due to the position of the elbow, and the changes in momentum occurring. The comparison of the leak rates between the types is discussed more in depth in the next section. The elbow leaks did not appear to show as much of an oscillatory affect from the leaks, or if they did, they are not visible in the videos.

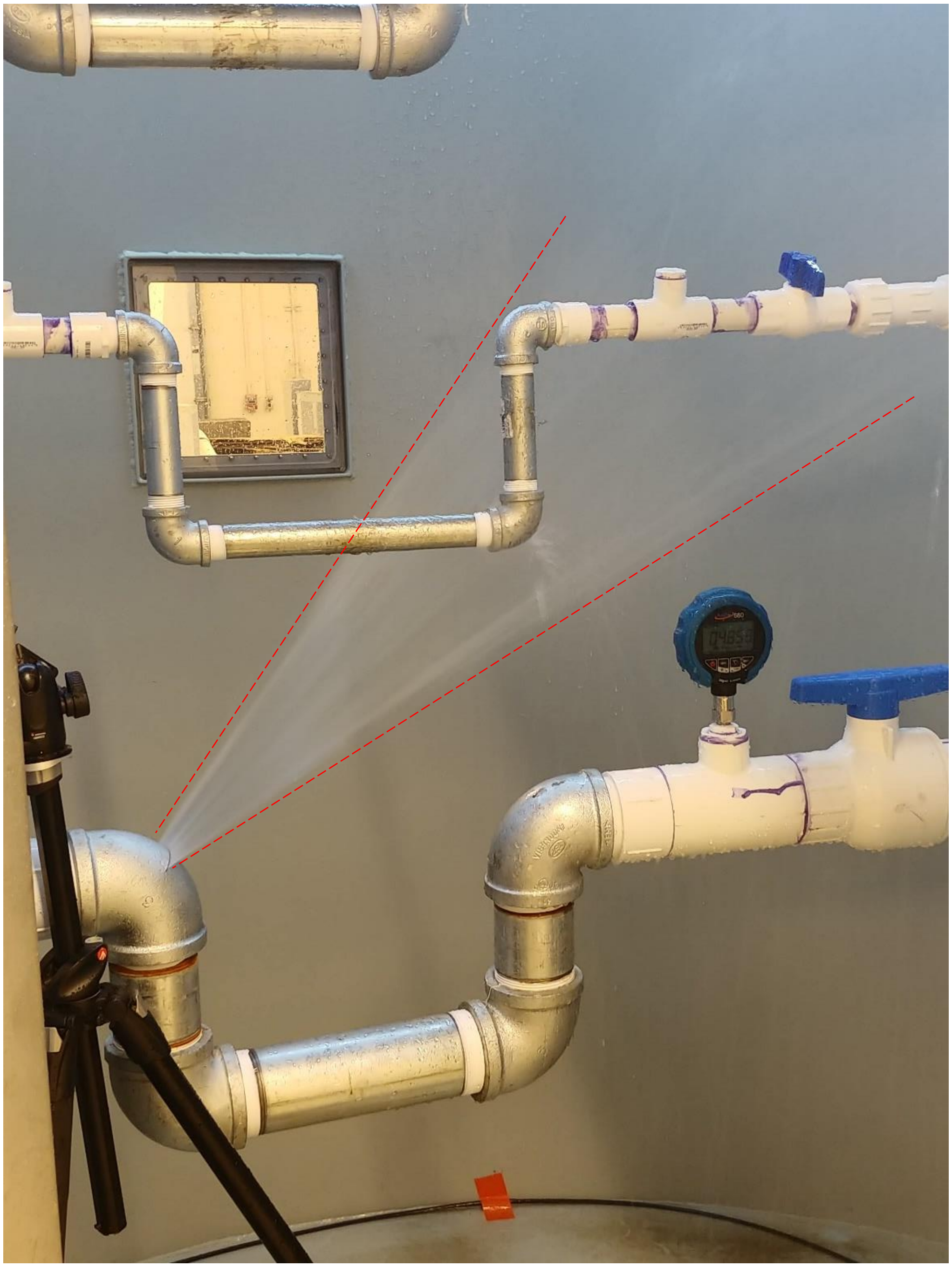

Figure 30. Spray from elbow, side view, 3-inch diameter.

Figure 31. Spray from elbow, straight on view, 3-inch diameter.

Qualitative Results

Throughout the course of these experiments three types of sprays were identified. The best way to categorize them is by how many valves were closed and the position of these valves. The three types are:

1. No valve closed leak
2. Upstream valves closed
3. Downstream valves closed

Type 1. No Valves

Type 1 leaks have the least amount of representation in these experiments, as each experiment only had one experiment with no valves closed. These leaks generally had moderately high leak rates, pressures, and leak velocities. There were no valves creating large drops in pressure and flow. The other types presented will show how this affects leaks.

Table 11. Type 1 Leak Data Example

	Leak rate (gpm)	**Error (gpm)**	**Pressure at Leak (psi)**	**Error (psi)**	**Velocity (ft/s)**	**Error (ft/s)**
Longitudinal						
3-inch	4.81	1.52	6.63	0.13	20.04	1.77
2-inch	4.87	1.10	8.31	0.25	16.12	1.03
1-inch	5.40	0.59	9.94	0.22	20.63	0.86
Circumferential						
3-inch	5.58	1.28	2.07	0.28	21.58	1.47
2-inch	2.89	1.27	3.35	0.75	10.19	1.08
1-inch	1.46	0.65	3.81	1.03	8.54	1.15
Elbow						
3-inch	6.82	1.43	7.05	0.10	19.76	1.22
2-inch	4.54	1.03	2.60	0.16	13.16	0.87
1-inch	3.22	0.77	1.65	0.08	9.35	0.64

Type 1 leaks can spray a large amount of water, but at lower velocities than the other categories as will be shown. Pictures showing this type of spray have already been presented above, in Figure 24, Figure 25, Figure 26, Figure 27, Figure 30, and Figure 31. These test act as a base line for comparing to Type 2 and Type 3.

Type 2. Upstream Valves Partially closed.

Departing from the Type 1 leaks, the Type 2 leaks happen when valves upstream of the leak are partially closed. More generally, if there are spots of large resistance upstream of the leak. Type 2 leaks have the lowest flow rates and the lowest velocities from the leaks compared to Type 1 and 3. Figure 32 shows a close view of a Type 2 leak from a longitudinal leak, and Figure 33 shows a wide angle. Figure 33 shows the leak from the pipe with a longitudinal leak. The water from the leak is barely reaching the back wall of the PET before hitting the ground. The misting from this type of leak is minimal, as can be seen in Figure 34 and Figure 35. These two figures show type leaks from an elbow and a circumferential leak respectively. Both leak types were characterized by the mist they created. At these lower flows and velocities though, very little mist is created. The distance away from this leak type at which components would be expected to be damaged is low, and would likely be only the components directly the failed piping.

Table 12 shows an example of the resultant data from Type 2 leaks. The data in the table is from the tests with both upstream valves half closed.

The data in Table 12, other than demonstrating Type 2 leak, also shows another comparison between the three leak types. At low flows the leakage from the elbow is still the greatest, even in the 1 and 2-inch piping, where the opening is smaller than the longitudinal slit. Conversely, the longitudinal crack leak parameters tend to be lower than the other two crack types. At best, the longitudinal is comparable to the other two, even though the leak area is larger than the other crack types (see TablesTable 3,Table 7, and Table 8).

Table 12. Type 2 Leak Data Example

	Leak rate (gpm)	Error (gpm)	Pressure at Leak (psi)	Error (psi)	Velocity (ft/s)	Error (psi)
Longitudinal						
3-inch	1.58	0.74	0.76	0.076	6.57	0.87
2-inch	4.26	0.59	10.14	0.076	17.77	0.91
1-inch	4.55	0.60	12.26	0.08	18.97	0.92
Circumferential						
3-inch	2.21	1.11	1.87	0.076	8.54	1.15
2-inch	4.14	0.80	7.48	0.076	16.03	0.96
1-inch	6.17	0.75	15.07	0.076	23.87	1.09
Elbow						
3-inch	3.22	0.77	1.65	0.076	9.35	0.66
2-inch	6.07	0.74	8.88	0.076	17.60	0.75
1-inch	7.35	0.59	13.13	0.076	21.30	0.76

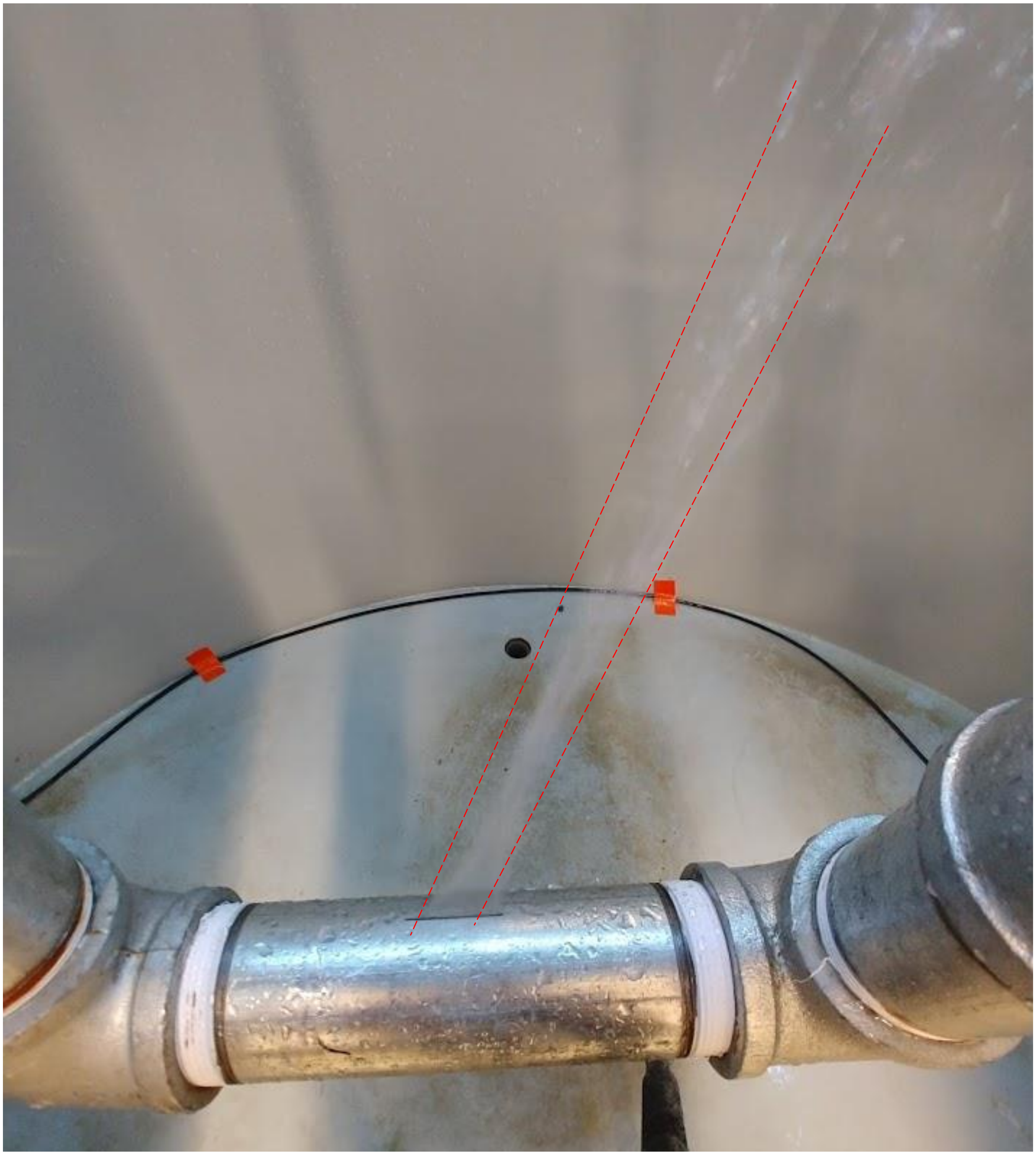

Figure 32. Type 2 leak from a longitudinal crack, close view, 3-inch diameter.

Figure 33. Type 2 leak from a longitudinal crack, wide view, 3-inch diameter.

Figure 34. Type 2 leak from an elbow leak, 3-inch diameter.

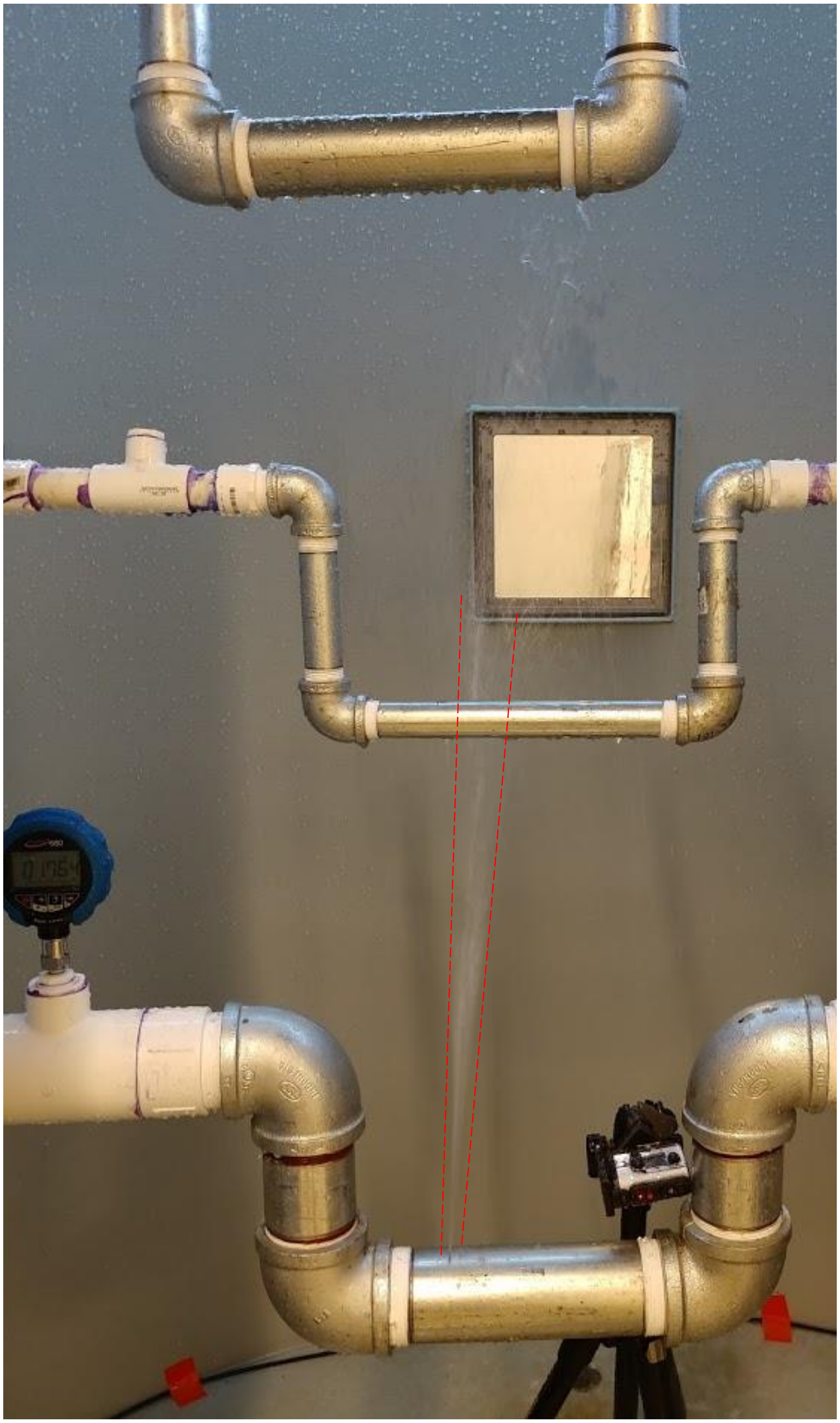

Figure 35. Type 2 leak from a circumferential leak, 3-inch diameter.

Type 3. Downstream Valves Partially Closed

The last type of leak identified in this experiment is called Type 3, and is categorized by leaks with valves, or other large losses, downstream of the leaks. Due to the experiment design and setup, this category had the most representative runs. These types of runs are characterized by large leak rates, large velocities, low pressure drops across leaks, but large pressures at leaks as well. These types of leaks tended to be the most violent, and the mistiest. Figure 36 shows a close view of a longitudinal crack, and Figure 37 a wide view. The wide view shows the leak hitting the back of the PET and splashing up and around the tank similar to the Type 1 in Figure 25. Additionally, the Type 3 leak comes out more normal to the pipe than the Type 1 or Type 2 (Figure 25 and Figure 33). Figure 38 shows a Type 3 leak from a circumferential leak and Figure 39 a Type 3 from an elbow. Both figures show the water being sharper and mistier than the other types. The angle is also more normal to the pipe than Type 2 (Figure 34 and Figure 35).

Type 3 leaks have the potential to be the most damaging to components. The high flow means more water leaving the pipes. The high velocity means the water will carry further and become mistier as it exits the pipe. The high pressure means the water leaves the pipe more a more normal angle, than other types and is more direct. As an example, Table 13 shows an example data from one valve configuration giving Type 3 leaks, which is the two downstream valves partially closed.

Table 13 numbers are vastly higher than the two previous types, including one test with a velocity of 72 ft/s, which was by far the largest velocity observed, due to the run also having the one of the highest pressures at the split. The same configuration with the longitudinal split had a comparable pressure at the leak, but due to the larger leak area, there is a larger pressure drop.

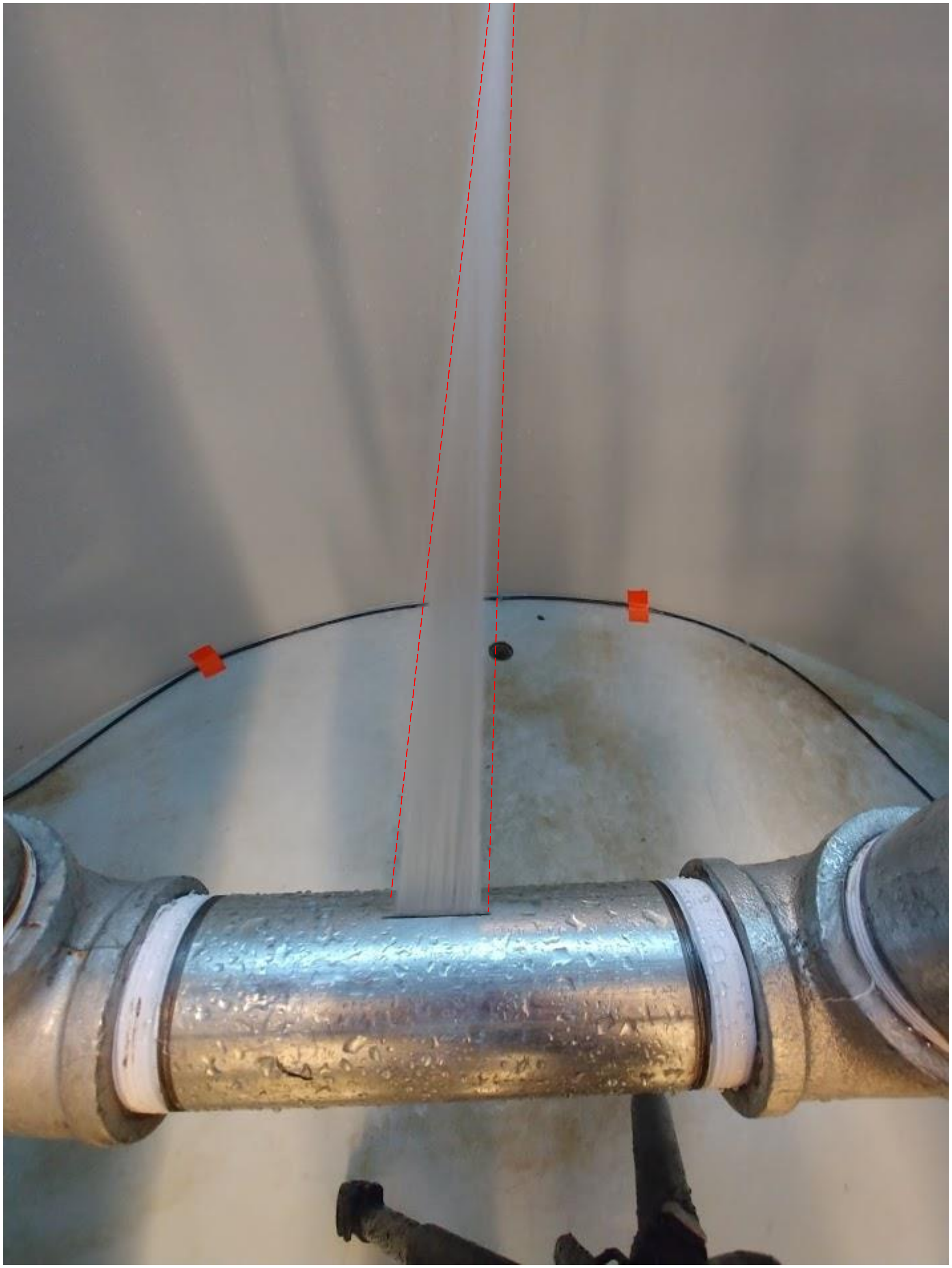

Figure 36. Type 3 leak from a longitudinal crack, close view, 3-inch diameter.

Figure 37. Type 3 leak from a longitudinal crack, wide view, 3-inch diameter.

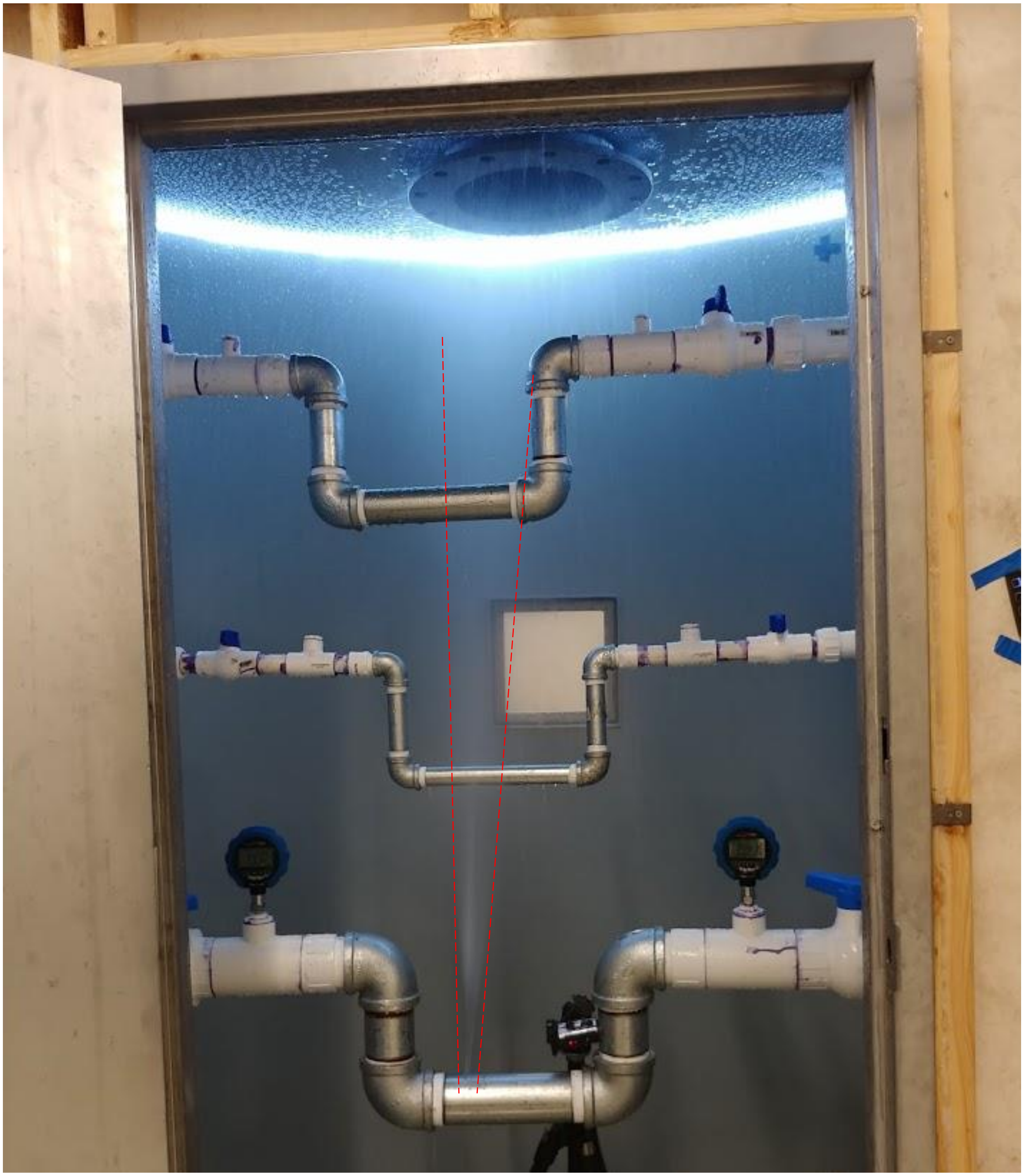

Figure 38. Type 3 leak from a circumferential leak, 3-inch diameter.

Figure 39. Type 3 leak from an elbow leak, 3-inch diameter.

Table 13. Type 3 Leak Data Example

	Leak rate (gpm)	Error (gpm)	Pressure at Leak (psi)	Error (psi)	Velocity (ft/s)	Error (psi)
Longitudinal						
3-inch	6.30	0.86	19.08	0.14	26.23	1.28
2-inch	4.6	0.59	10.51	0.19	14.35	0.64
1-inch	9.10	0.98	30.10	0.15	34.77	1.45
Circumferential						
3-inch	7.35	0.72	22.71	0.17	28.45	1.19
2-inch	3.03	0.69	15.25	0.23	15.71	1.37
1-inch	6.95	0.46	24.14	0.19	72.61	2.84
Elbow						
3-inch	9.34	0.74	21.49	0.16	27.08	0.96
2-inch	7.365	0.60	24.66	0.23	33.91	1.29
1-inch	7.44	6.00	30.06	0.16	59.02	12.52

Figure 40. 1-inch elbow Type 3 leak, 1-inch diameter.

Summary of Spray Types

The results presented in this section have described the three different spray Types identified by the experiments in this project. Type 1 is the base line leak, with no major losses around the leak, moderately high flows and velocities, but low pressures. Type 2 leaks are the leaks having many losses before the leak. Type 2 leaks have the lowest flows and velocities, but moderate pressures. Type 3 leaks have the highest of all three categories, high flows, pressures, and velocities.

It is impossible to say which Type of spray is the most damaging to NPP components in the context of this thesis. Some generalizations can be said for the Types. Type 2 would be most dangerous to components directly beneath piping, due to their low velocity. Types 1 and 3 would be dangerous to components far away, especially if the leak is on an elbow or is longitudinal, as these conditions lead to the leaks being the most directed. If misting is a concern for components, proximity to walls and ceilings would be of concern then, as Type 1 and Type 3 spraying against the walls created a large amount of mist, especially with circumferential cracks and elbow cracks.

Another way of describing these sprays is through the energy loss in the system. Type 1 has no major energy losses in the system, so it acts as the base line. Type 2 has major energy losses upstream of the leaks, so by the time the water reaches the leak there is not much energy left, and so very little to leave through the crack. Conversely, Type 3 leaks are trying to lose all their energy downstream of the leaks, causing a “back up” of energy, causing more energy to be dispersed through the leaks.

Minor Loss Coefficient

Part of characterizing the piping system used in this experiment was determining the minor loss coefficients of the system. Minor losses are used to calculate the head losses in piping components such as valves and elbows. It was also assumed when the leaks were introduced to the system they would introduce new minor losses. Part of the goal of this experiment was to determine engineering data valuable to leaks, and the minor loss coefficient, k, was of interest.

The original plan was to calculate the minor loss coefficient of the test sections using the one-dimensional energy equation, Equation 1, using the two pressure gauge points as the points in the equation. The minor loss coefficient is supposed to be constant for systems, independent of flow or velocity, however, this was not found to be the case. Figure 41 shows the results of these first calculations of k.

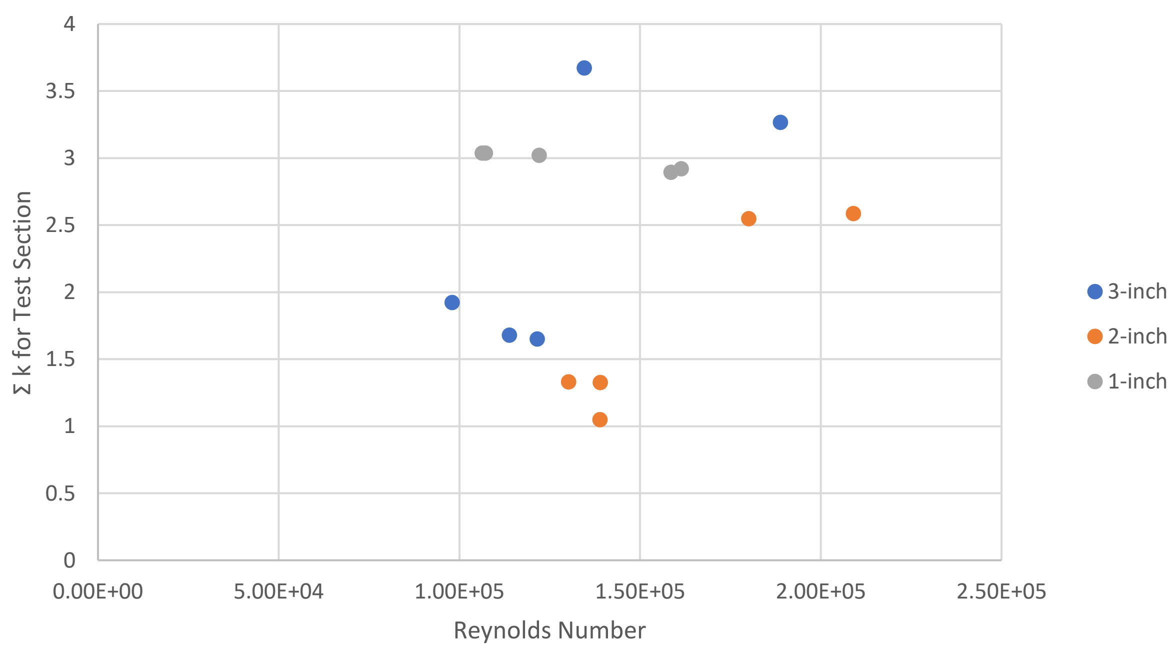

Figure 41. Initial minor loss coefficient calculations vs Reynolds number.

The results were inconsistent in general. The 1-inch line appears to converge around 3, but none of the others do. The two PVC valves in the system were discovered to be placed too close to the pressure gauge, especially the upstream one, caused interference with the pressure gauge. The calculations were performed again, changing the flow only with the downstream brass valve. The results of this can be seen in Figure 42. These results are more in line with what is expected. Averages of these values were then used to calculate k for the failures. Comparing the initial calculations and the new calculations revealed the initial the calculations done without the upstream PVC valve closed matched closely with the recalculated values.

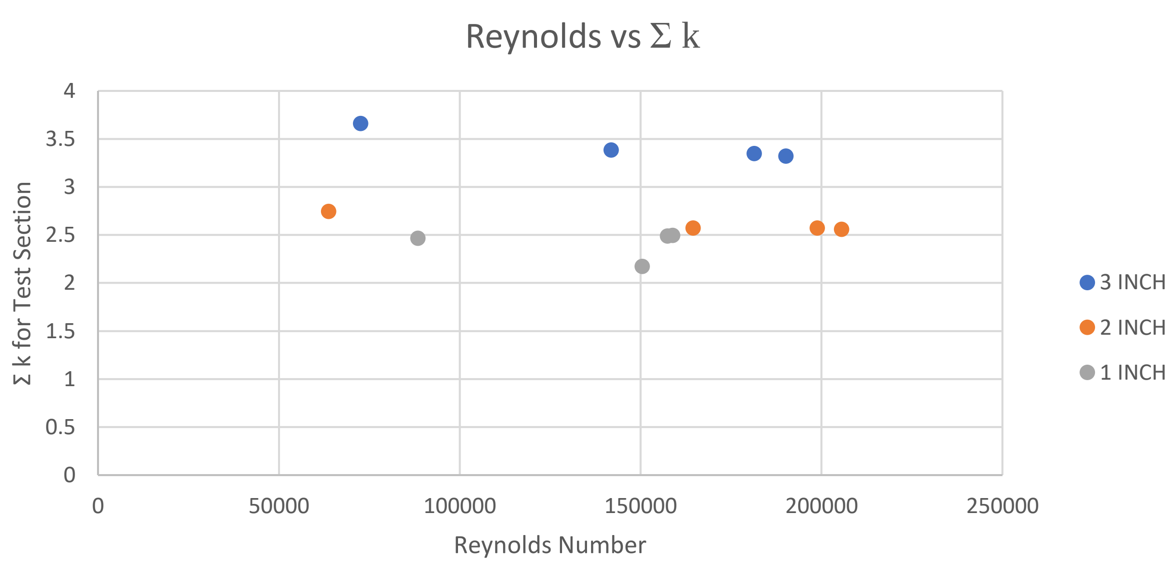

Figure 42. Recalculated minor loss coefficients.

The issue with the upstream PVC valve also made most of the pressure data recorded from it invalid. Any run then with the upstream PVC partially closed could not be used for any calculations. To overcome this, a different tactic was used, still using the one-dimensional energy equation, this time using the downstream pressure gauge as the first point, and the right side of the failure as point two.

It was also desired to explore the pressure losses across the different failures. The above method was used to find the pressure on the downstream side. Using tests not tainted by the PVC valves, the pressure at the upstream side could be calculated in some cases. In general, the pressure drop across the crack was minimal, and the difference was smaller than the error associated with the difference. Table 14 shows an example of the pressure calculations at the cracks, for longitudinal cracks in this case, using Equation 18. The cases with the pressure loss large enough to be observable in this system, were in the one-inch line. Two of the runs were large enough to be seen well, the other had a pressure at the highest end of what the gauge is rated for so it is not likely to be accurate.

Table 14. Longitudinal Pressure Calculation Example

	Upstream Side (psi)	Error (psi)	Downstream Side (psi)	Error (psi)	Difference (psi)	Error (psi)
3-inch up to down						
All Open	6.67	0.11	6.58	0.08	0.09	0.13
1 Closed	1.47	0.08	1.27	0.08	0.20	0.11
3-inch down to up						
1 Closed	16.16	0.11	16.07	0.08	0.08	0.13
2 Closed	19.14	0.12	19.02	0.08	0.11	0.14
2-inch up to down						
All Open	8.23	0.24	8.38	0.08	-0.15	0.25
1 Closed	3.10	0.18	3.19	0.08	-0.10	0.19
2-inch down to up						
1 Closed	6.05	0.19	6.19	0.08	-0.14	0.20
2 Closed	10.44	0.18	10.58	0.08	-0.15	0.19
1 inch up to down						
All Open	11.16	0.19	8.72	0.08	2.44	0.21
1 Closed	9.20	0.19	7.12	0.08	2.08	0.21
1 inch down to up						
1 Closed	13.13	0.21	10.97	0.08	2.15	0.23
2 Closed	30.03	0.12	30.18	0.08	-0.16	0.14

The pressures in Table 14, and similar calculations for circumferential and elbow leaks were used then to calculate the minor loss coefficients for the cracks. The pressure at the crack was assumed to be the average of the pressure at the crack on the upstream side and the pressure at the crack on the downstream side. If the upstream was not calculated due to the issue with the PVC valves, the downstream was assumed to be the crack pressure instead. Equation 21 was used to calculate the minor loss of the cracks. ΔP is the pressure loss across the slit to the atmosphere, v is the velocity through the crack, ρ is the density of water, g is the acceleration due to gravity, and k_{split} is the minor loss coefficient of interest.

$$\frac{\Delta P}{\rho g} = k_{split} * \frac{v^2}{2 * g}$$

Equation 21. Slit Minor loss calculation

Figure 43 through Figure 47 show the results from these calculations for the longitudinal, Figure 48 through Figure 52 for the circumferential, and Figure 53 through Figure 57 for the elbows. All of parameters in these figures for the minor loss coefficients are plotted with their associated errors, for both the independent and dependent variables. Several of the figures appear to have no horizontal error bars, but this is due to the small relative error in their calculation. No correlation was clear between the resulting minor loss coefficient for the crack and readily calculable parameters, though it was expected there would be one. The parameters compared for each crack type are the pressure in the pipe at the crack, the leak rate through the crack, they Reynolds number in the pipe, the velocity head in the pipe, and the total energy head in the pipe. Some of the calculated minor loss coefficients show some similarity or a trend, but it is not consistent throughout all the calculations. It is possible the pipes deformed during a test, but not in plastic deformation, so the cracks reset to their original size at the end of the test, or there are some other turbulent effects not being accounted for. Or it is possible there is some combination of parameters in the pipe that would reveal a pattern, but isn't inherently clear. It isn't clear what the issue is, or how to address it at this point, and will be reserved for future work. One thing that is clear, however, is the error in the calculations needs to be reduced, and more data need to be collected.

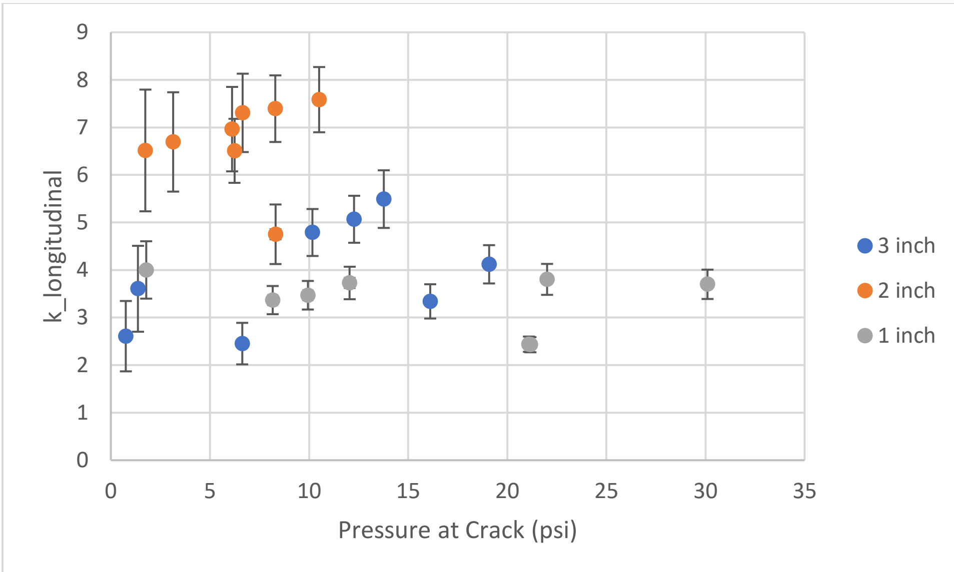

Figure 43. Longitudinal minor losses compared against pressure in the pipe.

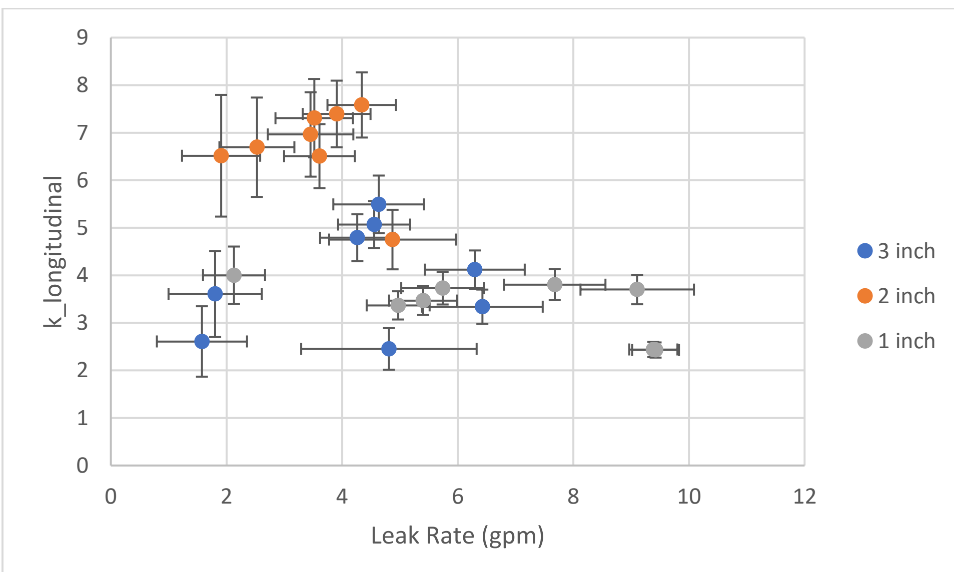

Figure 44. Longitudinal minor losses compared against the leak rate.

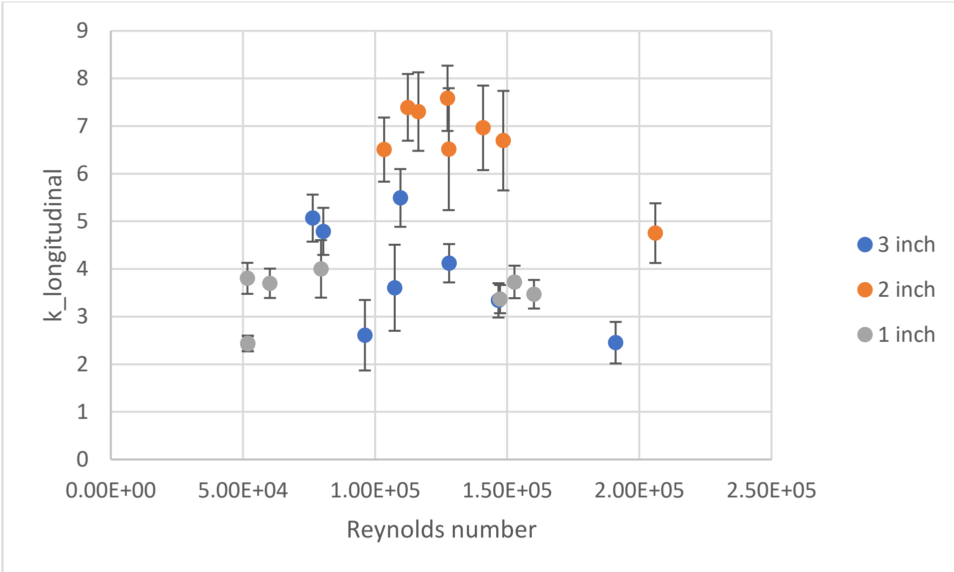

Figure 45. Longitudinal minor losses compared against Reynolds number in the pipe.

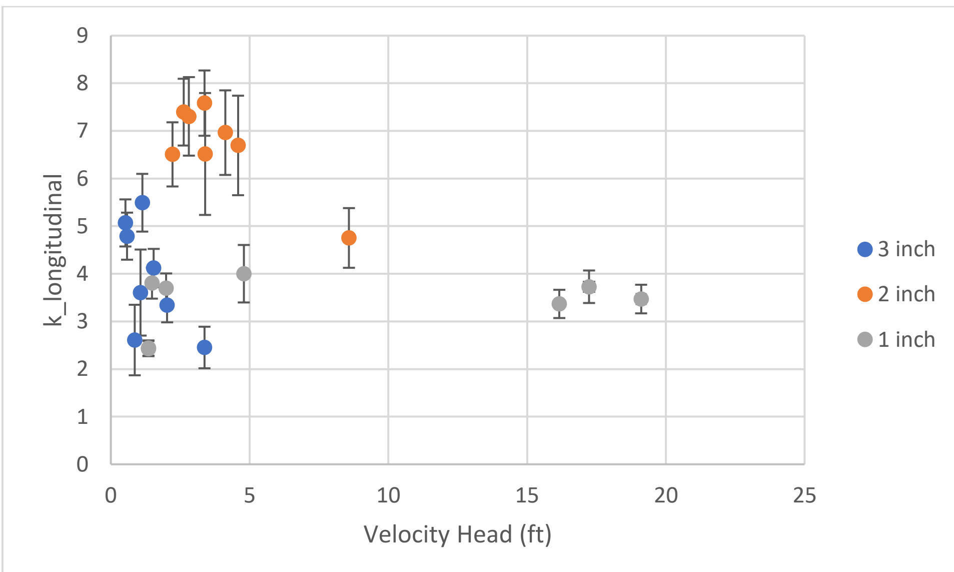

Figure 46. Longitudinal minor losses compared against velocity head in the pipe.

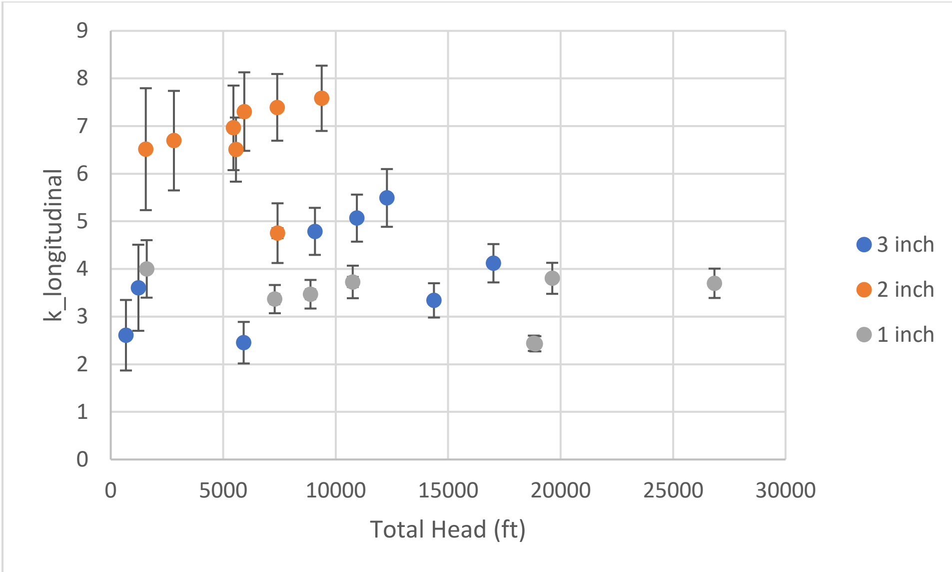

Figure 47. Longitudinal minor losses compared against the total energy head in the pipe.

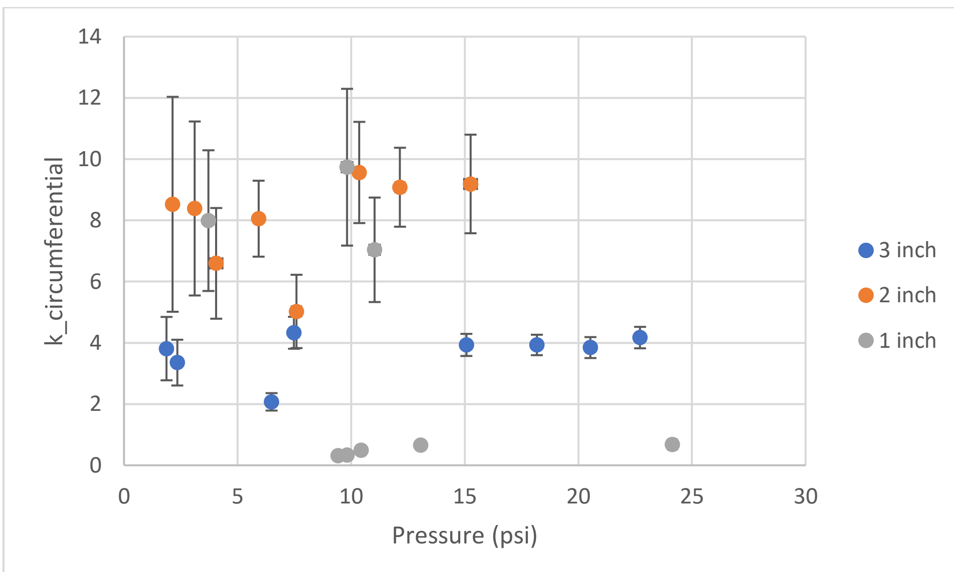

Figure 48. Circumferential minor losses compared against pressure in the pipe.

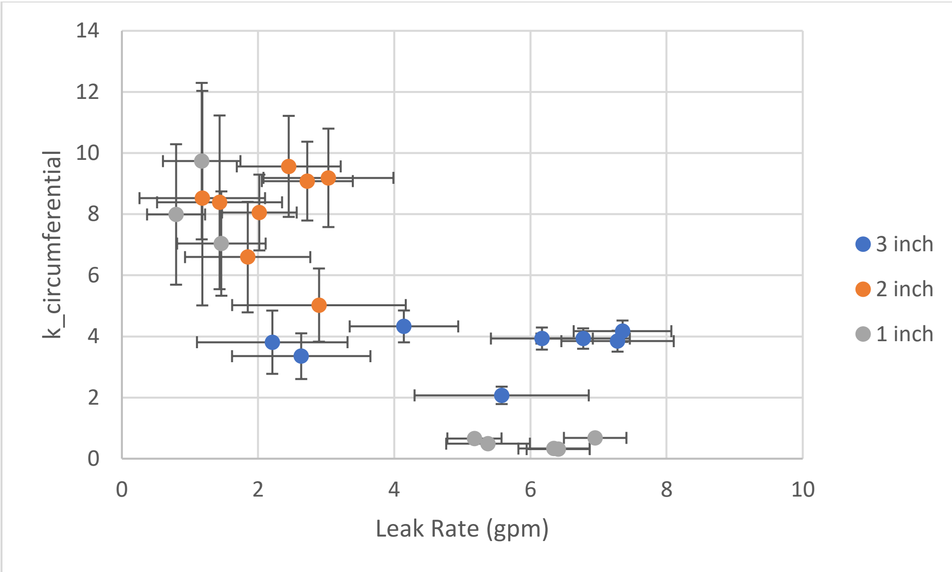

Figure 49. Circumferential minor losses compared against the leak rate.

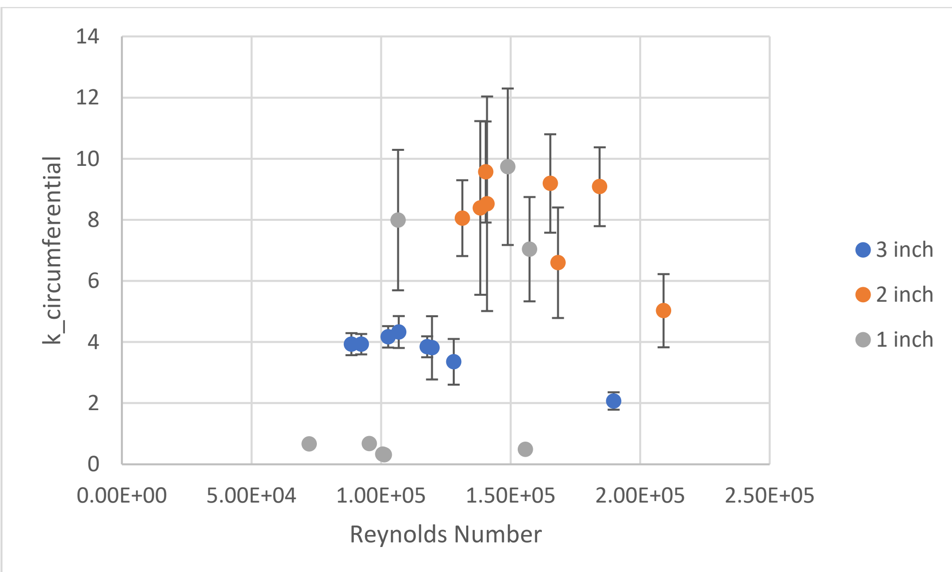

Figure 50. Circumferential minor losses compared against the Reynolds number in the pipe.

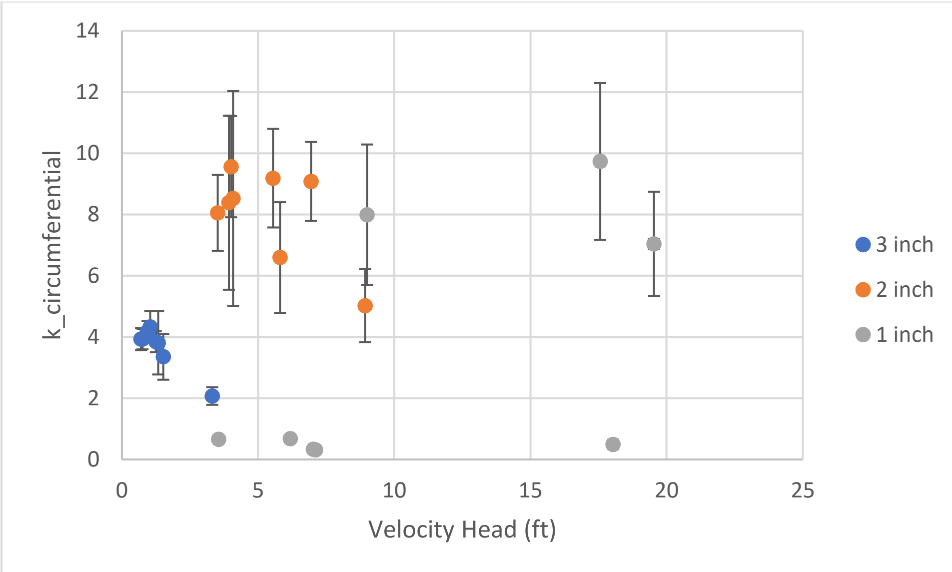

Figure 51. Circumferential minor losses compared against velocity head in the pipe.

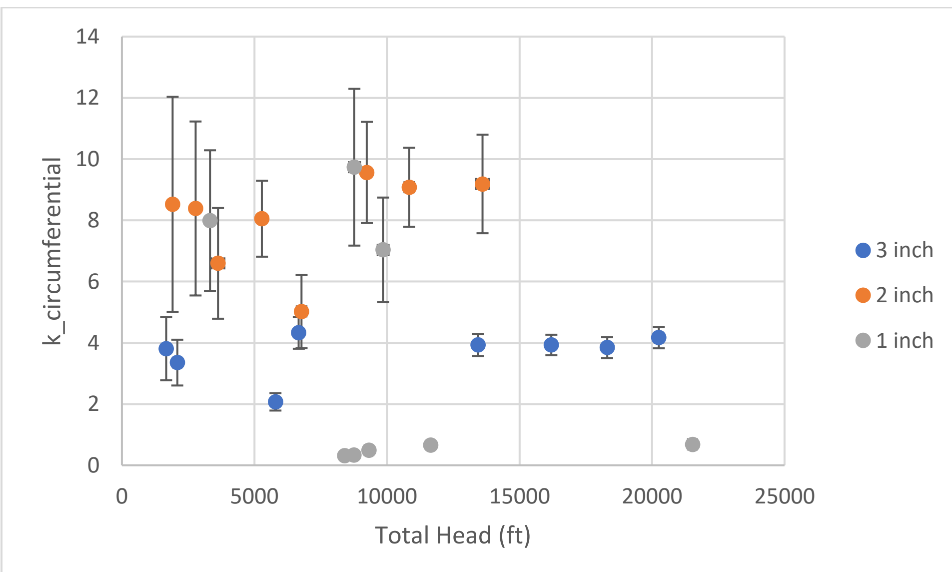

Figure 52. Circumferential minor losses compared against total head in the pipe.

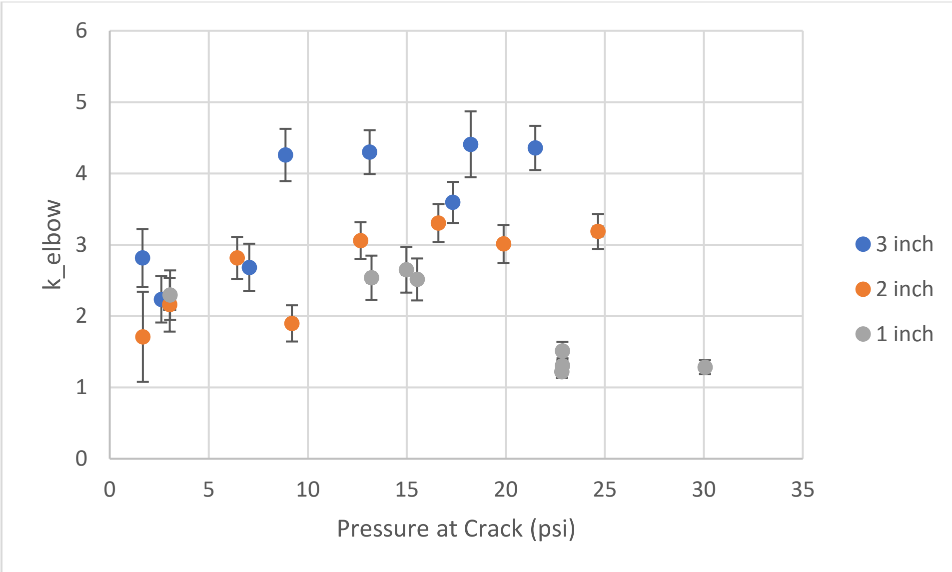

Figure 53. Elbow minor losses compared against pressure in the pipe.

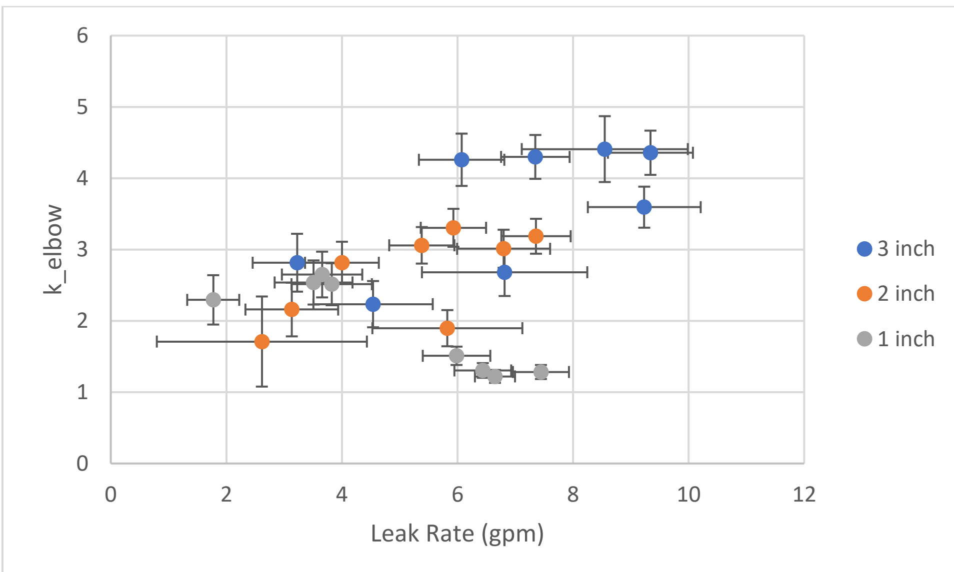

Figure 54. Elbow minor losses compared against leak rate.

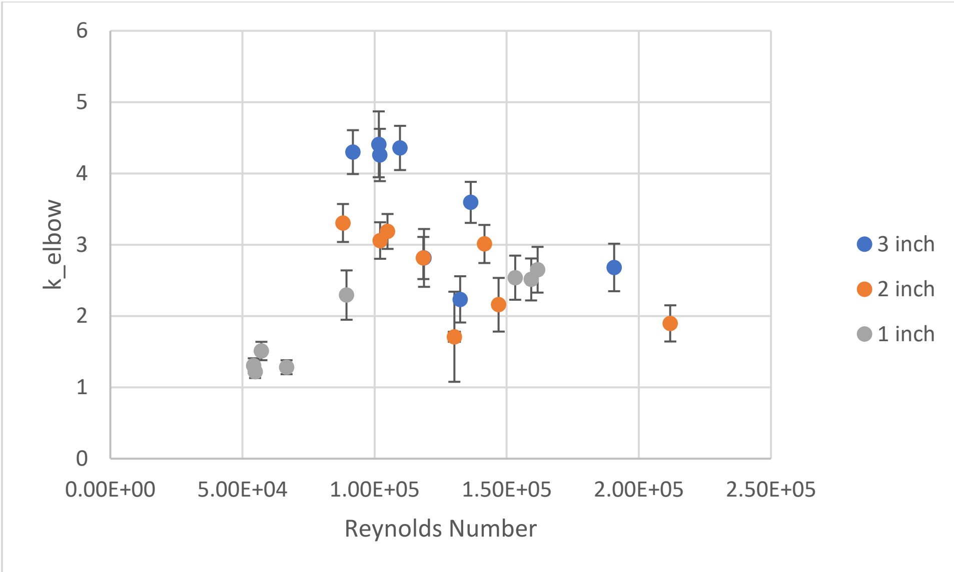

Figure 55. Elbow minor losses compared against Reynolds number in the pipe.

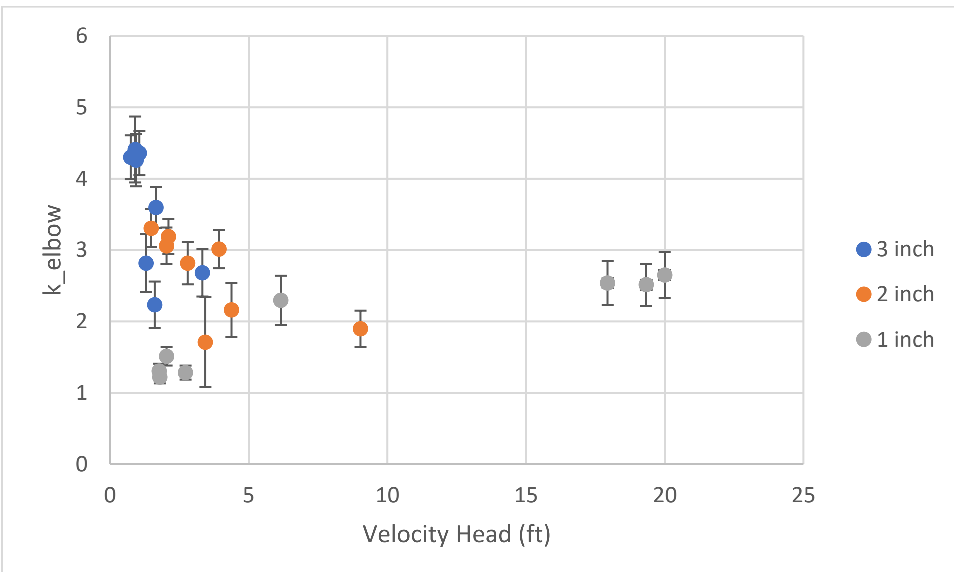

Figure 56. Elbow minor losses compared against velocity head in the pipe.

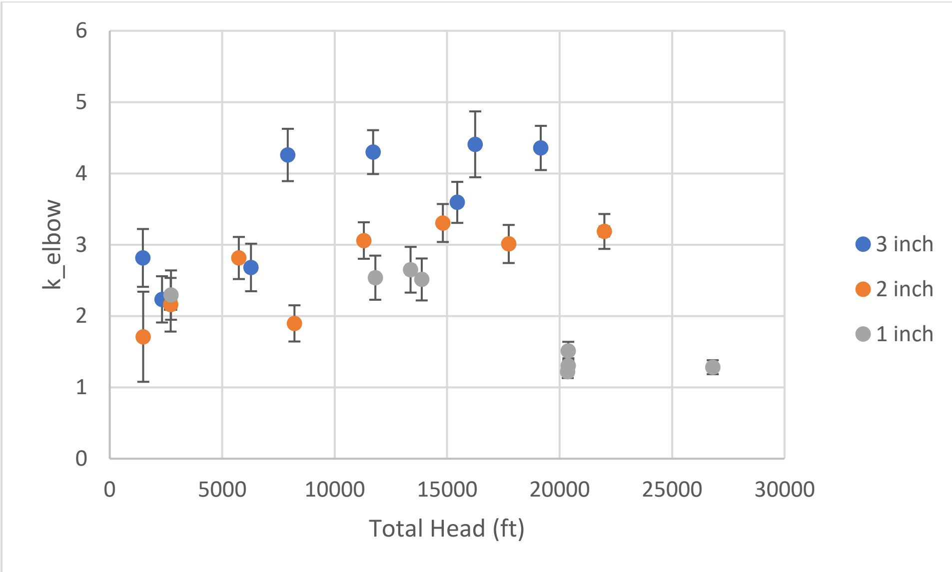

Figure 57. Elbow minor losses compared against total head in the pipe.

Conclusion

The results of this experiment demonstrate methods for describing three different leak scenarios, longitudinal cracks, circumferential cracks, and cracks in elbows. Longitudinal cracks were shown to be directed streams, producing very little mist. The angle of the stream from the longitudinal crack is also dependent on the pressure in the pipe at the crack. Circumferential cracks produce a fan like affect for the spray, producing more mist than the longitudinal crack. The last type of crack in elbows was a combination of the other two, though is more similar to the circumferential crack. Elbow leaks typically had higher leak rates and velocities due to the changes in momentum present in elbows. Three different leak Types were determined as well, Type 1 is the base line type with no valves partially closed in the system, exhibiting moderate leak rate and velocity. Type 2 shows the lowest of the flows and velocities from the cracks. Type 3 is the other end, with the highest leaks rates, pressures, and velocities.

The experiment setup is an area where this work needs improvement. The experiment was placed in the PET to help contain the spray which was beneficial. However, this created restrictions on the piping design. The PVC valves were placed too close to the pressure gauges, so when they were used to control the flow they influenced the data. A future iteration of this project should have its own apparatus allowing for easy change of parts, adequate room for instruments, and containment for spray.

Another improvement is the ability to measure the leak rate and the pressure. As can be seen in Table 11, Table 12, and Table 13 the error associated with the leak rate, and the error in the minor loss coefficients in Figure 43 through Figure 57 is quite large. The issue with the calibration in the flow meters increases these errors. Similar future experiments should make considerable effort to find flow meters better calibrated to each other to reduce error. Additionally, to prevent the issues with the upstream PVC valve, more piping should be installed between the two to reduce vortex affects. Alternatively, valves better capable of controlling the flow could be introduced upstream and downstream. Gate valves or butterfly valves would allow for more control over the reduction in flow than ball valves. A future iteration of this project could instead tie into the city water system via the fire hose present in the Water Resources Laboratory. The city water line would be expected to deliver a steadier flow with less oscillations. A steadier flow would aid in the reduction of variability in the flowmeters and possible pressure gauges as well.

There are several other areas future work in this area can develop. First, the cracks used to create the leaks were created artificially. The pipes failed should be failed in more realistic ways. The pipes used in this experiment were milled to create the cracks in them. A separate experiment would be useful to create failure in pipes more naturally, whether through corrosion, force, or vibration. Alternatively, or in addition to, it would be good to find failed pipes and have natural leaks from them being in service, then testing them with several different pressures and flows. It would be interesting in the future to see how these compare to organically caused cracks, whether through water hammer, or through corrosion.

Second, more flowrates and pressures should be measured. The experiments described in this thesis used a pump already in place in the lab. In the future, it would be better to design piping for specific pumps and test specific situations. The specific situations would be better to be suggested by people in industry or by the steering committee planned for the project. Additionally, during the experimentation process, it was thought enough data, with enough variation in the valve configurations were tested. Examining the data revealed more data was needed, from both the recording time and valve configurations. The variability between recording times for the flow meters was thought to be addressed by running the tests for four minutes, but more time is needed with this setup, or to use two HART modems to get rid of the multidrop problem.

Third, no tests were run with a downstream valve completely closed, making a situation in a pressurized wet stationary line with a leak. Tests with no downstream flow and a failure would best represent fire sprinkler lines, as this is generally how they are maintained. The no downstream flow condition was not tested out of fear of damaging the pump, but it would have been possible. It is expected this would end up being similar to a Type 3 leak, but testing would be needed to confirm this.

Another consideration to be made would be the temperature and the state of the water. The water in this experiment was room temperature, single phase water. It could be potentially valuable to examine two phase lines, or purely steam lines, as these types of lines are present in NPPs, but were outside of the scope of this thesis. The steam itself might not have much effect on components, but it may change how any water leaks out of the pipes.

Lastly, the most important future work will be testing real NPP components in leaks to failure. Electrical NPP components will require a much more robust setup. These components are likely large electrical components, such as presented as a battery room in the INL report [8]. These components would need to be isolated in a manner as not to be danger to any bystanders or operators. Designing such a setup will require a lot of considerations in the future of this project, and is important to other failure types than spray.

References

[1] S. Beliczey and H. Schulz, "The Probability of Leakage In Piping Systems of Pressurized Water Reactors on the Basis of Fracture Mechanics and Operating Experience," *Nuclear Engineering and Design: An International Journal Devoted to the Thermal, Mechanical, and Structural Problems of Nuclear Engineering,* vol. 102, pp. 431-438, 1987.

[2] G. T. E. B. H. D. Schulze, "Fracture Mechanics Analysis on the Initiation and Propogation of Circumferential and Logitudinal Cracks in Straight Pipes and Pipe Bends," *Nuclear Engineering and Design Vol. 58,* pp. 19-31, 1980.

[3] S. N. N. G. e. a. K. Matsumoto, "Study on Crack Opening Area and Coolant Leak Rates on Pipe Cracks," *International Journal of Pressure Vessesls and Piping Vol 46,* pp. Pages 35 - 50, 1991.

[4] Jai Hak Park, Young Ki Cho, Sun Hye Kim and Jin Ho Lee, "Estimation of Leak Rate Through Circumferential Cracks in Pipes in Nuclear Power Plants," *Nuclear Engineering and Technology,* pp. Volume 47, Issue 3, Pages 332-339, April 2015.

[5] S. Bush, M. Do, A. Slavich and A. Chockie, "Piping Failures in United States Nuclear Power Plants: 1961-1995 (SKI-R--96-20)," Swedish Nuclear Power Inspectorate, Sweden, 1996.

[6] National Energy Board, "Vibration fatigue failure of piping (Safety Advisory NEB SA03-1)," National Energy Board, Calgary, 2003.

[7] National Fire Protection Association, NFPA 13: Standard for the Installation of Sprinkler Systems, Chicago: National Fire Protection Association, 2016.

[8] Siemens, "Working with HART Networks (Application Guide AG012712)," Siemens Canada Limited/Siemens Milltronics Process Instruments, Peterborough.

[9] R. H. Szilard, J. L. Coleman, S. R. Prescott, C. Parisi and C. L. Smith, "RISMC Toolkit and Methodology Research and Development Plan for External Hazards Analysis (INL/EXT-16-38089)," Idaho National Laboratory, Idaho Falls, 2016.

[10] J. L. Coleman, C. Bolisetti, S. Veeraraghavan, C. Parisi, S. R. Prescott, A. Gupta and A. M. Kammerer, "Multi-Hazard Advanced Seismic Probabilistic Risk Assessment Tools and Applications (INL/EXT-16- 40055)," Idaho National Laboratory, Idaho Falls, 2016.

[11] Crane (Engineering Department), Flow of Fluids Through Valves, Fittings and Pipe (Technical Paper No. 410), Stamford: Crane Co., 2013.

Appendix

Appendix A: Equipment Setup

Compiled by Cody Muchmore and Antonio Tahan

The equipment setup appendix will describe the methods used to setup the equipment of the experiment. Some of the instruments used for this were difficult to setup, usually due to a lack of help in manuals. Such as, with the flow meters, things seemingly self-evident held up work for several weeks.

The first device to be discussed are the pressure gauges. The gauges used in this experiment are the Additel 680 Digital Pressure Gauge. They require a ¼ inch female threaded port to be used and are externally water proof up to a depth of 1 meter. To setup the gauges to record, two additional items are required, a USB receiver and the software they come with. By going through the settings, the pressure gauges can be put on a specific channel. The same channel should be used for each pressure gauge. The pressure gauges record their data locally, then upload it to the software via the USB transmission when requested. The software handles receiving and saving the data from two gauges, as well as starting and stopping the data recording. It is unknown how many gauges the software can handle.

The gauges transmission must be turned on each time they are turned on. Turning on the transmission is done by holding the settings key on the device. The menu can be navigated through with the same settings key until a symbol resembling a wi-fi signal is found.

Figure 58. Finding wireless transmission in menu

Figure 59. Accessing wireless communication menu

Figure 60. Setting wireless communication to on.

Figure 61. Exiting out of the menu with power button

The wireless menu can be entered using the zero key. Several different options are available, most importantly the option to turn it on, and the option to change the channel. It is unknown whether the channels themselves are important, but all gauges in use need to be set to the same channel. The wireless transmission will be activated when the same symbol as the menu is flashing in the top left. The software will then be able to find all gauges on each channel, then serial number can differentiate the gauges.

Once the USB is connected to the computer there is a green “play” button on the bottom right of the screen. Using this starts the transmission to the devices once a channel is selected.

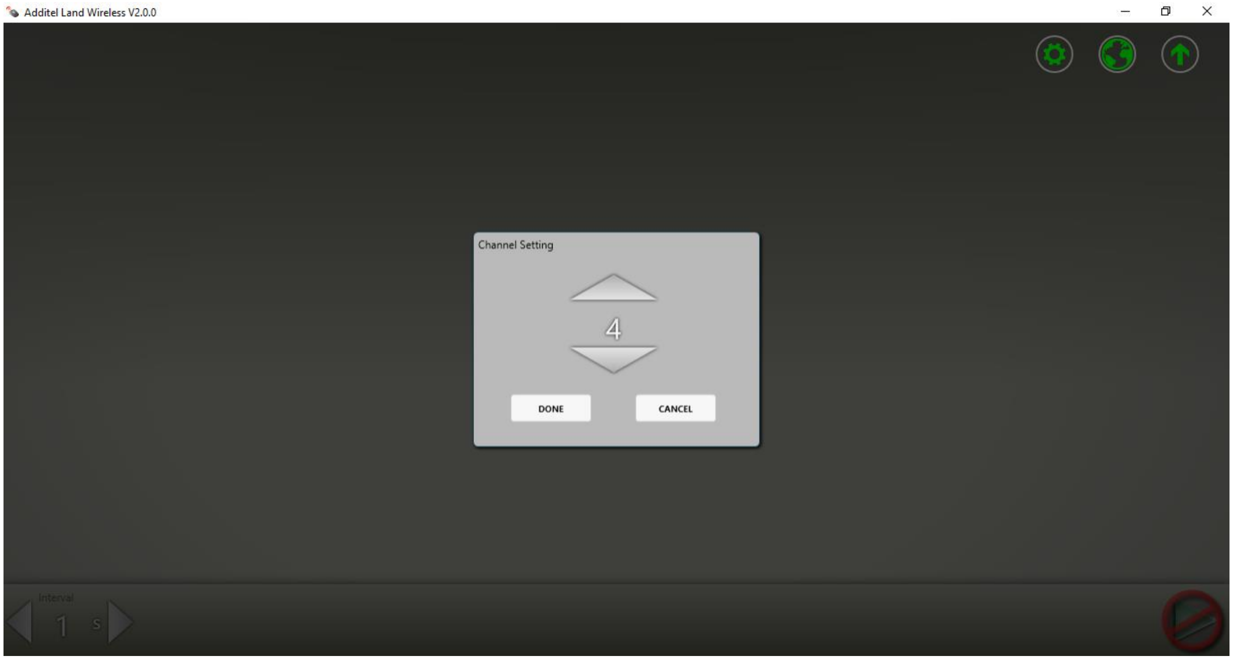

Figure 62. Setting the channel in the software

An icon representing a computer then appears, and once they connect, so do icons for each pressure gauge.

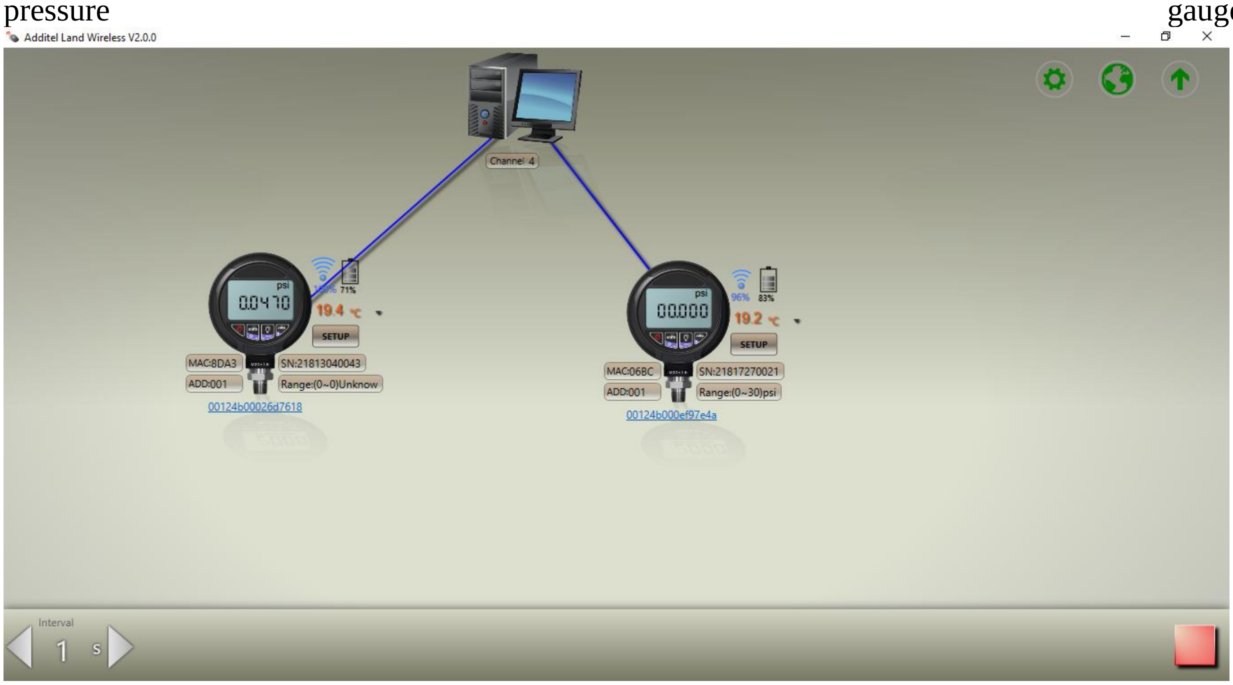

Figure 63. Pressure gauges communicating with the software.

Clicking the setup button will open the menu on the device on the left in the figure. The two most important options are Data Log and Export Data. Clicking Data Log opens the menu next to the right device. Clicking the Log Setting toggle will start the device recording pressure data. Clicking it again will end it.

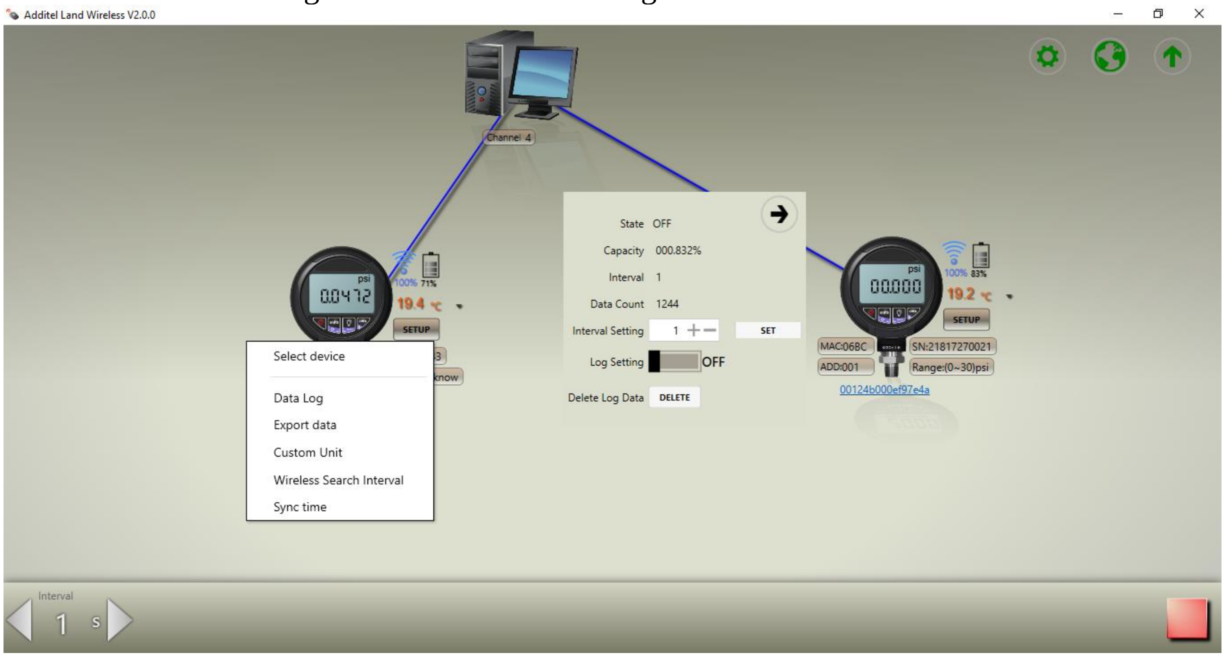

Figure 64. Opening the datalogging menu.

If it is wished to delete the old data on the device and start fresh, a password is required. The password is 218 by default.

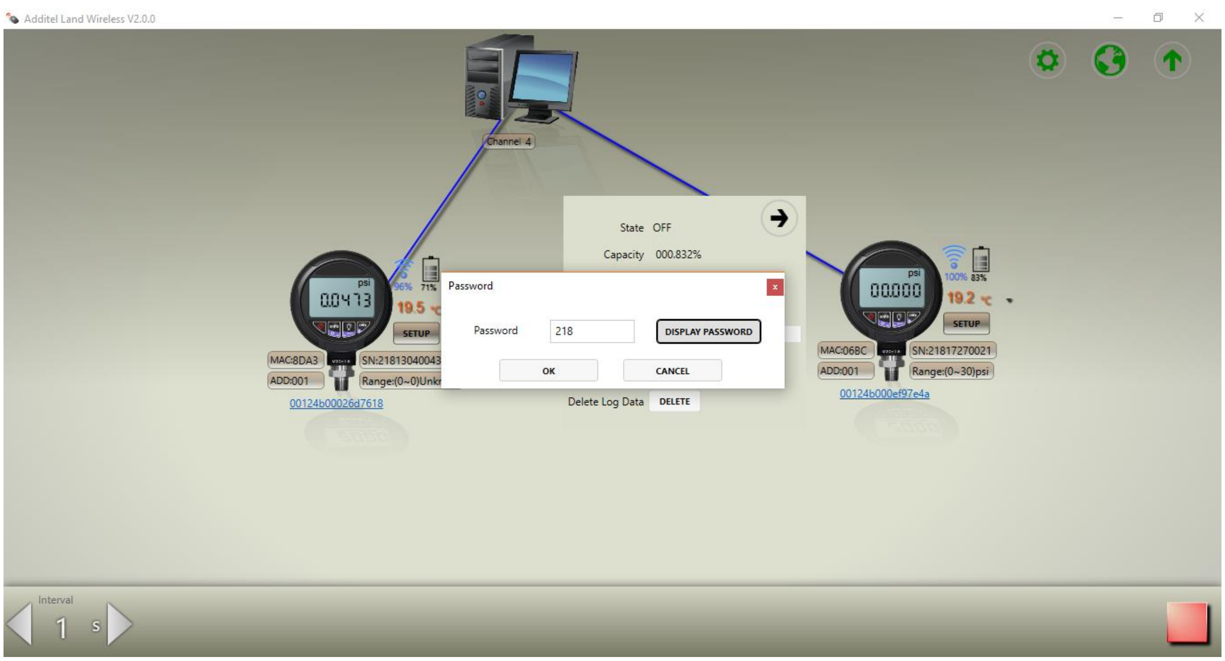

Figure 65. Deleting old data from the devices.

Once the data has been recorded to the device, it can be exported as a CSV file from with the Export Data. The data will be loaded from the device and a window will open as seen. Clicking export will open a save dialog window allowing the file to be saved wherever with a name of choice. Sometimes instead of a table window opening, a chart window will open by default. The chart window will show the most previously recorded session, with options to scroll through previous recordings. The chart opening by defaults is the only difference; a CSV file can still be exported from this window.

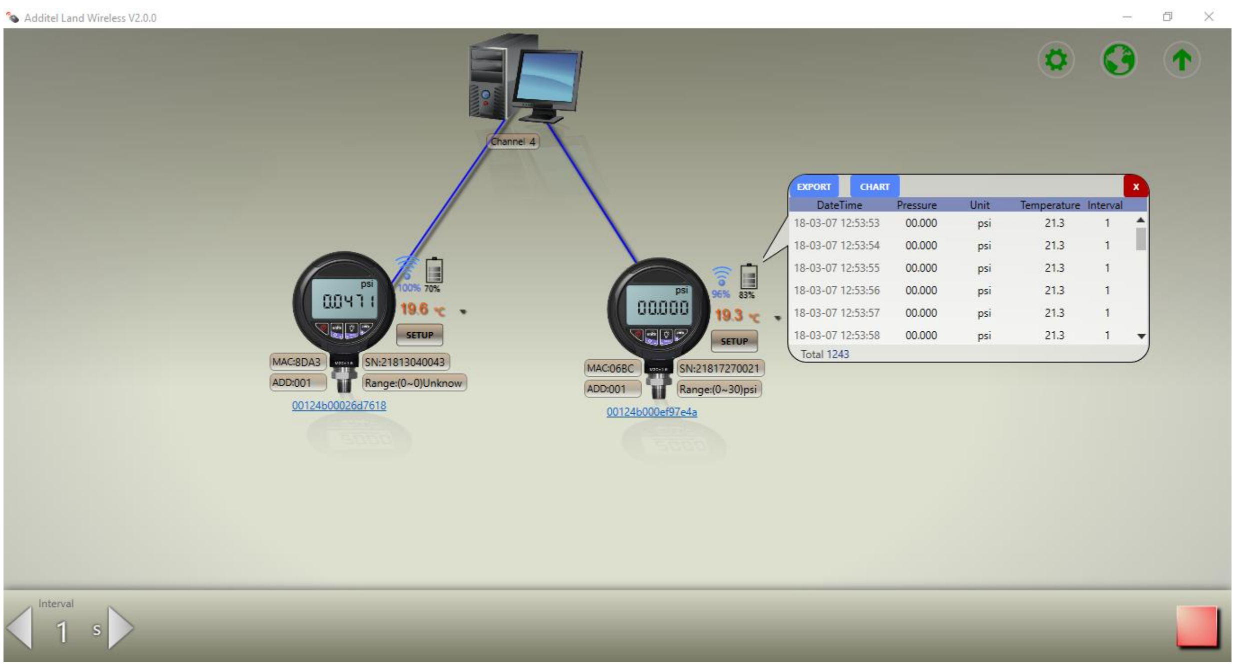

Figure 66. Saving recorded data.

The flow meters used for the leak tests are Krohne Optiflux 2000f 3-inch flow meters. The first is the physical setup. The manual for the flow meter has instructions about how to construct the piping that needs to be followed. The most important points are to have them at low points in your system so they will be filled completely. These flowmeters will not read correctly otherwise. Second, there should be at least 10*DN amount of pipe upstream of the flow meter (so for a 3-inch flow meter, 30 inches) after 3-dimensional bends. Downstream of the flow meter should be at least

2*DN amount of pipe (6 inches for a 3-inch flow meter. These upstream and downstream dimensions help ensure the flow has enough time to become uniform through the flow meter. The meter comes with grounding rings to help the signal be more consistent and stable. These need to be attached and placed between the meter and the pipe flanges. These are the parts of the manual most applicable to this experiment. The manual should be consulted if different setups are used.

These flowmeters have required wiring as well, for power and for HART monitoring. The power uses regular three prong grounded 120 V AC power to be wired in manually. A regular extension cord was used for this, cutting one end off and wiring it into the ports for power. The HART wiring is a bit more complicated, especially if more than one flow meter will be used. There are two ports to be wired to, in the manual they are described as active ports. Each flow meter will need to have these wired, then joined in parallel to another set of wires containing a 250-ohm resistor. It has been successful in the past to wire the both positive ports and negative ports to one side of the resistor.

Once the wiring has been completed, the flow meter channels need to be set. If only one channel is going to be used, the default is channel 0 and no changes need to be made. Otherwise, each flow meter need to be assigned a unique channel, from 1-15 for multidrop connections. Changing the HART channel can be done in the menus on the flow transmitter (the screen connected to the flow meters) by holding the far-left button on the transmitter (>) for 2.5 seconds then releasing it, which enters the menus. In the upper right of the screen is the address of the current menu. The menu to set the HART address is under Setup>HART>Address (C4.2). These menus can also be used to simulate a flow, to test and make sure the connection to the computer is working and reading what the transmitter is seeing.

With more flow meters used on the HART protocol, it should be noted, the worse the recording time is. The problem with the HART protocol is explained in a Siemens Application guide about working with HART networks. [9] When HART devices are multi-dropped, the analog channel can no longer be used, so the digital channel must be used. As the number of devices increases, so too does the update rate. For experiments where short term results are necessary, multidrop is a bad application. The problem of the lack of data was seen in the lab with the water rise experiments. Three flow meters were used initially, but later analysis of the data later revealed only a few data points from the test in the time of interest, sometimes having a difference between times of up to 17 seconds. For experiments where the time frame is longer, such as the pipe rupture experiments in this thesis, the multi-drop update rate is less of a problem. There is no fix to this using multi-drop, it is recommended to use as many HART modems as HART devices. The software should be able to handle it, and this will allow for point to point connections for each device.

The program used in the lab to record the flow meters is called PACTware. Figure 67 shows the screen when the program is first opened.

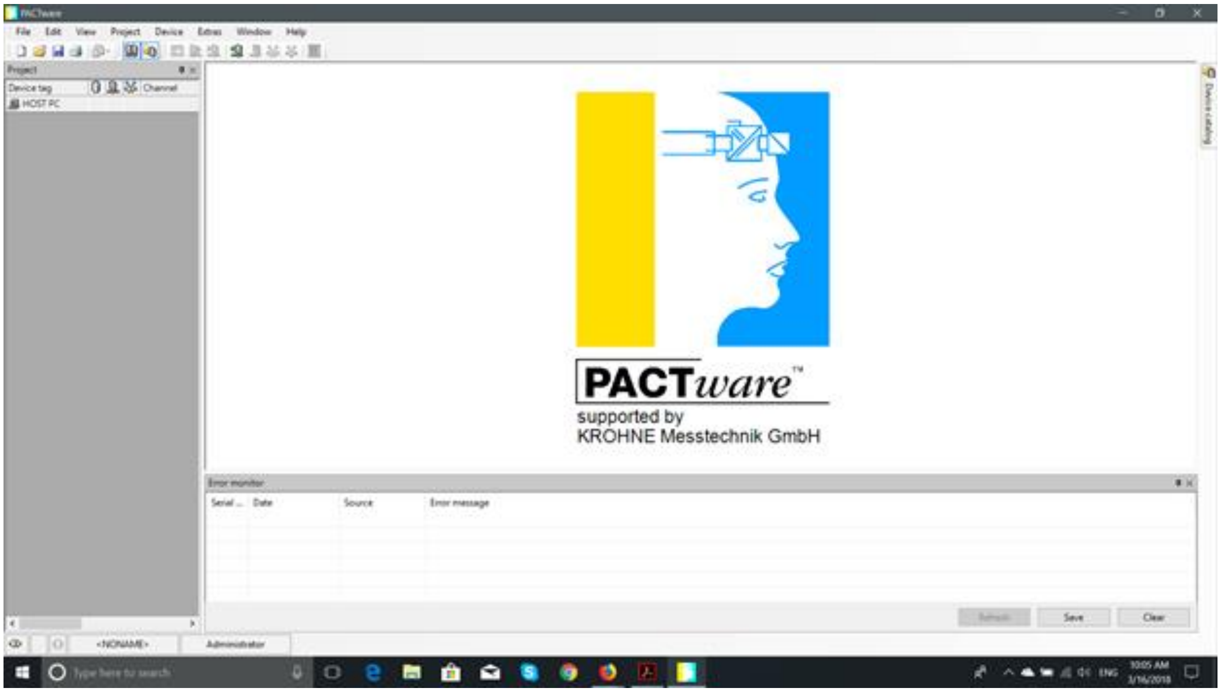

Figure 67. Pactware home screen.

To connect to the flow meters, be sure the physical connections are correct as described before. Next, right click on “HOST PC” on the left, as in Figure 68.

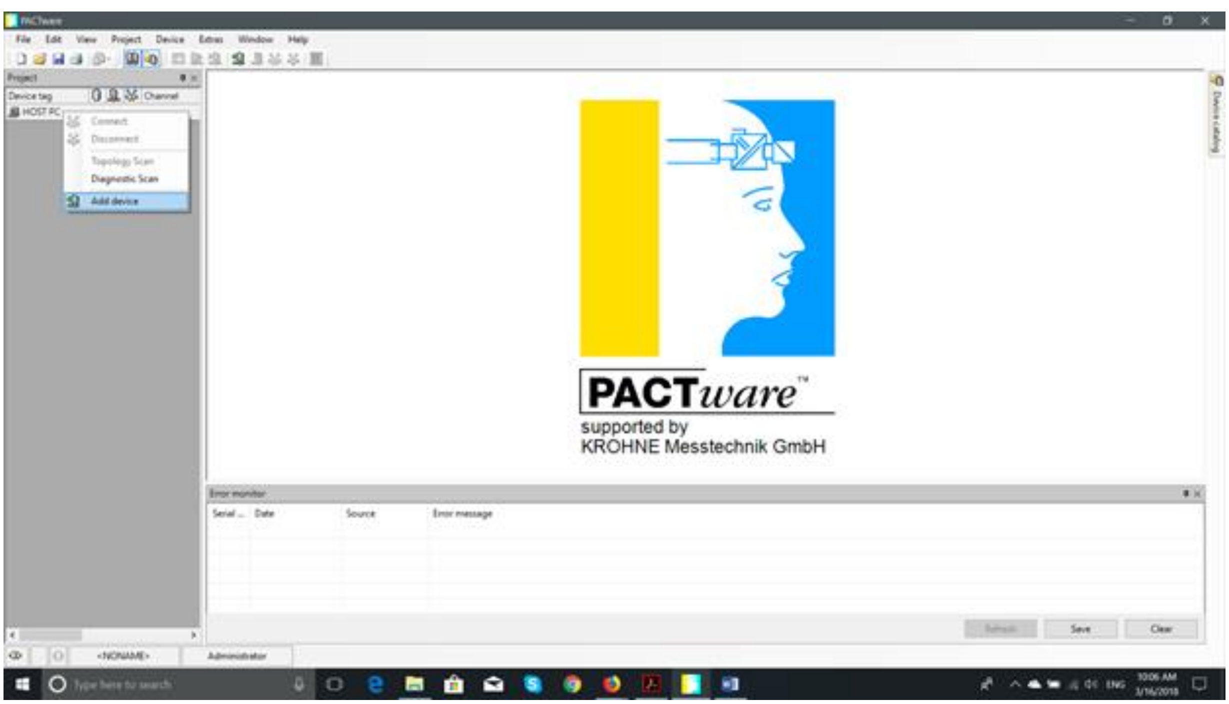

Figure 68. Adding connection to modem.

In the menu that opens click add device. A window will open with several device types, as in Figure 69. The device used is the HART Communication.

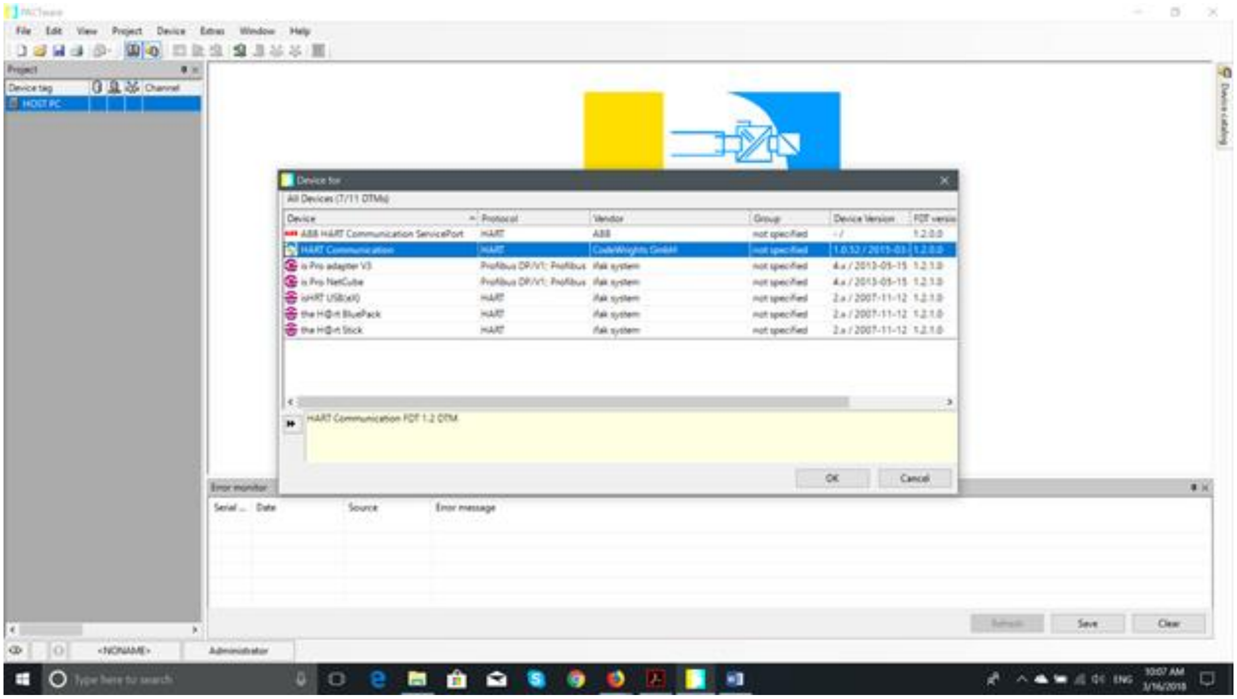

Figure 69. Selecting the appropriate modem.

The HART Communication device will now appear under the host PC with the name COM1. The COM1 icon represents the com port the USB HART modem is plugged into the computer, but it is not likely the modem will be in port 1. In the case of this example, the modem is connected in com port 3, but this may not always be the case. Open the device manager via the control panel to find which com port the modem is in. Back in PACTware, double click the modem device, or right click and select the parameters page.

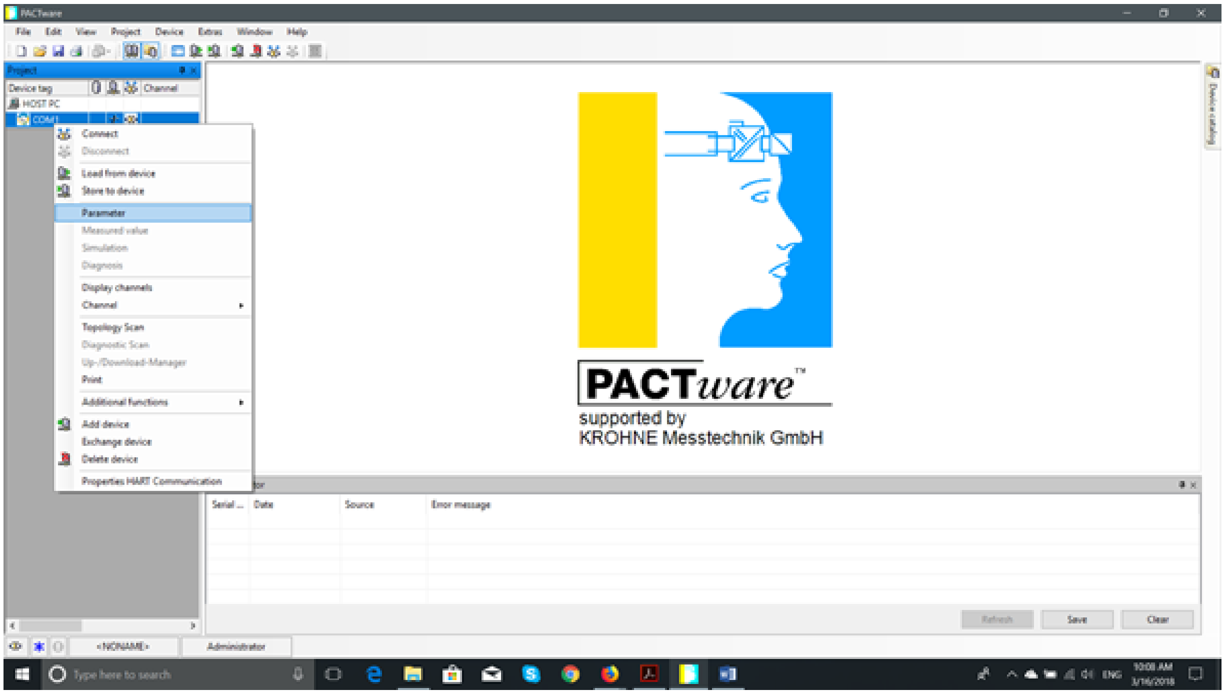

Figure 70. Opening parameter menu to set the COM port.

The parameters page allows you to select the correct com port for PACTware to attempt to find the HART modem.

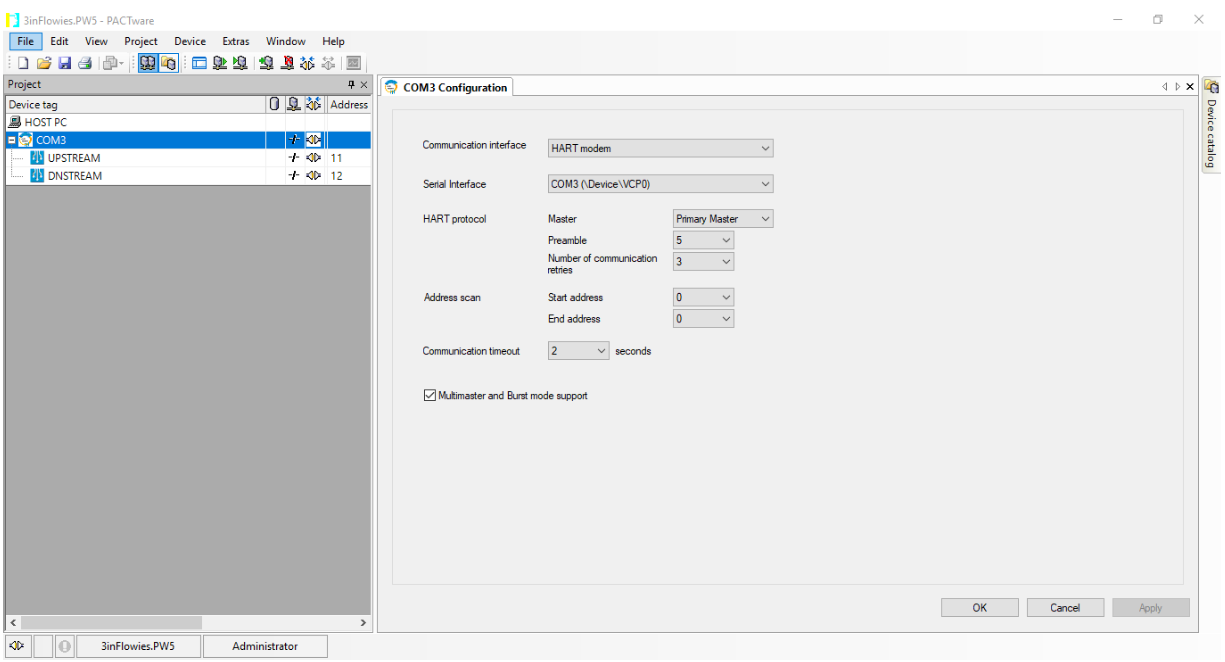

Figure 71. Menu to set the COM port and channels scanned for devices.

The above figure also shows the address scan. If multidrop is to be used, be sure to set these to a range appropriate to encapsulate the addresses used. 0 is reserved for point to point connections, and 1 to 15 is for multidrop. Otherwise, address designation is up to the users' discretion.

Once the correct port is chosen, once again from the right click menu, clicking connect should connect it. At this point, if the connection is successful, disconnect it again. Otherwise, troubleshoot and try to find the error in the setup.

IT IS EXTREMELY IMPORTANT TO DICONNECT THE MODEM AT THIS POINT. IF THE MODEM IS CONNECTED THE NEXT STEP WILL NOT WORK.

The next step is to connect to the flowmeters themselves. Right click the modem and select add device. From the window that opens choose the Microflex Generic HART DTM 6 as the device. These are referred to as Device Type Managers (DTMs).

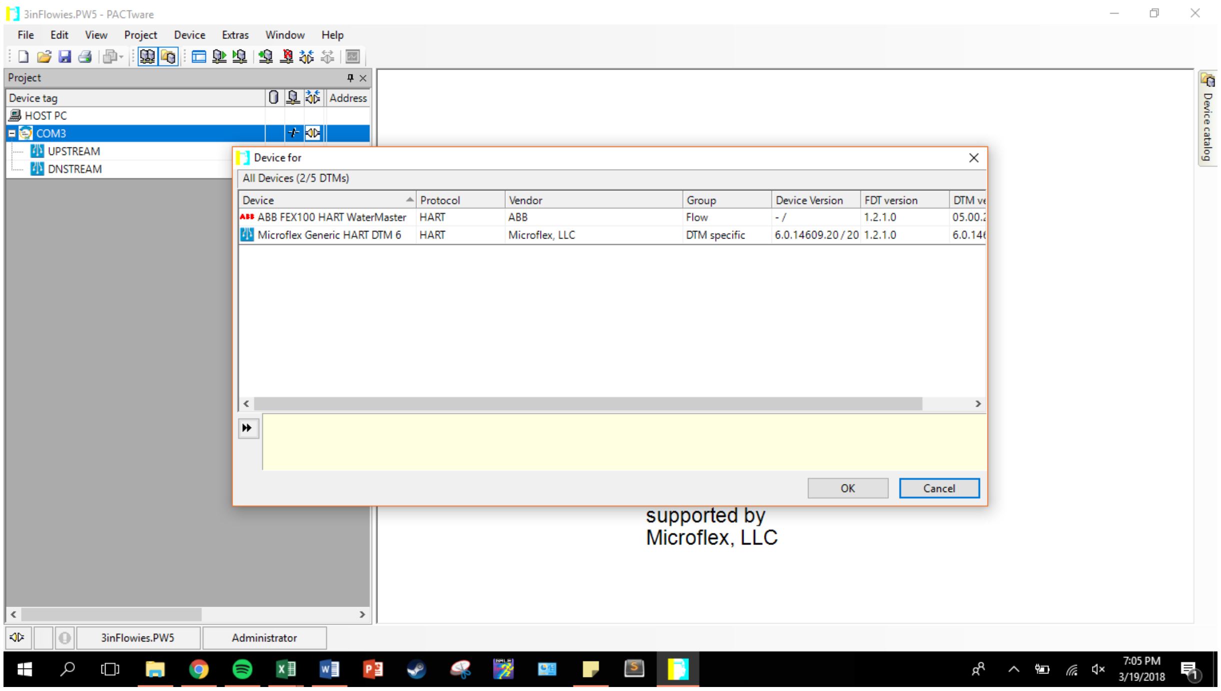

Figure 72. Adding a DTM to the modem.

If connecting to several flow meters via multidrop is desired, now is the time to set the address of the DTMs. Right click again on the COM device. Under Additional Functions is the option Change DTM Address. Open this window and change the new DTMs' addresses to match those of the devices. **If the modem is connected at this point, it is impossible to change the address of the DTMs.**

If multiple modems are in use, repeat the steps, adding the modem and just one DTM, being sure to observe the different ports for each modem. A multiple modem setup will allow for faster recording times for each flow meter, bypassing the inherent flaw in the HART protocol.

At this point, connecting to each flow meter should be possible. Right click each device you wish to connect to and click connect.

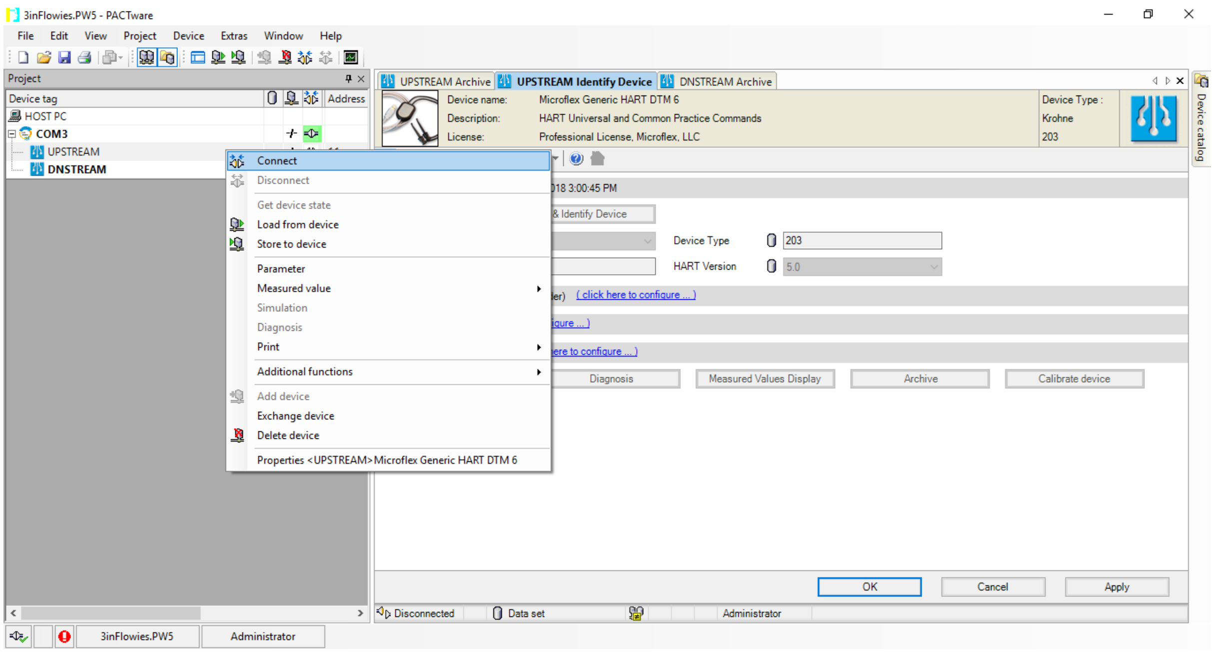

Figure 73. Connecting to the flow meters.

To record the values of the flow meters then right click them again, mouse down to the measured value tab, and click Archive to open a new tab. In this tab, it is possible to see the flow value for a flow meter and to save the resulting data. Each flow meter will open it its own tab.

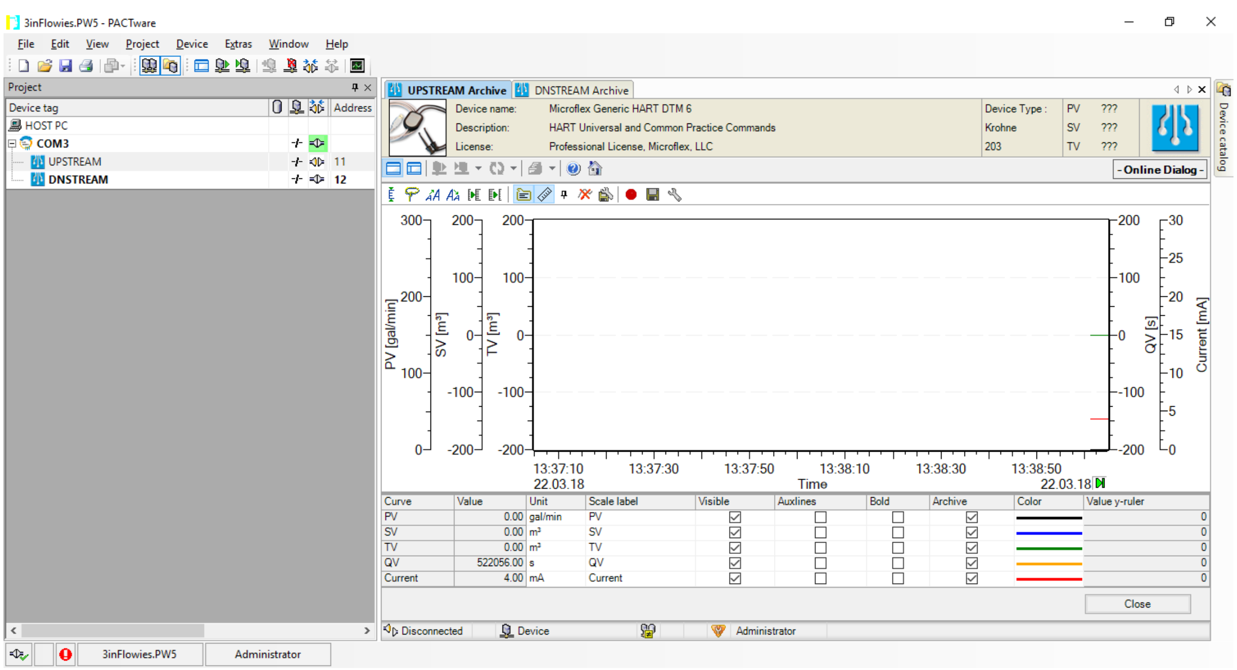

Figure 74. Window used to record flow data

After data is collected, clicking the save button will save a file called My Trend to a default location. If it is pressed again, it will attempt to do the same thing, but will be unable to. Saying no to overwriting the previous file will open a dialog allowing the user to save to a location of their choice. The file type is a CSV and opens best in Excel if the decimal and comma field are changed to a period and a comma from a comma and a semicolon, respectively.

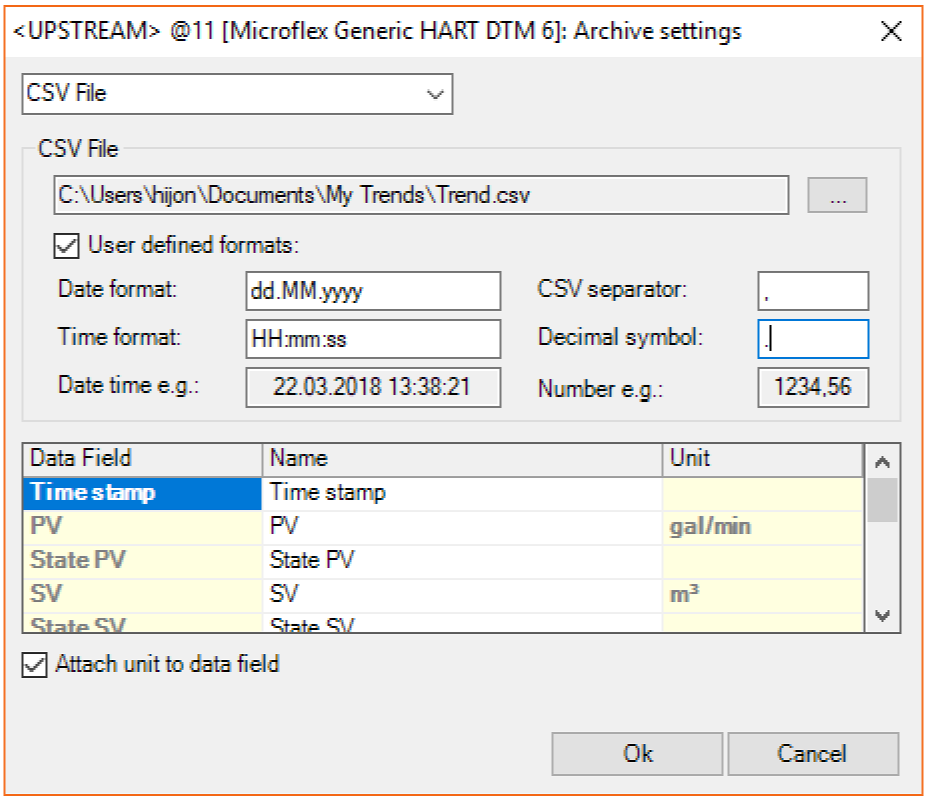

Figure 75. Window for saving recorded data

Appendix B: Pump Curve

The pump used in these pipe leak experiments is the 3GSUBSD5 High Volume Dewatering submersible pump from Global Pump. Figure 76 shows the pump curve provided by the manufacturer, and Figure 77 shows other specifications for the pump provided from the manual.

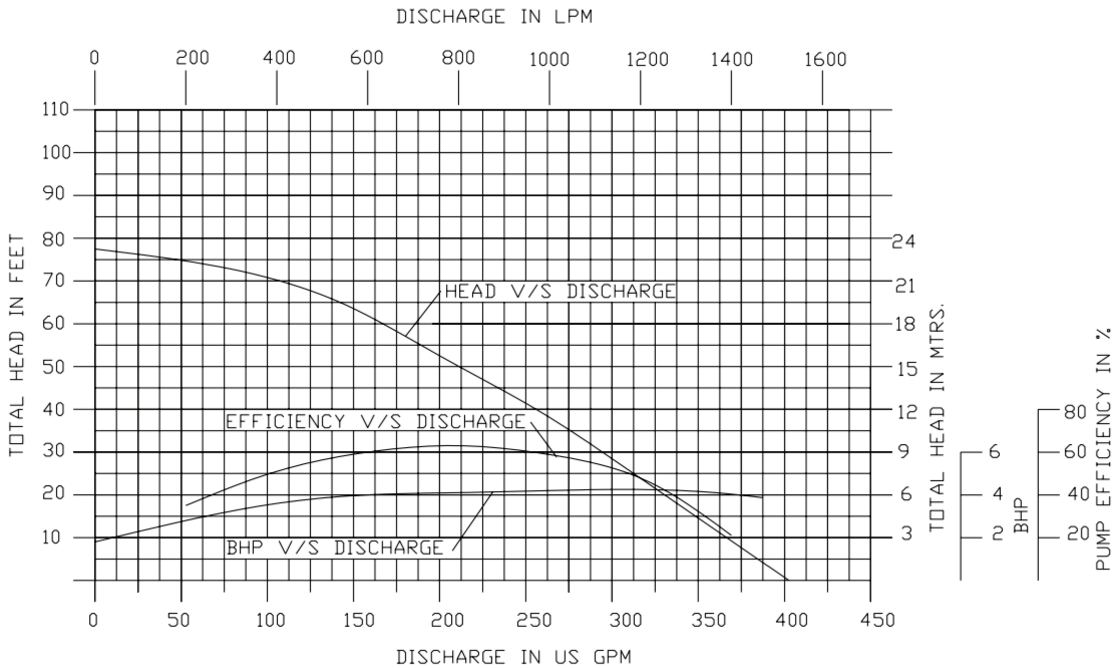

Figure 76. 3-inch submersible pump curve

SPECIFICATIONS	
Size	3" (75 mm)
Power	5 hp (3.7 kW)
Max Flow	400 gpm (91 m³/h)
Max Head	78' (24 m)
Motor	2-pole induction continuous rated motor with squirrel cage rotor. Stator insulation class 'H' (180°C)
Speed (motor)	3,400 RPM @ 60 Hz, 2,800RPM @ 50Hz
Power Rating (motor)	5 hp @ 60 Hz, 3.7 kW @ 50 Hz Full Load
Current FLA (motor)	7.1 Amps @ 460v, 8.1 Amps @ 400v
Max. temperature of the pump liquid (motor)	104°F/40°C
Max. start/stop per hour (motor)	15
Power Supply	3 phase, 50/60 Hz, AC Supply. Available in any voltage frequency combination (208/220/230/380/415/460/575/1,000V)
Power Cable	50' (15 m) length standard
pH Range	5 - 8
Submergence	Submergence below liquid surface min. 5" (127 mm) max. 50' (15 m)
Weight (approx. w/o cable)	90 lbs. (41Kg)

PUMP MATERIAL	
Outer Casing	Epoxy-coated aluminum
Stator Casing	Epoxy-coated extruded aluminum
Diffuser/Wearplate	Nitrile rubber-lined (polyurethane optional)
Shaft	431 Stainless steel
Shaft Seal	Tandem tungsten carbide/tungsten carbide and tungsten carbide/tungsten carbide mechanical seals wholly enclosed in an oil chamber
Hardware	304 Stainless Steel
Impeller	Nitride-hardened 410SS to 56HRC (Standard)
Ball Bearings	Two single row deep groove ball bearing. Bearings enclosed with high temperature grease-containing special anti-corrosion additive
Power Cable	Waterproof/oil proof, rubber-insulated, neoprene-sheathed copper conductor flexible cable. Type SOOW in North America, EPR in the Middle East and HO7RN in the EU. 6 Core or Control cable with thermal overloads optiona
Strainer	304 Stainless Steel with 0.25" (6 mm) round holes

Figure 77. 3-inch submersible pump data